COATING DEVELOPMENT FOR HIGH-SPEED TURNING OF STAINLESS STEEL ADDRESSING COMBINED WEAR MECHANISM

COATING DEVELOPMENT FOR HIGH-SPEED TURNING OF STAINLESS STEEL ADDRESSING COMBINED WEAR MECHANISM

By

QIANXI HE, M. SC., B. ENG

A Thesis Submitted to the School of Graduate Studies in Partial Fulfilment of the Requirements for the Degree Doctor of Philosophy

DOCTOR OF PHILOSOPHY (2022) McMaster University
(Mechanical Engineering) Hamilton, Ontario

TITLE Coating development for high-speed turning of stainless steel addressing combined wear mechanism

AUTHOR Qianxi He, M. Sc., B. Eng.

Mechanical Engineering

SUPERVISOR Dr. Stephen C. Veldhuis

Department of Mechanical Engineering

SUPERVISORY COMITTEE Dr. Eu-gene Ng

Department of Mechanical Engineering

Dr. Igor Zhitomirsky

Department of Materials Science and Engineering

Page Count xvii, 178

To my parents and family, for their unconditional love and support. I am truly thankful for having you all in my life.

Acknowledgements

First and foremost, I would like to express my deepest gratitude to my supervisor, Dr. Stephen C. Veldhuis. I am thankful to him for giving me the opportunity to be part of the McMaster Manufacturing Research Institute (MMRI). I appreciate that all the superior scientific research environment and the extremely preferable platform and resources provided by Dr. Veldhuis. Without his guidance and support, this research would not be possible. I am also grateful to my committee members, Dr. Eu-Gene Ng and Dr. Igor Zhitomirsky for their valuable comments and advice throughout this research work.

I need to thank all my mentors, friends, and colleagues at the McMaster Manufacturing Research Institute (MMRI), especially Dr. German Fox-Rabinovich, Dr. Jose Mario DePaiva, Dr. Julia Dosbaeva, and Dr. Abul Fazal Arif, for their continuous support and guidance along the journey. I feel extremely fortunate to work alongside so many amazing people, and I will always appreciate the knowledge and experience I gained at the MMRI over the years.

Finally, I thank my father, Weidong He, my mother, Jun Li, and my family for their understanding, patience, and support. No word can describe how grateful I am to have their endless love and support in my life.

Lay Abstract

Austenitic stainless steel is a material commonly employed in the mechanical, chemical, and oil and gas industries. However, the machining process for austenitic stainless steel is characterized by a high tendency to work-harden due to the material's high plasticity. This effect results in some machining issues such as high cutting forces, unstable chip formation, and rapid tool failure. The application of hard coatings is an effective way to improve cutting tool life during the machining of stainless steel. In the current research, an AlTiN physical vapour deposition (PVD) coating was developed for the high-speed turning of austenitic stainless steel (SS) 304. Development work was with an especial focus on the chemical composition, mechanical properties, and tribological characteristics. This novel AlTiN PVD coating prolonged the tool life in this application by over 1.3 - 4.6 times compared to commercially available coatings.

Abstract

Austenitic stainless steel 304 (SS304) is one of the most widely used materials for aerospace, vehicle accessories, medical equipment, and ship parts. One of the reasons is that this material provides corrosion resistance and mechanical properties because of its chemical composition of predominantly chromium (Cr) and nickel (Ni). However, austenitic stainless steels have a high tendency to work-hardening and low thermal conductivity. This results in machining problems such as high cutting forces, unstable chip formation, and rapid tool failure. In addition, the work-hardening intensifies the frictional force at the tool-chip interface, which leads to a high localized temperature and causes diffusion and oxidation at the tool-workpiece interface.

The aim of the current research was to develop novel compositions of adaptive PVD coatings for turning stainless steel, thereby cutting production costs, and improving product quality. The focus of this research was on a new generation of self-adaptive PVD coating designs and the use of these features to address machining issues during the cutting of stainless-steel material. It was found that during the high-speed turning of SS304, a complex combination of oxidation/diffusion wear mechanisms resulted in crater formation whereas abrasion/attrition led to flank wear. Therefore, the

coating was designed and investigated with consideration of the dominant tool wear mechanisms, mechanical properties, and the tribological characteristics that were present in the cutting zone.

In this research, different PVD and chemical vapour deposition (CVD) coating systems were studied for the semi-finish turning of SS304; monolayer AlTiN PVD coatings were investigated for the high-speed and ultra-high-speed turning of SS304 under various cooling conditions. Based on the research, a novel self-adaptive bilayer AlTiN PVD coating was developed and applied for the ultra-high-speed turning of SS304. The properties and performance of these coatings were comprehensively studied using X-Ray diffraction (XRD), scanning electron microscopy (SEM), nanomechanical indentation, scratch tests, optical 3D microscopy, tool wear studies, and tribological characterization. In addition, a chip cross-section analysis and surface integrity of the machined workpiece material were performed to study the machinability of SS304. The AlTiN PVD coating with the Al/Ti ratio of 60/40 was found to possess a favourable combination of tribological and micro-mechanical properties, and a novel self-adaptive bilayer AlTiN PVD coating was designed based on these findings. Tool life results have shown that the self-adaptive, bilayer AlTiN PVD coating improves tool life by over 1.3 - 4.6 times compared to the commercially available coatings.

Table of Contents

List of Figures

List of Tables

Abbreviations

BUE   Built-up edge

CCR   Chip compression ratio

CVD   Chemical vapor deposition

EBSD   Electron backscatter diffraction

EDS   Energy dispersive spectroscopy

PVD   Physical vapor deposition

SEM   Scanning electron microscope

SS304   Stainless steel 304

TCCL   Tool-chip contact length

WC   Tungsten carbide

XRD   X-ray diffraction

Chapter 1: Introduction

1.1. Background

Stainless steel is a material commonly employed in the mechanical, chemical, and oil & gas industries. Of the stainless steel varieties available, stainless steel 304 (SS304) is one of the most widely used for aerospace, vehicle accessories, medical equipment, and ship parts [1]. One of the reasons for its popularity is that this material provides very good corrosion resistance and mechanical properties as a result of its chemical composition made up predominantly of chromium (Cr) and nickel (Ni). This combination of properties renders SS304 for implementation in different industry fields.

It is known that austenitic stainless steels are prone to work-hardening (even at low deformation rates) and have low thermal conductivity. The machining process of austenitic stainless steel is characterized by a high tendency to work-harden due to its high plasticity. This effect results in some machining problems such as high cutting forces, unstable chip formation, and high residual stress levels on the machined surface [2]. In addition, the work-hardening elevates friction force at the tool-chip interface, which leads to a high localized temperature causing diffusion and oxidation wear at the tool-workpiece interface [3]. Due to the material's high plasticity and tendency to work-harden, the surface quality of machined parts is generally poor.

Because of cemented carbide's adequate combination of abrasion resistance, mechanical impact strength, high elastic modulus, thermal shock resistance, and corrosion resistance, cemented carbide tools are regarded as the most suitable tool material commercially available for the machining of stainless steels [4,5]. To avoid the chemical interaction between the tool and the workpiece material during stainless steel

machining, carbide cutting tool surfaces must be abrasion resistant, hard, and chemically inert [6]. By enhancing the surface properties of the cutting tool, surface engineering plays a key role in preventing extensive wear of the tool [2,7]. A cutting tool's surface properties, such as its hardness, thermal stability, friction coefficient, and chemical inertness, can be improved by applying a coating [8–10]. The two most regularly used coating depositions are: Chemical Vapor Deposition (CVD) and Physical Vapor Deposition (PVD). Both processes are employed to deposit a variety of cutting tool coatings that are useful for machining stainless steels [10–12].

The aim of the current research is to develop a novel composition and architecture for an adaptive PVD coating to be used in turning stainless steel, thereby reducing production costs and improving product quality. The focus of this research is on a new generation of self-lubricating and self-adaptive PVD coating designs and the use of these features to address machining issues during the process of cutting stainless steel materials. It is well known that applying self-lubricating or self-adaptive coatings can result in beneficial tribo-films being generated during the cutting process, improving the chip formation process, which results in better friction conditions at the cutting zone. Therefore, a precise understanding of how the coating system reacts with elements from the environment (mostly oxygen) to form lubricating films or tribo-ceramics with enhanced hardness, strength, adhesion to the substrate, and thermal barrier characteristics is needed [13]. Hence, the selection and design of coatings in this study considers the tribological compatibility of the tool and workpiece and the conditions under which they are operating.

1.2. Literature review

1.2.1. Stainless steel and machining challenges

Stainless steels are principally chosen for their favourable properties, such as corrosion resistance, high-temperature oxidation resistance, great strength, or cryogenic properties. There are numerous stainless steels commercially available, and these can be categorised according to their microstructure, into the following categories: Austenitic, Ferritic, Duplex/Super Duplex (Austenitic - Ferritic), Martensitic, and Precipitation Hardening. The Schaeffler diagram in Fig. 1.1 can be used to predict the expected microstructure for the various compositions of different grades of stainless steel.
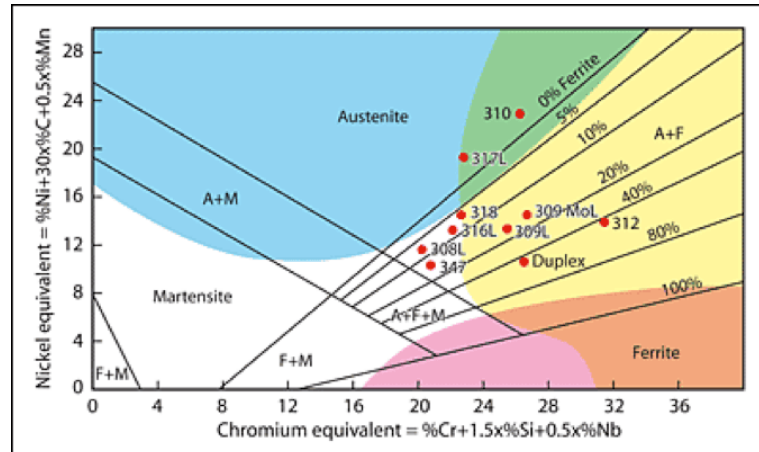
Fig. 1.1. Schaeffler constitution diagram for different grades of stainless steels [14].

SS304 contains at least 18 % Cr to increase hardness without compromising its ductility, which is achievable because Cr improves the grain refinement in the steel. Cr also enhances the strength of SS304 at elevated temperatures. In addition, SS304 contains no less than 8 % Ni. This improves toughness at low temperatures and

minimize scratches. Ni also provides heat resistance to the SS304, resulting in the material's low thermal conductivity [15,16]. This feature makes SS304 difficult to machine because the heat generated at the tool/chip/workpiece interfaces cannot be conducted away from the edge of the tool resulting in a substantial temperature rise. Almost 80 % of the heat will be transferred into the tool instead of dispersing with the chips, and this will accelerate tool wear due to diffusion and oxidation [17]. Moreover, SS304 has a high strain-hardening rate, which causes more adhesion of the workpiece material to the cutting tool surface. This produces unstable chips and built-up edge (BUE) [18]. Overall, the machining of stainless steels has several challenges due to BUE, work-hardening, thermal conductivity, and plastic deformation.

Built-up edge (BUE) is the accumulation of workpiece material welded to the rake face of the tool. The material adheres to the rake face of the tool due to high pressure and friction between the tool and the workpiece. When a critical amount of material deposits on the tool rake face, the welded material referred to as BUE itself contributes to the cutting process. Thus, the BUE effectively changes the geometry of the tool, which also affects the dimensional accuracy and surface finish of the final workpiece. If the balance of forces around the BUE varies, a portion of the BUE will detach along with the chips. Over a period of time, this may also lead to chipping on the flank face since the BUE can also remove a part of the tool material when it dislodges. Techinir and Yasilert [19] conducted turning experiments on SS304 at various cutting speeds, feed rates, and depths of cut, using a WC P10 cemented carbide tool. The study reported that although increasing the feed intensified the BUE, the BUE decreased as the cutting speed accelerated.

As shown in Fig. 1.2, machining processes involve a wide range of both mechanical and thermal physical phenomena. A part of the frictional heat generated between the cutting tool and the workpiece during machining transfers to the workpiece, resulting in a structural change of the material and the hardening of the workpiece surface. The work-hardened surface produces abrasive chips, which are responsible for the tool's abrasion and consequent notch wear. Another reason for notch wear may be the oxidation corrosion or other chemical processes that occur on the surface of the tool [20]. Selvaraj et al. [21] observed that tool wear was caused by diffusion, thermal softening, and notch wear at faster cutting speeds.
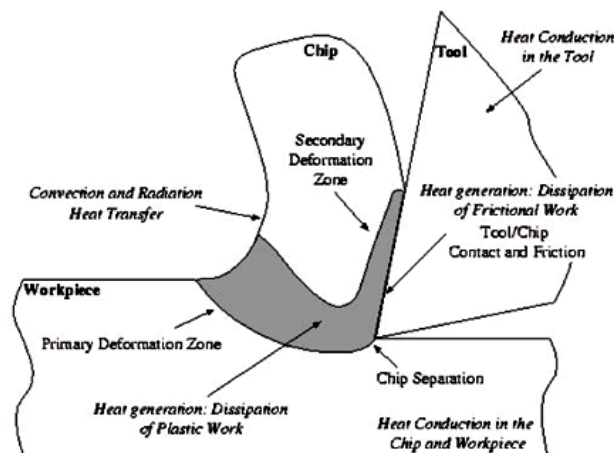
Fig. 1.2. Deformation zones during chip formation for orthogonal machining [22].

During machining, heat is generated from the plastic deformation of the workpiece material in the primary shear deformation zone. The sheared material forms chips that flow over the tool rake face. To overcome the friction at the chip-tool interface, chips undergo further plastic deformation in the secondary shear deformation zone, which increases the temperature at the tool-chip interface. Since stainless steel has low thermal conductivity, only a small amount of heat is conducted into the workpiece. Because of

this, nearly 80 % of the remaining heat transfers into the tool, causing the temperature of tool rake face to reach up to 1000˚C [17]. Diffusion and oxidization occur due to these high temperatures, leading to rapid tool wear.

Ductile materials are often difficult to machine because they plastically deform beyond their yield point and produce continuous chips which tend to stick to the tool. These high-temperature continuous chips aggressively bond to the cutting tool during cutting. When the chip moves through the cutting zone, it may carry a portion of the tool with it, resulting in rapid tool chipping and wear [23].

1.2.2. Cutting tools and machining conditions

Cemented carbide tools are commonly used to machine metal materials. Cemented carbide is a homogeneous mixture of tungsten carbide grains and tough cobalt binder. The tungsten carbide grains are fused into a solid matrix of cobalt metals with different grain sizes [24]. In accordance with ISO standard 4499-2:2008, Fig. 1.3 shows the different WC grain sizes of WC-Co microstructures.

| Ultrafine | Submicron | Fine | Medium | Coarse | Extra coarse |
| 0.2-0.5 µm | 0.5-0.9 µm | 1.0-1.3 µm | 1.4-3.4 µm | 2.5-5.0 µm | >5.0 µm |
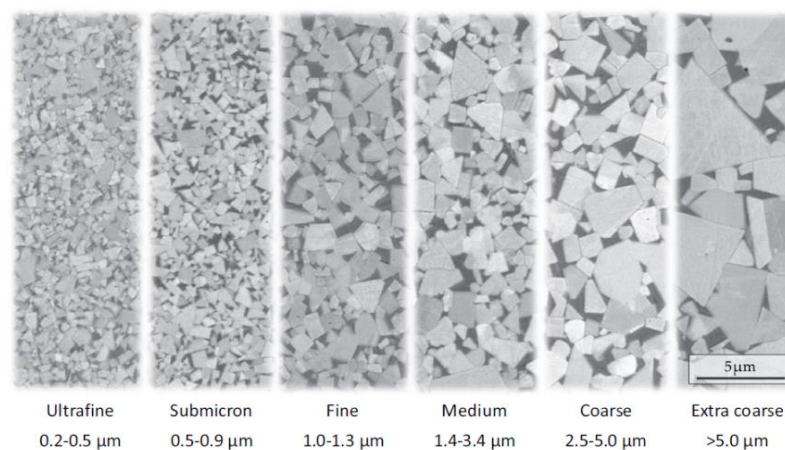
Fig. 1.3. Different WC grain sizes of WC-Co microstructures [25].

One of the main influences on the cutting temperature during any machining process is the cutting speed. As the cutting speed increases, the average cutting temperature at the tool-chip interface rises. The temperature will exceed 500 °C when the cutting speed approaches 140 m/min [4]. At these high temperatures, diffusion begins as elements transfer from the tool substrate to the stainless steel. This phenomenon causes rapid wear on the tool's rake face and weakens the edge of the tool. Moreover, adhesion and abrasion have been reported to be the dominant initial wear mechanisms on carbide tools during the machining of stainless steels [4]. Different cutting fluids have been used for SS304 turning to study their effects on tool wear and surface roughness [26]. However, researchers found that the cutting speed and feed have a more significant influence on tool wear than the choice of cutting fluid.

Mahdavinejad et al. [27] determined that the cutting speed had the greatest influence on tool life during machining. They also reported a significant improvement in tool life under wet conditions compared to dry machining.

Ahmed et al. [28] investigated the effect of BUE in the steady state zone of the tool life curve, using an uncoated WC tool for machining SS304 under wet conditions. It was found that tensile residual stress decreased as the BUE height increased.

Hossein and Yahya [29] reported notch wear to be the dominant tool failure mechanism when machining AISI 304 with a milling process using carbide inserts. Ciftci [12] reported a lower surface roughness resulting from reduced intensity of BUE formation, which was observed at a faster cutting speed. The multilayer CVD coated cemented carbide insert used in that study reduced the friction coefficient at the tool/chip interface.

Zafer and Sezgin determined the most suitable cutting conditions for the machining of AISI 304 stainless steel by considering the acoustic emissions during the cutting process [19]. Korkut et al. [18] conducted experiments using a multilayer coated cemented carbide tool on SS304 by varying the cutting speed from 120, 150, to 180 m/min. It was observed that, as the cutting speed increased, the surface roughness values decreased.

In terms of machining conditions, it is known that the fog generated by coolant during machining operations may result in aggressive health and environmental issues [30,31]. To address that, many manufacturing industries have focused on green and dry manufacturing in an effort to improve occupational health and safety and reduce the environmental impact of a process. The major benefits of dry machining include no water consumption and atmospheric pollution, no liquid residue on the part that requires cleaning, and no subsequent costs for disposing the liquids and cleaning chemicals. The use of liquid coolants and lubricants may also trigger skin irritation and long-term health issues due to inhalation of coolant mists. In general, it was found that machining costs can be reduced by 16-20 % during dry machining [32,33]. However, the adverse effects of dry machining include an increase in friction and adhesion at the tool/chip interface, which increases the temperature in the cutting zone, resulting in a faster wear rate and thus shorter tool life [34].

Many researchers have used different cutting tools, machining conditions, and coatings deposited by various methods to improve the machinability of stainless steels. Outeiro and M'Saoubi [35,36] reported that the dry turning of SS316 at accelerated cutting speeds increased the tensile superficial stresses in the hoop and axial directions, which greatly affects the properties of austenitic stainless steels and their ability to

withstand severe loading conditions. Xavior et al. [26] used different cutting fluids to study tool wear and surface roughness when turning SS304. Selvaraj and Chandramohan [37] minimized the surface roughness during the dry machining of SS304 by finding appropriate process parameters using the Taguchi method. However, achieving low surface roughness under dry machining conditions still presents a challenge.

1.2.3. Tool wear modes and mechanisms

1.2.3.1 General wear modes

Tool wear refers to the change in the shape of a tool from its original form due to the gradual loss of tool material or deformation of the tool during cutting (see Fig. 1.4). Tool wear is inevitable in all machining processes. It adversely affects product quality, dimensional accuracy, and overall productivity, so it is of the utmost importance to reduce tool wear in any machining process.

According to the ISO standard 3685:1993, there are multiple types of wear, namely flank wear, crater wear, BUE formation, notch wear, plastic deformation, thermal and mechanical fatigue, chipping, and fracture. When machining stainless steel, the most impactful wear types are flank wear and crater wear.

1. Flank wear
2. Crater wear
3. Plastic deformation
4. Notch wear
5. Thermal cracking
6. Mechanical fatigue cracking
7. Chipping
8. Fracture
9. BUE
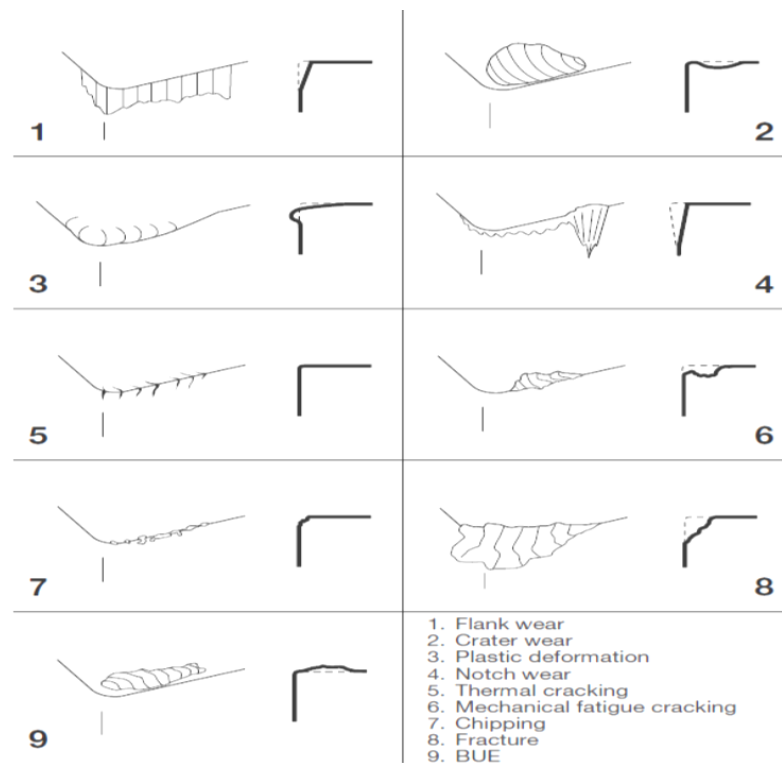
Fig. 1.4. Typical types of tool wear during machining [38].

Flank wear is observed in the form of a wear land on the flank face of the tool. Flank wear narrows the relief angle of the tool and increases frictional resistance [39]. It also reduces dimensional accuracy and can produce poor surface integrity in the machined part. According to ISO 3685:1993 and ISO 8688-2:1989, the tool life criterion is set at 300 µm of flank wear.

Crater wear happens on the rake face of the tool because of the sticking and sliding motion of the chips as they flow over the rake face of the tool at high stress levels and temperatures. Crater wear weakens the strength of the cutting edge and increases the probability of sudden tool breakage. Crater depth, KT, is the most widely used measurement to evaluate crater wear.

1.2.3.2 General wear mechanisms

There are different types of tool wear mechanisms, which are shown in Fig. 1.5. The most typical mechanisms of tool wear are briefly discussed below [39]. Most cutting processes are influenced by one or more of these wear mechanisms, the combination of which is dependent on the specifics of the cutting process (workpiece material, cutting zone temperature and stress, tool material, etc.).
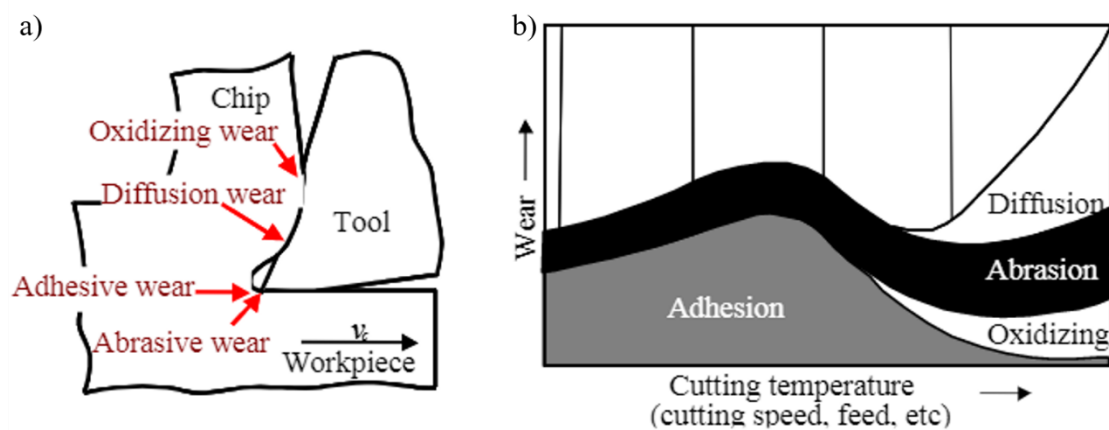
Fig. 1.5. Main wear mechanisms of inserts during the machining process [40].

Abrasive Wear: Abrasive wear occurs due to hard abrasive particles present in the workpiece scratching or scoring the workpiece material. Abrasion occurs mainly on the flank face of the tool. Abrasive wear is not a uniform form of wear and appears at various positions across the tool wear land. Typically, the abrasive wear volume is greater than the adhesive wear volume.

Adhesion Wear: Adhesion or attrition wear occurs when the workpiece material repeatedly adheres to the tool surface and breaks off at intervals, taking cutting tool fragments along with it. This adhesion of the workpiece material is referred to as built-up edge (BUE) and forms because of the high temperatures and pressures generated

during cutting. It is prevalent on both the flank and rake face. Adhesion wear volume is generally low.

Diffusion Wear: During cutting, high temperatures are generated, at which diffusion of the tool constituents into the workpiece, or vice versa, often takes place. This results in a smooth type of wear referred to as diffusion wear. The rate of diffusion is dictated by the chemical affinity between the tool and workpiece, the concentration gradient, and the cutting temperature. As the cutting temperature rises, the diffusion rate increases exponentially.

Oxidation Wear: Oxidation wear occurs due to the oxidation of tool materials, such as the tool binder, and takes place near the surface of the tool. Due to high cutting temperatures and pressures, oxygen often reacts with the tool material, giving rise to this type of wear. Oxidation wear typically results in localized notch wear that presents itself at the maximum depth-of-cut location on the tool.

1.2.4. Coatings for cutting tools (PVD/CVD)

An ongoing problem in machining is regulating the high temperatures it produces. The heat generated dissipates into the chip, tool, and workpiece. To minimize cutting temperature generation, coatings are applied on cutting tools to reduce friction at the tool-chip-workpiece interface. Surface engineering, which enhances the surface properties of the cutting tool, plays a key role in preventing the wear of the tool [7]. Coating a cutting tool improves its surface properties, such as hardness, thermal stability, friction coefficient, and chemical inertness [8–10]. There are two commonly used techniques for modifying the surface of cutting tools: Chemical Vapor Deposition (CVD) and Physical Vapor Deposition (PVD). Both processes can apply a number of different coatings to cutting tools relevant to the machining of SS304 [10–12]. Tool

coatings are traditionally expected to play multiple roles, such as reducing cutting temperatures and cutting forces and increasing abrasion resistance. The application of coated carbide tools has provided significant improvement within the cutting region, which has resulted in better tool wear performance. Tool coatings are thus expected to broaden the lowest wear zone on the feed rate and cutting speed wear map [41–43].

1.2.4.1 Coatings applied during the machining of stainless steels

Several PVD and CVD coatings have been used during the machining of stainless steel to provide the tools with improved wear resistance. CVD TiCN + Al_2O_3 as well as PVD TiCN and AlTiN coatings on cemented carbide substrates were investigated during the machining of super-duplex stainless steels [3]. It was found that the PVD coated cutting tool provided the longest tool life. Fox-Rabinovich et al. [44] investigated the structural characteristics and service properties of AlTiN and TiAlCrN coatings for different cutting tools during the machining of hard-to-cut materials. The influence of the coating design and composition on the oxidation behaviour of $Al_xCr_{1-x}N$ (x=0.70) coatings was studied, and the modified aluminum-rich AlCrN-based coatings were found to improve their oxidation resistance. Two different Al content levels in the nano-multilayered coatings were investigated during the machining of superalloys [45]. It was suggested that the composition of the coating and its characteristics should be tuned depending on the application. Krolczyk et al. [46] studied tool life and wear mechanisms during the machining of duplex stainless steel. They found that CVD - Ti(C, N)/Al_2O_3/TiN coated carbide tools show higher resistance to abrasive wear, and they are thus recommended for the rough machining of duplex stainless steel. In addition, it was also found [47] that the CVD TiC/TiCN/TiN coated cutting tools generate lower cutting forces than TiCN/TiC/Al_2O_3 coated tools, which is attributed to a lower friction

coefficient of the TiN top coating layer. Moreover, CVD Al_2O_3 coating is considered an excellent coating material for metal cutting applications as a result of its high chemical stability and favourable thermal properties [47].

Self-adaptive PVD coatings are a generation of coatings that respond selectively to cutting conditions. Such coating systems can provide an optimum response to external stimuli. They can react to outside conditions, such as temperature, stress and strain [48]. Self-adaptive coatings function by forming beneficial tribo-films through interacting with the environment (mostly oxygen) [49]. At high temperatures and under extreme friction, adaptive coatings react chemically with other materials and form tribo-films on the surface of the tool [50]. Consequently, there are two groups of adaptive coatings [51–53]: 1) Coatings that exhibit adaptive behaviour by virtue of their gradual change in composition or through the combination of hard phases with lubricant compounds; 2) Adaptive coatings that change their properties and structures under severe conditions by forming a tribo-film layer on the surface of the tool. Adaptive coatings can be applied for the machining of hard-to-cut materials since they can generate different tribo-films, and therefore they have a notable influence on frictional characteristics at the interfaces and on the wear performance of the tools.

Some self-adaptive coatings have been applied on different materials under various cutting conditions (such as TiAlCrSiYN/TiAlCrN PVD coatings for the dry machining of Inconel 781, hardened H13 steel, and 1040 steel, etc. [50,54–57]. The coatings studied formed an increasing number of protective tribo-films at the very beginning of the running-in stage of wear, demonstrating a very fast adaptive response to the external stimuli. This process exposes a reduced level of friction, which resulted in lower cutting forces and wear volume.

Based on the literature, self-adaptive PVD coatings could produce tribo-films as a reaction with the environment on the interlayer between the tool and workpiece material. Self-adaptive PVD coatings could be applied on cutting tools for the machining of stainless steels as a solution to improve tool wear performance.

1.2.4.2 Wear performance of coated tools applied during the machining of stainless steels

Flank wear is generally the most critical type of wear [58], and some researchers are studying this wear mechanism during the machining of stainless steels. Recent studies show that a tool's flank wear is reduced once AlTiN and AlTiSiN PVD coatings are applied on the cutting tool [59]. The higher performance with these two coatings is due to the generation of aluminum oxide (Al_2O_3), which is known to form chemically stable oxides that act as a protective thermal layer. The ongoing formation of this layer is prompted by the high content of aluminum present in both coatings.

Another wear mechanism that is commonly found during the machining of stainless steels is adhesion. Adhesion wear results in BUE formation, leading to poor friction conditions in the cutting zone. Ciftci [12] evaluated BUE formation using CVD coated carbide tools while machining AISI 304 and AISI 316 at two different cutting speeds (120 and 180 m/min). At a slow speed, it was noticed that the coated tool showed rapid and unexpected tool wear with occasional chipping, while at a faster cutting speed, less wear was observed on the cutting edge. One of the main reasons for this difference in performance is the lower level of adhesion observed between the BUE and cutting tool at accelerated cutting speeds.

Al-based PVD metallic coatings with different microstructures were investigated for the machining of AISI 304 [60]. Although the PVD coated tools that were developed

showed continuous flank wear, including abrasion wear with BUE periodically observed, the coatings were found to show good abrasion resistance (compared in most cases to that of a typical PVD ceramic coating, such as CrN) across a wide range of chemical compositions.

1.3. Main research gaps

According to the literature review, SS304 has a high tendency to work-harden and has low thermal conductivity, which makes it a hard-to-machine material. Limited information has been provided regarding the tribological interaction that occurs at the tool-chip-workpiece interface for semi-finish/finish operations during the machining of stainless steels, especially under high cutting speed conditions. A suitable and effective tool coating system has yet to be identified or developed to improve tool wear performance when machining stainless steels. Thus, this research aims to address the following research gaps not yet explored in the literature:

1. Most of the previous investigations were focused on the effects of coatings on tool wear and tool life only, but there is still a lack of information in the literature on the relationship between coating and substrate characteristics and its correlation with tool performance.

2. Although many researchers have proposed different coatings for improving the machinability of stainless steels, there is still an essential need to develop novel surface engineering methods in terms of architecture and coating composition, to prevent premature tool failure and prolong tool life.

3. The cutting tool's performance is strongly associated with the cutting conditions of the machining process. No research has been done yet to understand how the tool wear mechanisms change under various machining

conditions, especially for the high-speed (above 300 m/min) turning of stainless steels.

4. No systematic approach to coating design has been found in the literature for the machining of stainless steels. The current research focuses on the development of PVD coatings with different Al/Ti ratios and architectures to reduce tool wear during the semi-finish/finish turning of stainless steels.

5. The potential for a new generation of self-adaptive PVD coatings to improve tool wear performance during the machining of stainless steels has yet to be explored. A detailed study regarding tribo-film formation during stainless steel machining and how it effects tool wear is required.

1.4. Research objectives

As concluded from the available literature and research gaps shown above, increasing tool life and improving tool wear are essential requirements for the cost-effective machining of stainless steels. Thus, the general objectives of my Ph.D. research are as follows:

1. Investigate the wear behaviour of the cutting tool during the high-speed (above 300 m/min) machining of SS304.

2. Understand the correlation between different grades of substrates (cemented carbides) and the coatings deposited over them in terms of mechanical properties and tool wear performance.

3. Investigate the Al/Ti ratios in AlTiN-based PVD coatings regarding the coating architecture, mechanical/physical properties, wear behaviour, and tribological characteristics for the high-speed (above 300 m/min) machining of SS304 under different cooling conditions.

4. Develop a coating architecture (AlTiN-based multilayered, self-adaptive) to improve wear and tribological performance during the high-speed machining of SS304.

1.5. Thesis organization

In compliance with the regulations of McMaster University, the main body of this dissertation is assembled in a sandwich thesis format composed of published journal articles that address the objectives outlined above. The final chapter provides an overall conclusion and major findings of the current research. The structure of the thesis chapters and appendices is arranged as follows:

Chapter 1: This chapter introduces the research area along with the relevant background and research objectives to frame the scope of this thesis.

Chapter 2: This chapter presents a new approach to applying various CVD and PVD (coating + substrate) integrated systems during the semi-finish turning of SS304. The characteristics of the coating/carbide substrate design were evaluated in terms of chemical, phase composition, architecture, and mechanical properties in relation to the tribological and wear performance. A guideline is proposed for further study of the cutting tool life and wear performance of CVD and PVD coated cemented carbide inserts. This chapter addresses the first and second objectives of this research, and consists of the following journal paper publication: *Q. He, J.M. Paiva, J. Kohlscheen, B.D. Beake and S.C. Veldhuis. "An integrative approach to coating/carbide substrate design of CVD and PVD coated cutting tools during the machining of austenitic stainless steel". Ceramics International (IF 4.527). 46 (2020) 5149–5158.*

Chapter 3: This chapter studies AlTiN coatings with five different Al/Ti ratios (50/50, 60/40, 67/33, 70/30 and 73/27) deposited via the cathodic arc PVD method for

the ultra-high speed machining of SS304. The coating structure was characterized by SEM and XRD techniques. Assorted mechanical properties such as elastic modulus, coating adhesion, hardness and micro-scratch fracture toughness were assessed using nano-indentation and scratch testing. Chip characterization, tribological performance, and wear behaviour were also analyzed to gain a better understanding of the coating's performance. This chapter addresses the first and third objectives of this research and consists of the following journal paper publication: ***Qianxi He,*** *Jose M. Paiva, Joern Kohlscheen, Ben D. Beake, and Stephen C. Veldhuis. "Study of wear performance and tribological characterization of AlTiN PVD coatings with different Al/Ti ratios during ultra-high speed turning of stainless steel 304".* ***International Journal of Refractory Metals and Hard Materials*** *(IF 3.871). 96 (2021) 105488.*

Chapter 4: This chapter explores the tribological behaviour of AlTiN coatings with five different Al/Ti ratios and the effect of coolant under aggressive high-speed cutting conditions. During the experiments, the tool life, cutting forces, wear mechanisms, friction conditions, and surface integrity of the machined workpiece were investigated. Compared to the dry machining, all five coatings were found to exhibit 2-3 times longer tool life in the wet cutting conditions. This chapter addresses the first and third objectives of this research and consists of the following journal paper publication: ***Qianxi He***, *Jose M. Paiva, Joern Kohlscheen, and Stephen C. Veldhuis. "Analysis of the performance of PVD AlTiN coating with five different Al/Ti ratios during the high-speed turning of stainless steel 304 under dry and wet cooling conditions".* ***Wear*** *(IF 3.892). 492–493 (2022) 204213.*

Chapter 5: This chapter investigates a novel self-adaptive bilayer AlTiN PVD coating for the ultra-high speed finish turning of SS304. The coatings' mechanical

properties (hardness, elastic modulus, toughness, and adhesion) were evaluated using nano-indentation and scratch methods. The obtained data illustrated the influence of the mechanical properties of the coatings on tool wear performance. This chapter addresses the first and fourth objectives of this research and consists of the following journal paper publication: ***Q. He***, *J.M. DePaiva, J. Kohlscheen, and S.C. Veldhuis. "A study of mechanical and tribological properties as well as wear performance of a multifunctional bilayer AlTiN PVD coatings during the ultra-high-speed turning of 304 austenitic stainless steel".* ***Surface and Coatings Technology*** *(IF 4.158). 423 (2021) 127577.*

Chapter 6: This chapter contains a summary of and conclusions drawn from the current research studies, along with some suggestions for future work.

1.6. Note to the reader

Since this thesis consists of a series of journal articles, some repetitive material might be found while reading. In particular, there is some overlap in the introduction section of some chapters. In addition, the sections describing experimental instruments and measurement methodologies in some of the chapters contain significant repetition since the same facilities were used for all experiments. However, the background section of each chapter also provides references specific to the study presented in each paper.

1.7. References

[1]   Q. He, Z. Jin, G. Jiang, Y. Shi, The investigation on electrochemical denatured layer of 304 stainless steel, Mater. Manuf. Process. 33 (2018) 1661–1666. https://doi.org/10.1080/10426914.2018.1453152.

[2]   J.L. Endrino, G.S. Fox-rabinovich, C. Gey, Hard AlTiN , AlCrN PVD coatings for machining of austenitic stainless steel, Surf. Coatings Technol. 200 (2006) 6840–6845. https://doi.org/10.1016/j.surfcoat.2005.10.030.

[3]   J.M.F. d. Paiva, R.D. Torres, F.L. Amorim, D. Covelli, M. Tauhiduzzaman, S. Veldhuis, G. Dosbaeva, G. Fox-Rabinovich, Frictional and wear performance of hard coatings during machining of superduplex stainless steel, Int. J. Adv. Manuf. Technol. 92 (2017) 423–432. https://doi.org/10.1007/s00170-017-0141-4.

[4]   D. Jianxin, Z. Jiantou, Z. Hui, Y. Pei, Wear mechanisms of cemented carbide tools in dry cutting of precipitation hardening semi-austenitic stainless steels, Wear. 270 (2011) 520–527. https://doi.org/https://doi.org/10.1016/j.wear.2011.01.006.

[5]   C.M. Fernandes, A.M.R. Senos, Cemented carbide phase diagrams: A review, Int. J. Refract. Met. Hard Mater. 29 (2011) 405–418. https://doi.org/https://doi.org/10.1016/j.ijrmhm.2011.02.004.

[6]   J.G. Corrêa, R.B. Schroeter, Á.R. Machado, Tool life and wear mechanism analysis of carbide tools used in the machining of martensitic and supermartensitic stainless steels, Tribol. Int. 105 (2017) 102–117. https://doi.org/https://doi.org/10.1016/j.triboint.2016.09.035.

[7]   J.L. Mo, M.H. Zhu, A. Leyland, A. Matthews, Impact wear and abrasion

resistance of CrN, AlCrN and AlTiN PVD coatings, Surf. Coatings Technol. 215 (2013) 170–177. https://doi.org/https://doi.org/10.1016/j.surfcoat.2012.08.077.

[8]   I. Sik, A. Amanov, J. Deok, Tribology International The effects of AlCrN coating , surface modi fi cation and their combination on the tribological properties of high speed steel under dry conditions, Tribiology Int. 81 (2015) 61–72. https://doi.org/10.1016/j.triboint.2014.08.003.

[9]   M. Çöl, D. Kir, E. Eri\csir, Wear and blanking performance of AlCrN PVD-coated punches, Mater. Sci. 48 (2013) 514–520. https://doi.org/10.1007/s11003-013-9532-3.

[10]   K. Bobzin, High-performance coatings for cutting tools, CIRP J. Manuf. Sci. Technol. 18 (2017) 1–9. https://doi.org/https://doi.org/10.1016/j.cirpj.2016.11.004.

[11]   M. Sokovic, L.A. Dobrzański, J. Kopač, L. Kosec, Cutting Properties of PVD and CVD Coated A2lO 3 + TiC Tool Ceramic, in: THERMEC 2006, Trans Tech Publications, 2007: pp. 1159–1164. https://doi.org/10.4028/www.scientific.net/MSF.539-543.1159.

[12]   I. Ciftci, Machining of austenitic stainless steels using CVD multi-layer coated cemented carbide tools, 39 (2006) 565–569. https://doi.org/10.1016/j.triboint.2005.05.005.

[13]   G.S. Fox-Rabinovich, J.E.K. and S.C.V. Iosif Gershman, Mohamed A. El Hakim, Mohamed A. Shalaby, Tribofilm Formation As a Result of Complex Interaction at the Tool/Chip Interface during Cutting, Lubricants. 2 (2014) 113–123. https://doi.org/https://doi.org/10.3390/lubricants2030113.

[14] C. Hong, J. Shi, L. Sheng, W. Cao, W. Hui, H. Dong, Influence of hot working on microstructure and mechanical behavior of high nitrogen stainless steel, J. Mater. Sci. 46 (2011) 5097–5103. https://doi.org/10.1007/s10853-011-5439-2.

[15] A. Di Schino], J.M. Kenny, Grain size dependence of the fatigue behaviour of a ultrafine-grained AISI 304 stainless steel, Mater. Lett. 57 (2003) 3182–3185. https://doi.org/https://doi.org/10.1016/S0167-577X(03)00021-1.

[16] A. Biksa, K. Yamamoto, G. Dosbaeva, S.C. Veldhuis, G.S. Fox-Rabinovich, A. Elfizy, T. Wagg, L.S. Shuster, Wear behavior of adaptive nano-multilayered AlTiN/MexN PVD coatings during machining of aerospace alloys, Tribol. Int. 43 (2010) 1491–1499.
https://doi.org/https://doi.org/10.1016/j.triboint.2010.02.008.

[17] P.S. Bapat, P.D. Dhikale, S.M. Shinde, A.P. Kulkarni, S.S. Chinchanikar, A Numerical Model to Obtain Temperature Distribution During Hard Turning of AISI 52100 Steel, Mater. Today Proc. 2 (2015) 1907–1914.
https://doi.org/https://doi.org/10.1016/j.matpr.2015.07.150.

[18] I. Korkut, M. Kasap, I. Ciftci, U. Seker, Determination of optimum cutting parameters during machining of AISI 304 austenitic stainless steel, Mater. Des. 25 (2004) 303–305.
https://doi.org/https://doi.org/10.1016/j.matdes.2003.10.011.

[19] Z. Tekıner, S. Yeşılyurt, Investigation of the cutting parameters depending on process sound during turning of AISI 304 austenitic stainless steel, Mater. Des. 25 (2004) 507–513.
https://doi.org/https://doi.org/10.1016/j.matdes.2003.12.011.

[20] D. A. Stephenson and J. S. Agapiou, Metal Cutting Theory and Practice, 2016.

[21]   D.P. Selvaraj, P. Chandramohan, M. Mohanraj, Optimization of surface roughness, cutting force and tool wear of nitrogen alloyed duplex stainless steel in a dry turning process using Taguchi method, Measurement. 49 (2014) 205–215. https://doi.org/https://doi.org/10.1016/j.measurement.2013.11.037.

[22]   R.S. Rajpoot, S.K. Saluja, D. Of, I.G.E.C.S. Mp, An investigation of the chip formation process by applying Finite Element Method in orthogonal machining, Int. J. Mod. Eng. Res. 6 (2016) 12–21.

[23]   I. Sushil, P. Amit, P. Rohit, Machining challenges in stainless steel--A review, Int. J. Adv. Res. Ideas Innov. Technol. 3 (2017) 1395–1402.

[24]   J. García, V.C. Ciprés, A. Blomqvist, B. Kaplan, Cemented carbide microstructures: a review, Int. J. Refract. Met. Hard Mater. 80 (2019) 40–68. https://doi.org/https://doi.org/10.1016/j.ijrmhm.2018.12.004.

[25]   H.M. Ortner, P. Ettmayer, H. Kolaska, The history of the technological progress of hardmetals, Int. J. Refract. Met. Hard Mater. 44 (2014) 148–159. https://doi.org/https://doi.org/10.1016/j.ijrmhm.2013.07.014.

[26]   M.A. Xavior, M. Adithan, Determining the influence of cutting fluids on tool wear and surface roughness during turning of AISI 304 austenitic stainless steel, J. Mater. Process. Technol. 209 (2009) 900–909. https://doi.org/https://doi.org/10.1016/j.jmatprotec.2008.02.068.

[27]   R.A. MAHDAVINEJAD, S. SAEEDY, Investigation of the influential parameters of machining of AISI 304 stainless steel, Sadhana. 36 (2011) 963–970. https://doi.org/10.1007/s12046-011-0055-z.

[28]   Y.S. Ahmed, G. Fox-Rabinovich, J.M. Paiva, T. Wagg, S.C. Veldhuis, Effect of Built-Up Edge Formation during Stable State of Wear in AISI 304 Stainless

Steel on Machining Performance and Surface Integrity of the Machined Part, Mater. (Basel, Switzerland). 10 (2017) 1230. https://doi.org/10.3390/ma10111230.

[29] K.A. Abou-El-Hossein, Z. Yahya, High-speed end-milling of AISI 304 stainless steels using new geometrically developed carbide inserts, J. Mater. Process. Technol. 162–163 (2005) 596–602. https://doi.org/https://doi.org/10.1016/j.jmatprotec.2005.02.129.

[30] V.T. Gatade, V.T. Patil, P. Kuppan, A.S.S. Balan, R. Oyyaravelu, Experimental investigation of machining parameter under {MQL} milling of {SS}304, {IOP} Conf. Ser. Mater. Sci. Eng. 149 (2016) 12023. https://doi.org/10.1088/1757-899x/149/1/012023.

[31] S.A. Bagaber, A.R. Yusoff, Multi-objective optimization of cutting parameters to minimize power consumption in dry turning of stainless steel 316, J. Clean. Prod. 157 (2017) 30–46. https://doi.org/https://doi.org/10.1016/j.jclepro.2017.03.231.

[32] P.S. Sreejith, B.K.A. Ngoi, Dry machining: Machining of the future, J. Mater. Process. Technol. 101 (2000) 287–291. https://doi.org/https://doi.org/10.1016/S0924-0136(00)00445-3.

[33] A.K. Sharma, A.K. Tiwari, A.R. Dixit, Effects of Minimum Quantity Lubrication (MQL) in machining processes using conventional and nanofluid based cutting fluids: A comprehensive review, J. Clean. Prod. 127 (2016) 1–18. https://doi.org/https://doi.org/10.1016/j.jclepro.2016.03.146.

[34] S. Zhang, J.F. Li, Y.W. Wang, Tool life and cutting forces in end milling Inconel 718 under dry and minimum quantity cooling lubrication cutting

conditions, J. Clean. Prod. 32 (2012) 81–87.

https://doi.org/https://doi.org/10.1016/j.jclepro.2012.03.014.

[35] J.C. Outeiro, D. Umbrello, R. M'Saoubi, Experimental and numerical

modelling of the residual stresses induced in orthogonal cutting of AISI 316L

steel, Int. J. Mach. Tools Manuf. 46 (2006) 1786–1794.

https://doi.org/https://doi.org/10.1016/j.ijmachtools.2005.11.013.

[36] T. Leppert, R.L. Peng, Residual stresses in surface layer after dry and MQL

turning of AISI 316L steel, Prod. Eng. 6 (2012) 367–374.

https://doi.org/10.1007/s11740-012-0389-3.

[37] D.P. Selvaraj, P. Chandramohan, OPTIMIZATION OF SURFACE

ROUGHNESS OF AISI 304 AUSTENITIC STAINLESS STEEL IN DRY

TURNING OPERATION USING TAGUCHI DESIGN METHOD, in: 2010.

[38] V.P.A. and J.P. Davim, Machining-Fundamentals and Recen Advances,

Springer, 2008. https://doi.org/10.1007/978-1-84800-213-5.

[39] M. Shaw, Metal cutting principles, 2°, Oxford Unversity Press, New York,

2005.

[40] O.M. Oduola, O.O. Awopetu, C.A. Ikutegbe, K.J. Akinluwade, An Outlook on

Tool Wear Mechanisms of Selected Cutting Tool Materials, 14 (2016) 1–9.

https://doi.org/10.9734/BJAST/2016/22211.

[41] A.M. K. Holmberg, Chapter 5 Coating Characterization and Evaluation, in: K.

Holmberg, A. Matthews (Eds.), Coat. Tribol. Princ. Tech. Appl. Surf. Eng.,

Elsevier, 1994: pp. 257–308. https://doi.org/https://doi.org/10.1016/S0167-

8922(08)70755-7.

[42] E. Sayit, K. Aslantas, A. Çiçek, Tool Wear Mechanism in Interrupted Cutting

Conditions, Mater. Manuf. Process. 24 (2009) 476–483.

https://doi.org/10.1080/10426910802714423.

[43] M.Y. Noordin, V.C. Venkatesh, C.L. Chan, A. Abdullah, Performance

evaluation of cemented carbide tools in turning AISI 1010 steel, J. Mater.

Process. Technol. 116 (2001) 16–21.

https://doi.org/https://doi.org/10.1016/S0924-0136(01)00838-X.

[44] G.S. Fox-Rabinovich, A.I. Kovalev, M.H. Aguirre, B.D. Beake, K. Yamamoto,

S.C. Veldhuis, J.L. Endrino, D.L. Wainstein, A.Y. Rashkovskiy, Design and

performance of AlTiN and TiAlCrN PVD coatings for machining of hard to cut

materials, Surf. Coatings Technol. 204 (2009) 489–496.

https://doi.org/10.1016/j.surfcoat.2009.08.021.

[45] J.L. Endrino, G.S. Fox-Rabinovich, A. Reiter, S. V Veldhuis, R.E. Galindo,

J.M. Albella, J.F. Marco, Oxidation tuning in AlCrN coatings, Surf. Coatings

Technol. 201 (2007) 4505–4511.

https://doi.org/https://doi.org/10.1016/j.surfcoat.2006.09.089.

[46] G.M. Krolczyk, P. Nieslony, S. Legutko, Determination of tool life and

research wear during duplex stainless steel turning, Arch. Civ. Mech. Eng. 15

(2015) 347–354. https://doi.org/https://doi.org/10.1016/j.acme.2014.05.001.

[47] S. Ruppi, Deposition, microstructure and properties of texture-controlled CVD

α-Al2O3 coatings, Int. J. Refract. Met. Hard Mater. 23 (2005) 306–316.

https://doi.org/10.1016/j.ijrmhm.2005.05.004.

[48] L. Ning, Nano-multilayered Self-adaptive Hard PVD Coatings for Dry High

Performance Machining, 2007.

[49] G. Fox-Rabinovich, G.E. Totten, Self-organization During Friction - Advanced

Surface-Engineered Materials and Systems Design, 1st ed., CRC Press, Boca Raton, 2006.

[50] G. Fox-rabinovich, J.M. Paiva, I. Gershman, M. Aramesh, D. Cavelli, K. Yamamoto, G. Dosbaeva, S. Veldhuis, Control of Self-Organized Criticality through Adaptive Behavior of Nano-Structured Thin Film Coatings, Entropy. 18 (2016) 290. https://doi.org/10.3390/e18080290.

[51] C. Donnet, A. Erdemir, Historical developments and new trends in tribological and solid lubricant coatings, Surf. Coatings Technol. 180–181 (2004) 76–84. https://doi.org/https://doi.org/10.1016/j.surfcoat.2003.10.022.

[52] I.A. Podchernyaeva, D. V Yurechko, V.M. Panashenko, Some trends in the development of wear-resistant functional coatings, Powder Metall. Met. Ceram. 52 (2013) 176–188. https://doi.org/10.1007/s11106-013-9511-0.

[53] H.A. Jehn, Multicomponent and multiphase hard coatings for tribological applications, Surf. Coatings Technol. 131 (2000) 433–440. https://doi.org/https://doi.org/10.1016/S0257-8972(00)00783-0.

[54] T. Conditions, G. Fox-rabinovich, A. Kovalev, I. Gershman, D. Wainstein, M.H. Aguirre, D. Covelli, J. Paiva, K. Yamamoto, S. Veldhuis, Complex Behavior of Nano-Scale Tribo-Ceramic Films in Adaptive PVD Coatings under Extreme, (2018) 1–15. https://doi.org/10.3390/e20120989.

[55] I.S. Gershman, A.E. Mironov, E.I. Gershman, Self-Organization during Friction of Slide Bearing Antifriction Materials Self-Organization during Friction of Slide Bearing Antifriction Materials, (2015). https://doi.org/10.3390/e17127855.

[56] G.S. Fox-rabinovich, K. Yamomoto, S.C. Veldhuis, A.I. Kovalev, G.K.

Dosbaeva, Tribological adaptability of TiAlCrN PVD coatings under high performance dry machining conditions, 200 (2005) 1804–1813. https://doi.org/10.1016/j.surfcoat.2005.08.057.

[57] J. Yuan, K. Yamamoto, D. Covelli, M. Tauhiduzzaman, T. Arif, I.S. Gershman, S.C. Veldhuis, G.S. Fox-rabinovich, Tribo- films control in adaptive TiAlCrSiYN / TiAlCrN multilayer PVD coating by accelerating the initial machining conditions, Surf. Coat. Technol. 294 (2016) 54–61. https://doi.org/10.1016/j.surfcoat.2016.02.041.

[58] A.E. Diniz, Á.R. Machado, J.G. Corrêa, Tool wear mechanisms in the machining of steels and stainless steels, Int. J. Adv. Manuf. Technol. 87 (2016) 3157–3168. https://doi.org/10.1007/s00170-016-8704-3.

[59] A.I. Fernández-Abia, J. Barreiro, J. Fernández-Larrinoa, L.N.L. de Lacalle, A. Fernández-Valdivielso, O.M. Pereira, Behaviour of PVD Coatings in the Turning of Austenitic Stainless Steels, Procedia Eng. 63 (2013) 133–141. https://doi.org/https://doi.org/10.1016/j.proeng.2013.08.241.

[60] J. Lawal, P. Kiryukhantsev-Korneev, A. Matthews, A. Leyland, Mechanical properties and abrasive wear behaviour of Al-based PVD amorphous/nanostructured coatings, Surf. Coatings Technol. 310 (2017) 59–69. https://doi.org/https://doi.org/10.1016/j.surfcoat.2016.12.031.

Chapter 2: An integrative approach to coating/carbide substrate design of CVD and PVD coated cutting tools during the machining of austenitic stainless steel

Q. He[1], J.M. Paiva[1,2,], J. Kohlscheen[3], B.D. Beake[4] and S.C. Veldhuis[1]*

1- McMaster Manufacturing Research Institute, McMaster University, Hamilton – L8S4L8, Canada.

2- Engineering Graduate Program – PPGEM, Pontificia Universidade Católica do Paraná, Curitiba – 80215901, Brazil.

3- Kennametal Shared Services Gmbh, Altweiherstr 27-31, 91320 Ebermannstadt, Germany.

4- Micro Materials Ltd., Willow House, Yale Business Village, Ellice Way, Wrexham - LL13 7YL, UK.

∗ Corresponding author: paivajj@mcmaster.ca (J.M. Paiva).

Author's Contribution

Qianxi He	Designed and conducted the experiments
	Analyzed the results.
	Wrote the manuscript.
Jose M. Paiva	Assisted with designing the research methodology.
	Assisted with writing and editing the manuscript.
Joern Kohlscheen	Deposited the coating.
Ben D. Beake	Assisted with data collection for coating layer mechanical properties
Stephen C. Veldhuis	Supervised the project.

Abstract

Machining of hard to cut materials such as austenitic stainless steel presents a challenge due the thermo-mechanical properties of this material, which contribute to intensive buildup edge formation and negatively affect tool life. CVD TiCN + Al_2O_3 and PVD AlTiN coatings deposited on cemented carbide substrates are generally recommended for machining austenitic stainless steel. These coatings were deposited by two different methods: (i) PVD AlTiN was deposited on the same substrate material at two different thicknesses (2.5 and 5 μm); (ii) CVD TiCN + Al_2O_3 was deposited with the same thickness (5 μm) on two different substrates. A new approach to applying various PVD and CVD (coating + substrate) integrated systems is introduced in this study for austenitic stainless steel machining. The relationship between the coating and substrate characteristics of these material systems and tool performance was assessed. The characteristics of the coating/carbide substrate design were evaluated in terms of chemical, phase composition, architecture, mechanical properties in relation to the tribological and wear performance. The obtained results demonstrate an improvement in tool wear performance and tool life brought about by the surface engineered layer/carbide material with an optimal combination of coating/substrate properties. Based on these findings, a guideline is proposed for further study of the cutting tool life and wear performance of CVD and PVD coated cemented carbide inserts.

2.1. Introduction

The low thermal conductivity and high tendency for work hardening of Austenitic Stainless Steel 304 (SS304) render it a hard-to-cut material. The machining process of SS304 is characterized by an unstable attrition wear mechanism, which eventually leads to intense build-up-edge (BUE) formation and consequent chipping on the cutting edge [1,2].

To improve chemical interaction between the tool and the workpiece material during stainless steel machining, the carbide cutting tool surfaces must be abrasion resistant, hard and chemically inert [3]. In order to enhance the surface properties of the cutting tool, surface engineering plays a key role in preventing the wear of the tool [4,5]. A cutting tool's surface properties such as hardness, thermal stability, friction coefficient, and chemical inertness are improved by the application of a coating [6-8]. The two most regularly used coating deposition are: Chemical Vapor Deposition (CVD) and Physical Vapor Deposition (PVD). Both processes make use of a variety of cutting tool coatings for machining 304 stainless steel [8-10].

CVD TiCN + Al_2O_3, as well as PVD AlTiN coatings on cemented carbide substrates are considered optimal for the stainless steel machining [11]. Depending on the application, different levels of Al composition in nano-multilayered coatings can improve tool life through the formation of aluminum oxide tribofilms [12,13]. In addition, the Al_2O_3 outer layer on the coating is considered to be an excellent coating material for metal cutting applications due to its high chemical stability and favorable thermal properties [14]. Al_2O_3 outer layer in CVD coatings are usually deposited on the top of coated TiCN cemented carbide tools to provide superior properties, such as mechanical and physical characteristics. Therefore, these coatings are commonly used

for the machining of stainless steel [14,15]. However, the entire system (substrate and coating layer) feature naturally different mechanical and physical properties. The content and composition of the Co within the carbides, the C/N ratio and the α-Al_2O_3 top-layer affect their wear performance during machining. The majority of previous investigations only analyzed the effects of a coating on tool wear and tool life. There is a notable lack of published studies concerning the influence of different integrated systems (PVD or CVD coating + substrate) on tool performance.

In this paper, not only coating characteristics were investigated, but also the effect of cutting substrates. An emphasis was made on the frictional characteristics of the cutting process based on the chip characteristics (microstructure, chip compression ratio - CCR, details of the metal flow, and shear bands). The goal of this study is to determine the relationship between the wear resistance of different coatings (CVD and PVD) and the characteristics of the entire coating layer/substrate material system. On this basis, guidelines to select the most appropriate tool system might be formulated for the machining of grade 304 stainless steel.

2.2. Experimental procedure

For the investigation recorded, commercial Kennametal PVD and CVD coated carbide tools were deposited on three different cemented carbide grades. The PVD coated tool is an advanced PVD AlTiN coating deposited on a very deformation-resistant unalloyed carbide substrate, whereas CVD 1 and CVD 2 are both multilayer TiN-MT-TiCN-Al_2O_3 CVD coatings deposited on carbide substrates that have different chemical compositions and mechanical properties. Two different thicknesses of PVD coatings were tested: 2.5 and 5 microns. These cutting tools will be henceforth referred to in this paper as PVD 1 and PVD 2, respectively. According to the manufacturer

guidelines, those three different coating/substrate systems are suitable for general-purpose machining of austenitic stainless steels at various speeds and feeds. The cutting insert geometry selected for the cutting tests was a CNMG120408-MP geometry (according to ISO 1832). The workpiece material considered in this work is an austenitic AISI 304 stainless steel, whose microstructure, chemical composition, and mechanical properties are summarized in Table 2.1.

Table 2.1. Chemical composition, and mechanical properties of Austenitic Stainless Steel AISI 304.

Element	Weight (%)	Yield strength (MPa)	Tensile strength (MPa)	Elongation (% in 50 mm)	Hardness	
					Rockwell B (HR B) max	Brinell (HB) max
C	< 0.08	205	515	40	92	201
Mn	< 2					
Si	< 0.75					
P	< 0.045					
S	< 0.03					
Cr	18 - 20					
Ni	8 - 10.5					
N	< 0.1					
Fe	Balance					
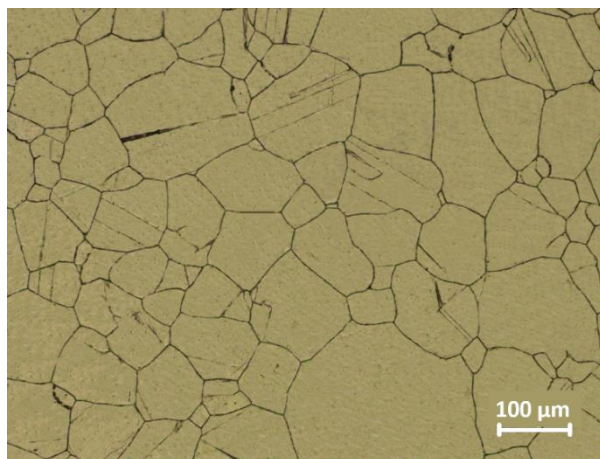
The cutting tests were performed by single point turning using a SS304 bar with a 180 mm diameter and 250 mm length. A CNC Okuma Crown L1060 Lathe was employed for the cutting tests. All turning tests were conducted under a semi-finishing process with a cutting speed of 320 m/min, a feed rate of 0.2 mm/rev and a depth of cut

of 1 mm under wet conditions using a semi-synthetic coolant with a 7 % concentration. These cutting conditions were based upon those widely prevalent in industry for the machining of stainless steels. The tool life criterion adopted in this work was a flank wear of 0.3 mm, according to ISO 3685. A Keyence optical microscope was used to inspect the tool wear on the cutting tools.

Cross-section studies of the cutting tools were conducted by a JEOL-6610 scanning electron microscope (SEM) coupled with Energy Dispersive Spectroscopy (EDS) to verify the chemical composition of the coatings and the substrates. The uncertainties for these measurements were around 5 %. Moreover, SEM imaging was used to investigate the tool wear performance. The wear mechanism and morphology of the worn cutting inserts were evaluated. A D8 Discover X-ray diffractometer was used to assess evaluate the phase composition of the coatings deposited on the cemented carbide substrates. The analyses were conducted in the standard θ–2θ configuration to identify the phase and coating composition during the deposition. Frame exposure was 600s at a collection range of 20-85°. 2D frames were acquired by Diffract Measurement Centre Version 6.5 Software. A source of Co K alpha radiation was configured in the diffractometer to avoid the superposition of signals from the substrate material and the coating. This was done so that only the results from the surface layer of AlTiN PVD and Al_2O_3 CVD coatings.

The micro-mechanical characteristics (hardness and reduced elastic modulus) of the coatings and corresponding carbide substrates were measured using a Fischerscope HM2000 Hardness Tester (Fischer, Germany) with a load of 20 mN. A Vickers indenter geometry was employed for this analysis as well as for the fracture toughness studies. Fracture toughness of the studied carbide substrates was measured by Revetest Tester

(Anton Paar, Austria), with 50N-150N load. The load applied during toughness measurement was 100N. Cracks formed at the corners of the indentations, can be used to derive a nominal surface toughness value. Fracture toughness was evaluated using the following equation: $K_{IC} = A\sqrt{H}\sqrt{\frac{P}{\Sigma L}}$ (where H is the hardness (N/mm^2), P is the applied load (N), ΣL is the sum of crack lengths (mm), and A is a constant with a value of 0.0028) [16].

To evaluate the wear performance and tribological conditions during the cutting tests, progressive 3D studies of wear volume and surface texture of the chips were carried out with an Infinite Focus G5 focus variation microscope (Alicona, Austria). An Electron backscattered diffraction (EBSD) method was used to evaluate crystal orientation, phase identification, and grain size in the chip cross-sections. A JEOL JSM-7000F SEM combined with an AZtec EBSD (Oxford, U.K.) microscope was used for this analysis.

The chip compression ratio (CCR), the shear angle, the cutting force, and the friction coefficient at the tool-chip interface were determined by standard methods proposed by Shaw (2005) [17]. The proposed methodology is based on the plastic deformation inherent to the process of metal cutting which can be represented by the CCR. Shaw (2005) states that CCR can be used to represent the ratio of the complete plastic deformation performed by the external force applied by metal cutting. That is to say, the influence of cutting conditions, tool geometry and tool surface were also described by Shaw (2005) in terms of the friction conditions and the energy consumed in the cutting zone (tool-chip and tool-workpiece interfaces).

2.3. Results and Discussion

2.3.1. Coating/carbide substrates system structure

Fig. 2.1 shows the SEM images of the different cemented carbide substrates. The main phases of the cemented carbides are the WC phase (brighter phase) and the Co binder phase (darker phase). The cemented carbide provides an optimal combination of soft and ductile Co and hard, wear-resistant WC carbides, which improves the high-temperature resistance of the cutting tools [18]. It is possible to see an additional phase of the CVD 1 carbide grade, showing coarse grains. Through SEM and EDS analysis, it was possible to identify and quantify the phases present in different substrates. The results show that PVD and CVD 2 are cemented carbide grades composed of tungsten carbide and cobalt (WC-Co). The cemented carbide grade used in the PVD coating is WC-Co (92.5-7.5 wt. % respectively) with a microstructure characterized by fine grain sizes combined with a homogenous distribution of binder, whereas CVD 2 is WC-Co (90-10 wt. % respectively) with medium grain size. Usually, fine/ultrafine grains of WC benefit the mechanical properties of the cutting tool and consequently enhance the resistance of the carbide alloy to abrasion wear and chipping on the cutting edges [19].
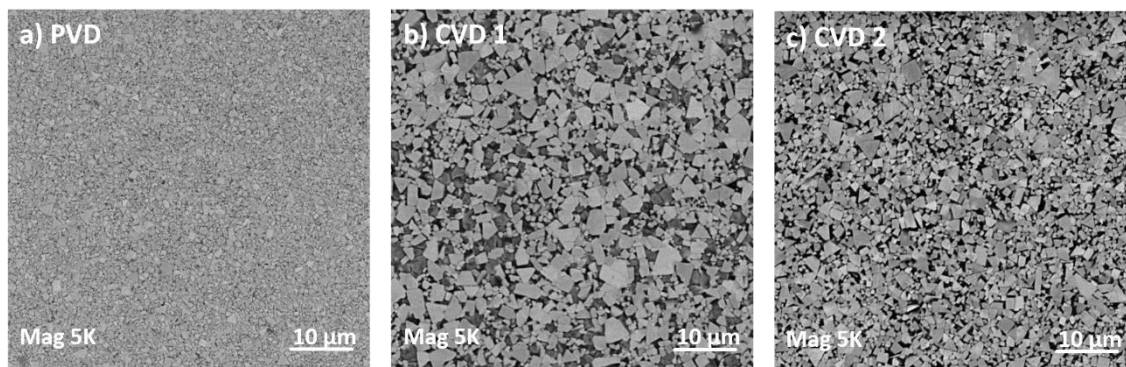
Fig. 2.1 Backscattered electron SEM images showing the microstructure of different cemented carbide grades: a) cemented carbide grade used for AlTiN PVD 1 and PVD 2, b) cemented carbide grade used for TiN-MT-TiCN-Al_2O_3 CVD 1, and c) cemented carbide grade used for TiN-MT-TiCN-Al_2O_3 CVD 2.

The CVD 1 carbide grade shows the presence of a Cobalt binder phase of around 10 wt. % and an additional TiC phase (2.6 wt. %). In particular, the combination Co binder with TiC decreases hardness and substantially improves fracture toughness (see Table 2.2). Therefore, the wear behavior of the cutting tools used in machining operations at high cutting zone temperatures is improved once a certain amount of TiC is added to the WC-Co cemented carbides [20,21]. Another advantage of the presence of TiC in cemented carbide is that it delivers resistance against crater producing diffusion wear, and inhibits rapid flank wear during austenitic stainless steel cutting [22].

SEM images of the coatings cross-sections are shown in Fig. 2.2. Fig. 2.2a and b shows that the AlTiN PVD 1 is a 2.5 µm monolayer and PVD 2 is a 5 µm monolayer coating. Both have a uniform and dense microstructure. Fig. 2.2c and d shows the microstructure of the fracture cross-section of both CVD coatings. An architecture composed of three different layers is revealed: Al_2O_3 is the top layer, TiCN is the sublayer with a columnar microstructure and TiN is the base layer of this sandwich

coating system. The total coating thickness is 5 μm, with Al_2O_3 ~1.5 μm, TiCN ~2.5 μm and TiN ~0.5 μm. A thin layer of TiN is commonly used as an interlayer in CVD coatings to improve the interatomic bonds at the interface between the substrate and the coating, which improves the adhesion of the coating to the substrate [23]. Furthermore, the SEM image displays surface defects of different sizes and shapes present on the top surfaces of all coatings studied in this work as it is shown in Fig. 2.2. Overall, the coatings demonstrate adequate adhesion within the interlayer between the coating and the substrates.
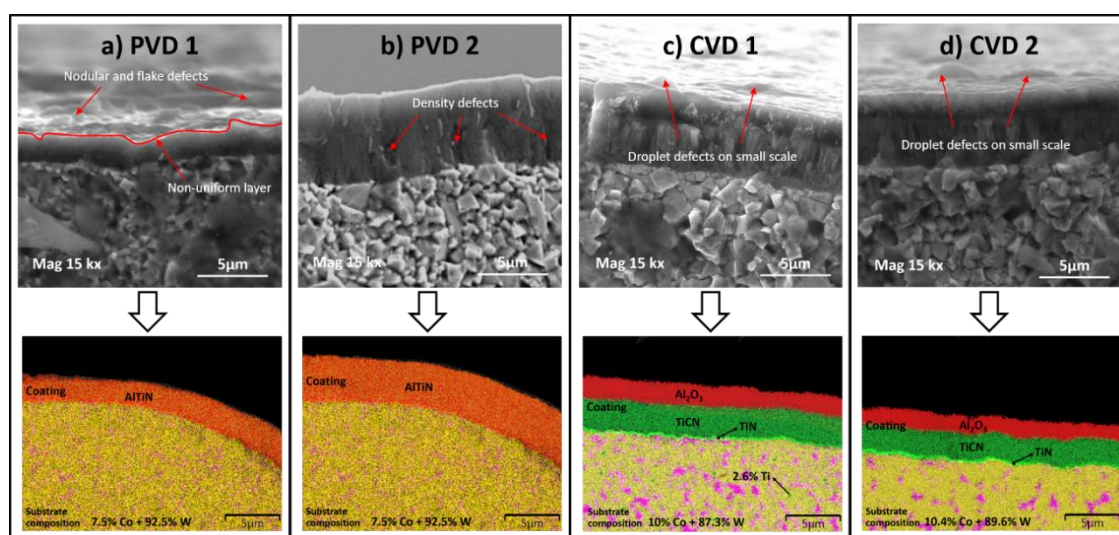
Fig. 2.2 The SEM images of the inserts cross-section and the corresponding EDS elemental maps results of the chemical composition for each coating/carbide substrate system: a) PVD 1; b) PVD 2; c) CVD 1; and d) CVD 2.

The XRD patterns of the AlTiN PVD and TiN-MT-TiCN-Al_2O_3 CVD coatings deposited over the three different cemented carbide substrates are shown in Fig. 2.3. The phase composition analysis demonstrates that the PVD coating has Face Center Cubic (FCC) structural characteristic peaks with a (111), (200), and (220) texture. The

XRD spectrum in Fig. 2.3a displays a strong (200) preferred orientation of the AlTiN coating, which represents the minimum surface and strain energies during the deposition process. In this way, a coating is generated with the lowest surface energy among the crystal planes after deposition [24].
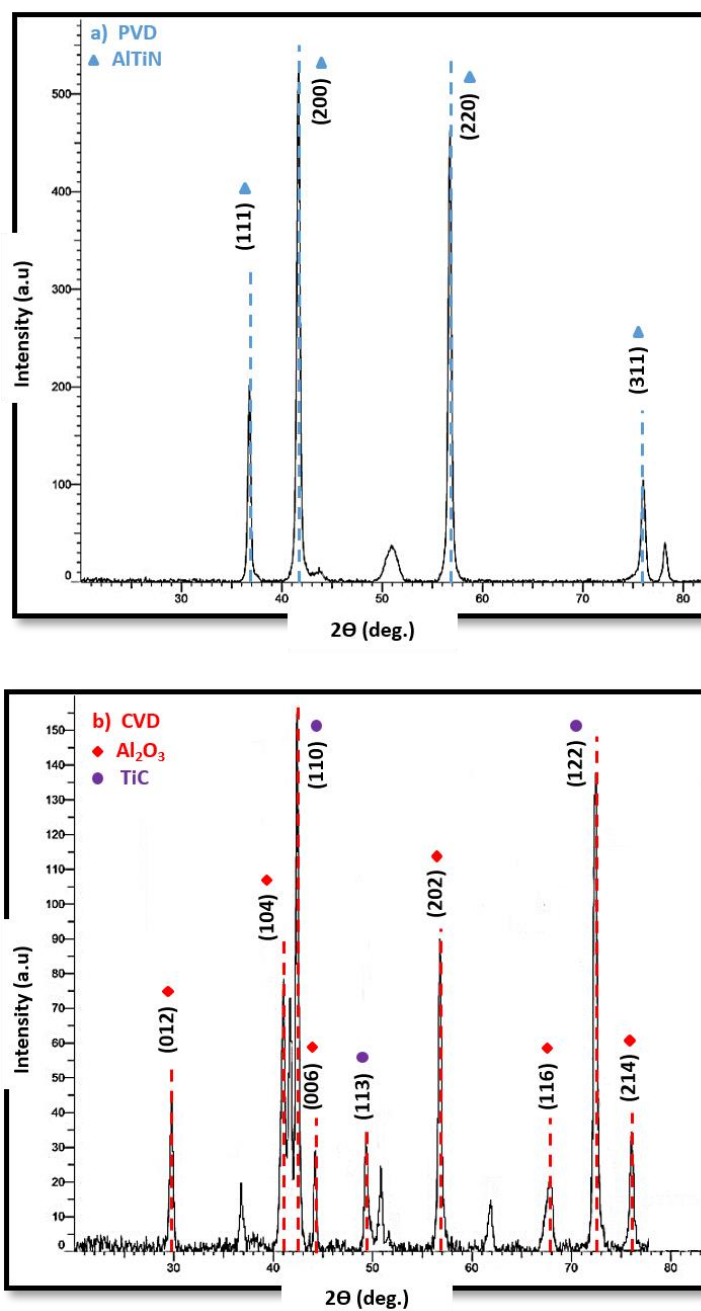
Fig. 2.3. XRD patterns of coated cutting tools: a) AlTiN PVD, b) Outer layer Al_2O_3 CVD.

However, the XRD results obtained from the α-Al$_2$O$_3$ CVD coating deposited on top of an intermediate TiCN layer (Fig. 2.3b) demonstrate that the coating consists of only α-Al$_2$O$_3$ crystals with random orientations [25]. This α-Al$_2$O$_3$ phase distribution is confirmed by the diffractions peaks at 2θ values of, 29.58˚ for (012), 41.06˚ for (104), 42.57˚ for (110), 44.03˚ for (006), 49.12˚ for (113), and 76.29˚ for (214). This result shows that α-Al$_2$O$_3$ is a constant alumina phase with a high melting point (2050 °C) and a corundum structure [26]. Therefore, the elevated melting point of this coating makes suitable for the machining of stainless steels.

2.3.2. Tool life data

Fig. 2.4 presents the flank wear values vs. machined cutting length for uncoated and coated inserts. The cutting tool life results shown in Fig. 2.4 are derived from an average of three tests for each kind of cutting tool. The obtained results are plotted with the specific error bars for each condition tested. PVD 1 and PVD 2 coated cemented carbide tools feature almost identical wear resistance (Fig. 2.4). This means that the integrative performance of the coated carbide material system is of major importance (as will be discussed in section 3.3). The data indicates that the CVD 1 coated cemented carbide cutting tool has the lowest wear rate compared to the other cutting tools investigated in this work. Chipping wear was detected in all the cutting tools with different scales, as shown in Fig. 2.4b.
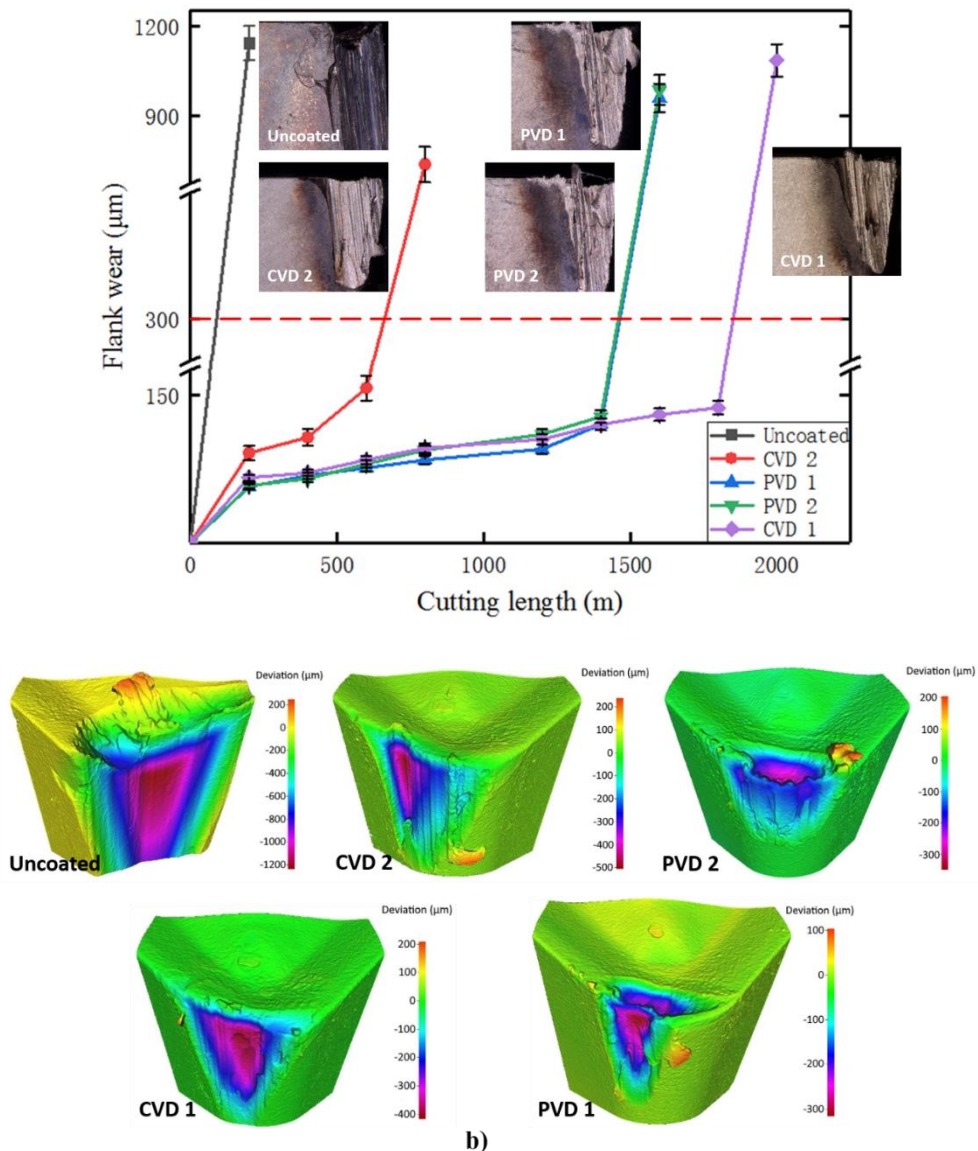
Fig. 2.4. Cutting tests results: a) Flank wear versus Cutting length and b) Wear Alicona images of the inserts at the end of tool life during machining SS304.

Another important observation to be made is that both the PVD 1 and PVD 2 cutting tools have significant crater wear, which may be a response of the integrated system (coating + substrate). Since PVD 1 and PVD 2 cutting tools had similar wear performance during the cutting tests, the thickness of the monolayer coating did not noticeably affect the wear performance of both PVD coatings systems. Therefore,

complete wear analysis will only be performed on PVD 1.

2.3.3. Mechanical properties and characterizations

To link the tool life results with the integrative design of the tribo-system, tool micro-mechanical characteristics (including hardness, elastic modulus, plasticity index, and fracture toughness) for the three coating/substrate systems are summarized in Table 2.2. The mechanical properties of the cemented carbide grade tool used in the PVD coating feature the lowest Co content (Fig. 2.2a), which results in the highest hardness (H) ~ 23 GPa and elastic modulus (E) ~550 GPa.

Table 2.2. Micro-mechanical characteristics for the coatings/carbide substrates.

Grade	PVD	CVD 1	CVD 2
Carbide substrate			
Hardness (GPa)	22.8±3.5	17.5±2.9	16.5±3.1
Grain size (μm)	1.225	3.725	2.15
Density (g/cm^3)	14.9	14.7	14.2
Fracture toughness (MPa m$^{1/2}$)	14.3±1.2	16.8±1.3	14.5±1.2
Elastic modulus (GPa)	550±28	538.7±23	443±23
H/E	0.0414	0.0325	0.0372
Plasticity Index	0.588	0.685	0.657

Coating layer	PVD 1	CVD 1 and CVD 2		
	AlTiN	Al$_2$O$_3$ top layer	TiCN sublayer	TiN base layer
Hardness (GPa)	30.0±4.1	33±3.2	30±2.8	30±3.5
Elastic modulus (GPa)	360±27	390±25	420±28	380±24
H/E	0.0833	0.0846	0.0714	0.0789
H^3/E^2 (GPa)	0.208	0.236	0.153	0.187

Outer coating layer	PVD 1	CVD 1	CVD 2
	AlTiN	Al$_2$O$_3$	Al$_2$O$_3$
Fracture toughness (MPa m$^{1/2}$)	1.35±0.07	2.0±0.1	1.71±0.09

Also, it is worth mentioning that the density of the cemented carbide grade in the PVD tool shows a discrete tendency to reduce the solid-solution content [27]. This means that a smaller grain size present in the tool cemented carbide substrate used for PVD will provide higher values of density and elastic modulus than the cemented carbide substrates used for both CVD coated materials, which reduces the fracture toughness resistance (Table 2.2). Alternatively, the cemented carbide substrate used in both CVDs has greater Co content (Fig. 2.2c and d), resulting in lower hardness and high fracture toughness. These differences in the chemical compositions of the cemented carbide substrates may explain why the coated tools had different values of toughness resistance (Table 2.2).

The H/E ratios and Plasticity Index (PI) values were calculated for all the three carbide substrate materials (Table 2.2). The H/E ratio of the PVD coated material is greater than that of the CVD coated material. The lowest value of H/E is obtained in the CVD 1 material. According to literature, a carbide substrate material with a low H/E ratio (elastic strain to failure) corresponds to a higher tool life [28]. CVD 1 has the highest PI. It is known that the higher PI values are associated with the high capacity of a substrate material to dissipate loading [29]. Thus, the PI value obtained for PVD is lower than that of CVD 1 and CVD 2. The PI index parameter indicates that the PVD substrate might fail by plastic deformation at high temperatures during the cutting process [29]. This indicates that tool wear failure occurs due to oxidation on the rake face. This hypothesis is confirmed in Fig. 2.4b, where both PVD coated tools exhibit plastic deformation on the rake face.

The high *H/E* ratio of the CVD coating is primarily caused by its elevated hardness. In this case, considering only the outer layer (Al_2O_3) of the CVD coating, wear

resistance during cutting with predominant adhesive wear can be lower than that of coatings with a low *H/E* ratio.

Under heavy loaded tooling applications where intensive surface deformation of surface layers during friction is taking place, an optimum *H/E* (elastic strain to failure) is necessary to achieve better tool life [28]. This should be considered in combination with PI values (Table 2.2) [30]. Higher values of PI are associated with higher energy dissipation under loading. The more energy is dissipated by plastic deformation, the less is available for carbide fracture, which reduces the severity of the wear process. The carbides are strictly described as "quasi-plastic", since deformation involves interrelated micro-mechanisms: (i) constrained plastic deformation of the Co binder (ii) slip within WC (iii) formation of micro-cracks at high strains [31,32]. Góez et al have noted that damage tolerance necessarily involves a competition between deformation and fracture [33]. In their analysis of the microstructural design of carbide systems for enhanced damage tolerance quasi-plasticity, Góez et al concluded quasi-plasticity to be the optimal dominant damage mode against cracking [33]. The PI parameter is highly correlated with the *H/E* parameter, being almost linearly related to the inverse of *H/E* [28,32,33]. Both of these parameters could, therefore, be used in a complementary fashion to characterize the wear behavior of heavy-loaded tribo-systems under conditions of unstable attrition wear resulting in strong buildup edge formation. The CVD coated carbide material with lower hardness and *H/E* ratio, as well as higher PI and toughness, features better wear performance as well as longer tool life. Based on the data presented in Table 2.2, the entire set of the coating + cemented carbide grade provided by CVD 1 delivered superior wear performance. Among the studied tools, the CVD 1 coating system featured the best performance results, indicating that a

combination of factors (CVD 1 has better plasticity and better load carrying capacity) which contribute to a greater tool life and improved tool wear resistance.

2.3.4. Tool wear analysis

Fig. 2.5 shows the SEM images of the cutting tools used in the cutting tests. Machining of austenitic stainless steels at high cutting speeds promote interactions between the tool, chip and workpiece which always cause tool wear and other damage to the tool, due to the intense thermal and mechanical loads that occur in the cutting zone. In this case, the main wear mechanism is generated by the combination of abrasion, diffusion and attrition wear. With different coating system combinations, the cutting inserts show different wear patterns as a result of their tool life performance. It is known from literature that an unstable attrition wear mechanism predominates during the machining of austenitic stainless steel, which eventually leads to intense BUE formation and consequent chipping of sharp cutting edges [34]. As shown in Fig. 2.5, the uncoated insert suffers more intensive wear than any other insert. A large amount of adhered workpiece material results in BUE formation. The other three inserts with different coatings show abrasion combined with attrition wear. Also, CVD 2 has a noticeable BUE, which is detrimental to machining processes that affect the chip flow. PVD features significant crater wear on the rake face, which may be produced by intense diffusion combined with abrasion and attrition between the tool rake face and the chip, resulting in sliding and adhesion. However, crater wear was minimized in the CVD 1 tool and was not the main cause of tool failure. The high chemical stability of the coatings was considered as the reason for the shallow crater wear. As such, this coating tends to perform better under heavy load operations, demonstrating superior resistance to wear and plastic deformation than the previous coated tools. The combined

effect of the mechanical properties of the entire coating/substrate system account for the improvement of tool life under extreme cutting conditions.
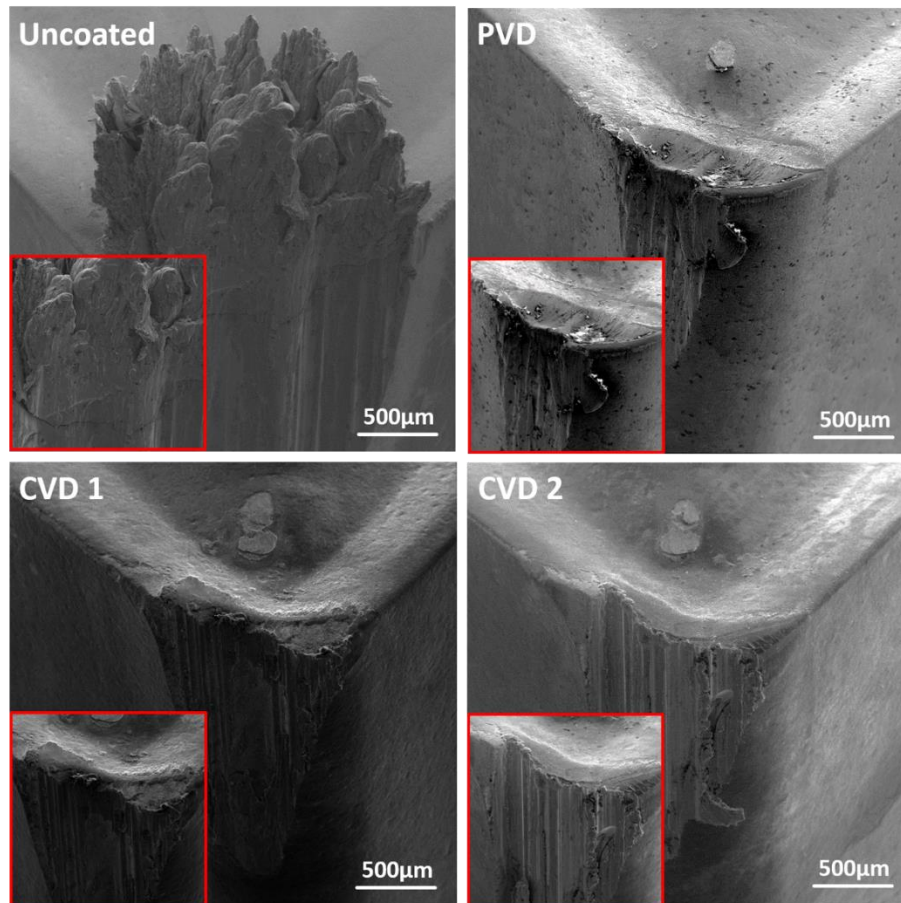
Fig. 2.5. Tool wear patterns evaluated by SEM on the cutting inserts after machining SS304 (end of tool life data).

Fig. 2.6 shows SEM images and elemental map data from the rake surface for the best performing coated tools (PVD 1 and CVD 1) at a cutting length of 1500 m (this cutting length representing the end of life for the PVD 1 tool). The elemental maps obtained from PVD tools confirm that a substantial amount of workpiece material adheres on the tool flank and rake face (see Cr and Fe maps). The images also indicate substrate exposure, i.e., coating detachment from the chip/tool interface, with the

substrate already being exposed and covered by a BUE. The elemental data obtained for PVD provide evidence of chipping wear on the cutting tool. In contrast, the elemental maps of CVD 1 show reduced BUE and only minor chipping is visible at this cutting length. The presence of Cr and Fe signals close to the tip of the cutting tool indicates the formation of chromium and iron oxides. These oxides are composites naturally observed in BUE structures. At this stage, oxidation is the primary wear mechanism taking place on the tool rake surface during cutting.
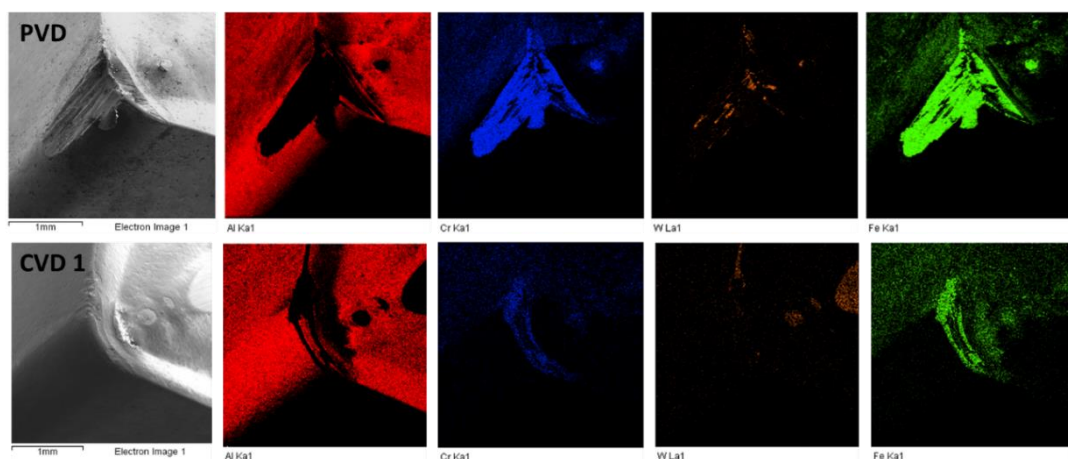
Fig. 2.6. The SEM image of the tool rake face and the corresponding EDX elemental maps: a) AlTiN PVD and b) CVD 1.

The minimum and maximum deviations in tool wear statistics of the unworn reference tool obtained by Alicona were calculated with a 95 % accuracy. These values represent the minimum and maximum deviations above the reference plane. The magnitude of BUE formed at the end of each cutting tool's life are shown in Fig. 2.7a. The values in Fig. 2.7b present the deviation related to tool wear damage (volume below the reference plane) occurring at the cutting edge. The CVD 1 cutting insert exhibited the lowest BUE formation compared to the other tested cutting tools. Moreover, the tool

wear volume data presented in Fig. 2.7 show chipping wear and intensity of BUE formation are significantly reduced in CVD 1 cutting tools using the investigated cutting inserts. For the uncoated, CVD 2 and PVD coated tools, intensive adhesion of the workpiece material to the rake surface was observed during the initial wear stage, which results in faster tool wear. The formation of an unstable buildup structure leads to further tearing and subsequent chipping at the cutting edge. Also, chipping of the cutting edge intensifies BUE formation. Fracture of the build-up-edge can also carry away a part of the cutting edge with it, which aggravates chipping on the cutting edge.
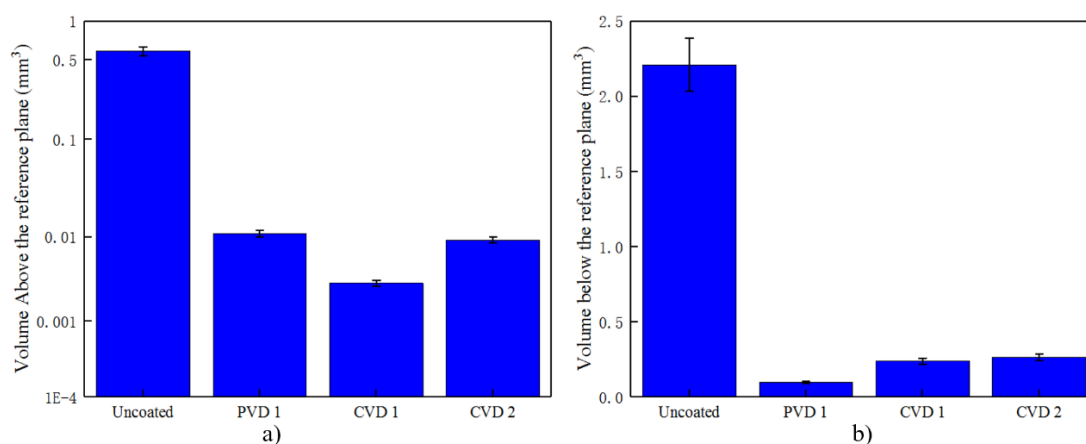
Fig. 2.7. Numerical wears statistics data obtained from the cutting tools proposed in this work: a) Volume above the reference plane and b) Volume below the reference plane.

Tool wear statistics obtained from Alicona confirm that the CVD 1 cutting tool system features lower tool edge failure compared to the other studied coatings. Therefore, this system was demonstrated to deliver improved and more efficient tool performance for this type of application.

2.3.5. Evaluation of tribological properties

To understand how the behavior of the entire coating/substrate material system

contributes to chip formation, in-situ tribological evaluations were based on chip characterization studies. SEM images of the chips' undersurface are shown in Fig. 2.8. Although all chips produced by the investigated cutting tools feature a curling geometry, the chips formed by the cutting tool with a CVD 1 coating have the greatest degree of curl. This indicates that the chip flow in the cutting zone is accelerated as a consequence of the minimal friction being present there [35]. This behavior is confirmed by images of chip undersurface morphology. Metal flow produced by the uncoated, PVD and CVD 2 coated tools causes intensive sticking at the chip/tool rake surface and subsequent tearing at the undersurface of the chips. This tearing indicates that the metal flow is strongly arrested at the cutting tool/chip interface, which generates intensive friction. In contrast, the chips produced by CVD 1 coated tools have a smoother undersurface, confirming that the tool rake surface has the lowest friction compared with the other tools. This behavior of the entire CVD 1 coating/substrate system significantly reduces the intensity of attrition wear. This coating/substrate system delivers high mechanical resistance (due to the presence of TiCN) associated with the low thermal conductivity of the outer Al_2O_3 layer, which protects the surface of the tool from heat transfer [36].
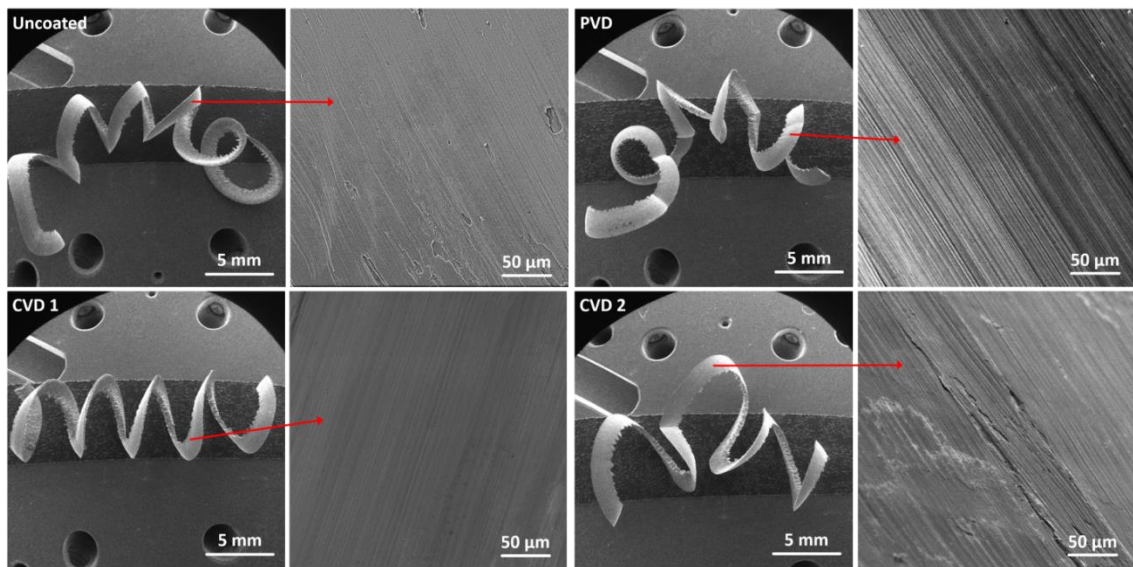
Fig. 2.8. Chip type and morphology of the chip undersurface for the coated insert during machining of SS304: a) Uncoated, b) AlTiN PVD, c) TiN-MT-TiCN-Al$_2$O$_3$ CVD 1, and d) TiN-MT-TiCN-Al$_2$O$_3$ CVD 2 coating.

To confirm the hypothesis that the CVD 1 integrative coating/substrate system provides superior chip flow at the tool/chip interface, surface topography of the chip undersurface acquired during machining was compared in all tools investigated in this work, using an Alicona 3D digital microscope. Surface textures of the chip undersurfaces obtained by the studied cutting tools following the machining of SS304, are shown in Fig. 2.9. The length and width of all examined chips are 3 mm and 2 mm, respectively. It can be clearly seen that compared to PVD (SA = 0.3419 μm), the chip yielded by the CVD 1 coated tool has a smoother surface, with SA = 0.3252 μm. These results confirm the superior characteristics of the CVD 1 coating/substrate system.
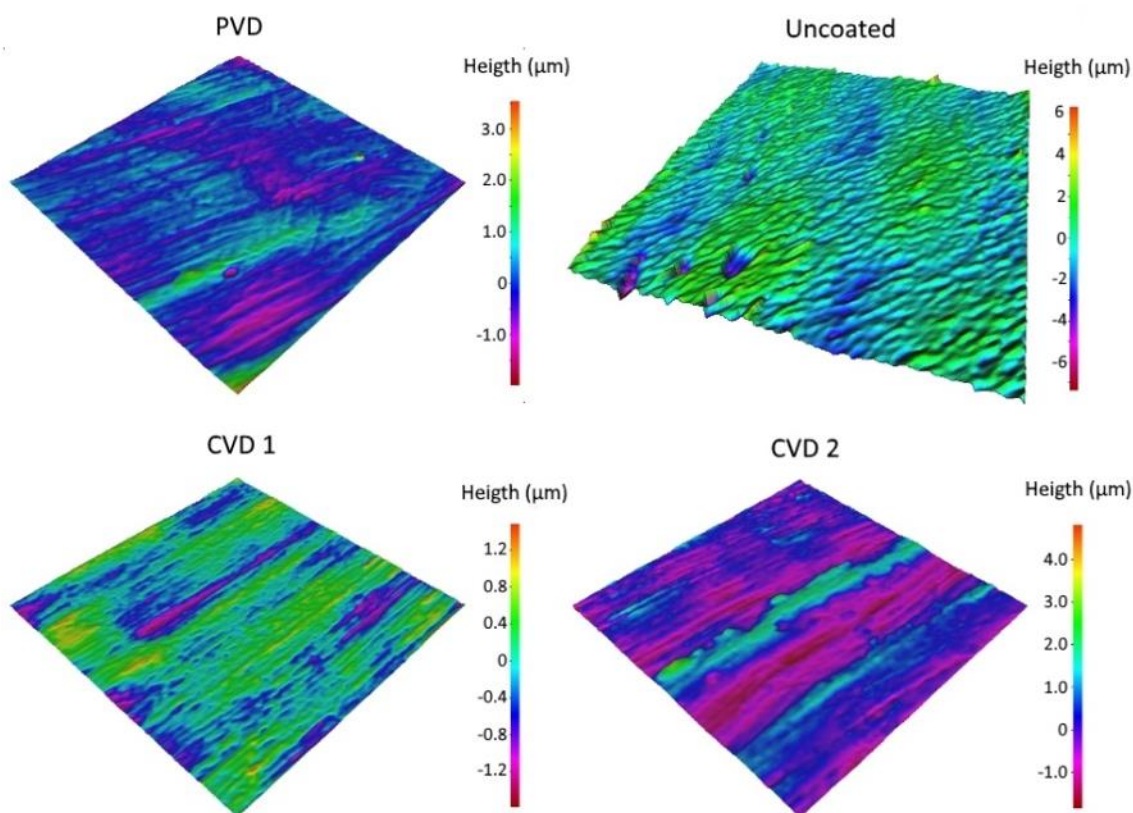
Fig. 2.9. Three-dimensional surface texturing of the chips' undersurface.

At this point, the tribological conditions generated by the combination of different coating/substrate systems play an essential role during the chip formation process in all the tools tested in this work. A study of tribological characteristics of shearing work material was conducted to assess the frictional conditions at the tool-chip interface [37]. Chips were collected at the beginning of cut (around 5 m of cutting length), and the data concerning chip thickness, chip compression ratio, shear angle, friction angle, shear strain, chip sliding velocity, chip flow angle and friction coefficient are summarized in Table 2.3.

Table 2.3. Results of the chip characteristic studies (chip thickness, chip compression ratio, shear angle, friction angle, shear strain, chip is sliding velocity, chip flow angle and friction coefficient) evaluated for all different integrated substrate/coating systems.

Coating	Chip thickness (mm)	Chip compression ratio - CCR	Φ - Shear angle (°)	β - Friction angle (°)	(ϒ) Shear Strain	Chip sliding velocity (m/min)	Chip flow angle (°)	Friction coefficient (μ)
Uncoated	0.245	0.813	41.08	8.9	0.92	260.23	20.17	0.227
PVD	0.277	0.719	37.39	12.6	0.97	230.16	26.16	0.368
CVD 1	0.236	0.844	42.23	7.7	0.87	270.15	28.33	0.185
CVD 2	0.289	0.689	36.15	13.8	0.95	220.61	22.15	0.418

Based on the Table 2.3 summary, chip thickness, chip compression ratio and shear angle are superior in the CVD 1 coating system compared to all other tools studied in this work. The data confirm a significant improvement of friction conditions occurs in the cutting zone while machining with CVD 1. All obtained results demonstrate that the chip characteristics were enhanced in the CVD 1 integrated system. Therefore, it can be concluded that the integrated coating/substrate system represented by CVD 1 reduces friction, leading to an overall improvement in tool life (Fig. 2.4).

Another critical point to be observed is that the sliding velocity was increased in CVD 1, indicating that this system accelerates the metal flow process. An accelerated metal flow causes intense plastic deformation in the chips. To assess the level of plastic deformation within the chips obtained by the CVD 1 and PVD integrated substrate/coating systems, an evaluation of the chips' microstructures was performed by SEM and EBSD, with the results presented in Fig. 2.10. Cross-section images of the chips examined by EBSD confirm that the grains are strongly refined in the chips produced by CVD 1. Therefore, chip flow is accelerated, and strain plastic deformation is induced within the chip. The high amount of shear strain material found in the chips

produced by the CVD 1 system can be attributed to the low value of the friction angle and greater chip compression compared to chips produced by PVD (Table 2.3). The images displayed in Fig. 2.10 clearly present zones of intensity strengthening within the chips generated by the CVD 1 system, which specify a preferential deformation texture {1 1 0} for the austenitic matrix structure. These results are strongly corroborated by the experimental pole figures obtained by R'Saoubi and Ryde [38] based on X-ray diffraction analysis of the chips close to the tool–work friction zones in different stainless steels. Therefore, the results confirm that the higher stress values of CVD 1 were related to the differences in chip formation characteristics between the integrated coating/substrate systems. Shear-located chips and severe plastic deformation were present in CVD 1, in contrast to PVD, which had a lower chip sliding velocity and more homogeneous plastic deformation (Fig. 2.10).
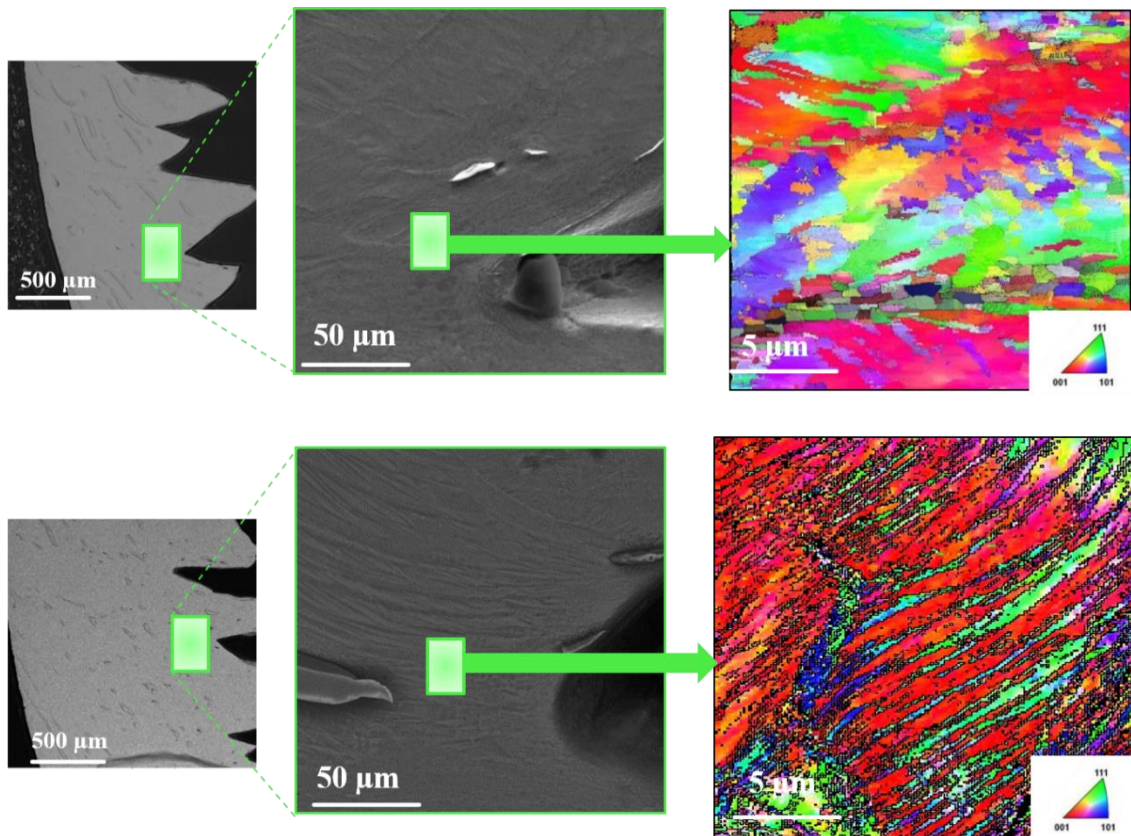
Fig. 2.10. Cross sections and EBSD images of the chips' microstructures produced by different integrated substrate /coating system: a) PVD and b) CVD 1.

Fig. 2.11 shows the effect of the integrated coating/substrate system (PVD and CVD 1) on the chip segmentation characteristics during the machining of austenitic stainless steel. It can be seen that the segments are curved and slightly different in each tool system. Although chips produced by PVD show a regular lamellar structure, the spacing between the segments is inconsistent due to the intense friction conditions on the tool-chip interface. Chips produced by CVD 1 show the same trend of a regular lamellar structure and spacing between the segments. However, fracture patterns were clearly observed on the entire surface of the lamellar chip band. This is a combined effect of the higher chip sliding velocity as well as the milder friction conditions at the tool-chip interface. Based on this analysis, it can be concluded that the segmented chips

produced by the CVD 1 system result from interrupted primary shear banding processes that initiate from the tool-contact surface. These processes rapidly propagate towards the valleys on the chips, causing sequential tearing along the chip shear band. In this case, the shear band may be developed by a high level of shear during the chip flow which enhances chip formation by accelerating the deformation within the chip. This in turn, creates a discontinuity and brittle shear bands, entirely due to ductile flow [39].
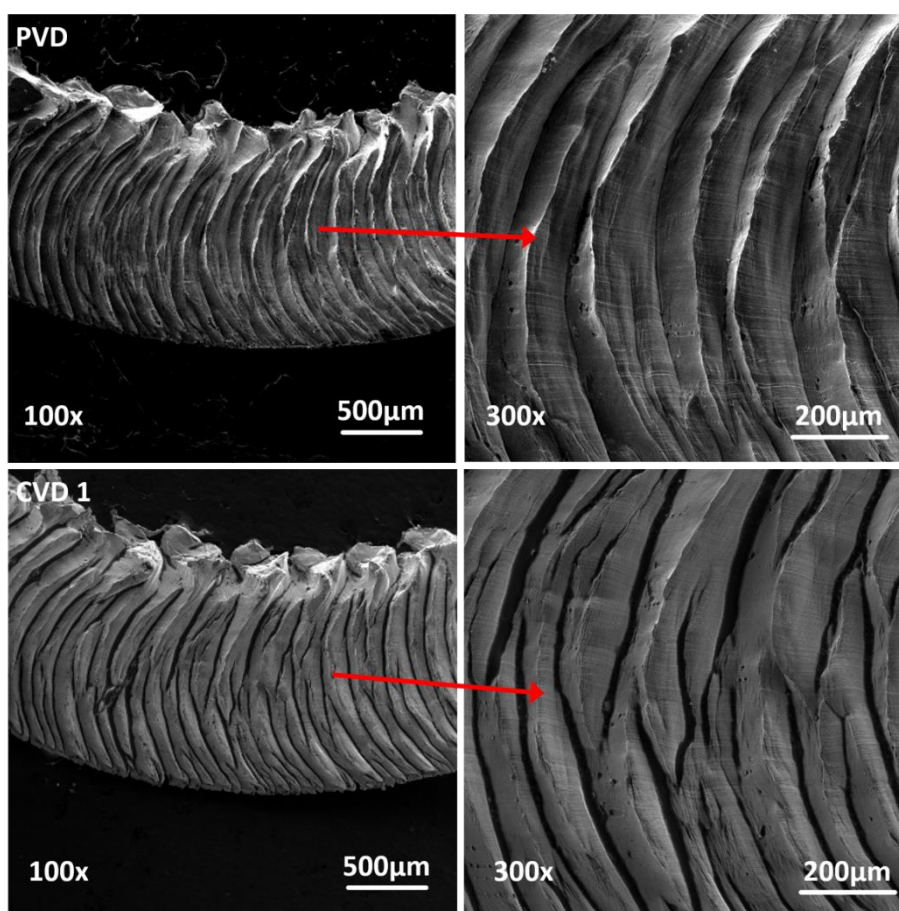
Fig. 2.11. SEM images showing the shear bands lines of chips produced by PVD and CVD 1.

2.4. Conclusions

The results of cutting experiments and characterization measurements on different

coating/substrate systems (2 PVDs and 2 CVDs) were analyzed and compared during the machining of 304 austenitic stainless steel. This research reveals that superior wear performance and toll life are provided by a surface engineered layer/carbide material with the most optimal combination of the coating/substrate properties. The following conclusions are drawn in this study:

i. The tribological evaluation, tool life test, wear performance and mechanical characteristics of the CVD 1 coating system show that the best results are an outcome of the integrative coating/carbide substrate design.

ii. The CVD 1 coating features the best performance due to a combination of factors (e.g., better plasticity and better load carrying capacity) contribute to the greater tool life.

iii. The enhanced mechanical properties of CVD 1 affect tribological characteristics during cutting (such as CCR, metal flow and shear band), wear performance, and overall tool life.

iv. A combination of Co binder with the presence of TiC in CVD 1 reduces hardness and substantially improves fracture toughness, which mitigates the crater wear pattern on the cutting tools during cutting caused by high temperatures and adhesive wear.

v. Finally, this study reveals that the difference in thickness of the PVD AlTiN did not change the wear behavior, confirming that an integrative approach to coating/carbide substrate design plays a significant role in tool wear performanceand tool selection.

2.5. References

[1]   I. Korkut, M. Kasap, I. Ciftci, and U. Seker, "Determination of optimum cutting parameters during machining of AISI 304 austenitic stainless steel," *Mater. Des.*, vol. 25, no. 4, pp. 303–305, 2004.

[2]   A. P. Junaidh, G. Yuvaraj, J. Peter, V. Bhuvaneshwari, Kanagasabapathi, and K. Karthik, "Influence of Process Parameters on the Machining Characteristics of Austensite Stainless Steel (AISI 304)," *Mater. Today Proc.*, vol. 5, no. 5, Part 2, pp. 13321–13333, 2018.

[3]   J. G. Corrêa, R. B. Schroeter, and Á. R. Machado, "Tool life and wear mechanism analysis of carbide tools used in the machining of martensitic and supermartensitic stainless steels," *Tribol. Int.*, vol. 105, pp. 102–117, 2017.

[4]   J. L. Mo, M. H. Zhu, A. Leyland, and A. Matthews, "Impact wear and abrasion resistance of CrN, AlCrN and AlTiN PVD coatings," *Surf. Coatings Technol.*, vol. 215, pp. 170–177, 2013.

[5]   J. L. Endrino, G. S. Fox-rabinovich, and C. Gey, "Hard AlTiN , AlCrN PVD coatings for machining of austenitic stainless steel," vol. 200, pp. 6840–6845, 2006.

[6]   I. Sik, A. Amanov, and J. Deok, "Tribology International The effects of AlCrN coating , surface modi fi cation and their combination on the tribological properties of high speed steel under dry conditions," *Tribiology Int.*, vol. 81, pp. 61–72, 2015.

[7]   M. Çöl, D. Kir, and E. Eri\csir, "Wear and blanking performance of AlCrN PVD-coated punches," *Mater. Sci.*, vol. 48, no. 4, pp. 514–520, Jan. 2013.

[8]   K. Bobzin, "High-performance coatings for cutting tools," *CIRP J. Manuf. Sci.*

Technol., vol. 18, pp. 1–9, 2017.

[9] M. Sokovic, L. A. Dobrzański, J. Kopač, and L. Kosec, "Cutting Properties of PVD and CVD Coated A2lO 3 + TiC Tool Ceramic," in *THERMEC 2006*, 2007, vol. 539, pp. 1159–1164.

[10] I. Ciftci, "Machining of austenitic stainless steels using CVD multi-layer coated cemented carbide tools," vol. 39, pp. 565–569, 2006.

[11] J. M. F. de Paiva *et al.*, "Frictional and wear performance of hard coatings during machining of superduplex stainless steel," *Int. J. Adv. Manuf. Technol.*, vol. 92, no. 1–4, pp. 423–432, 2017.

[12] J. L. Endrino *et al.*, "Oxidation tuning in AlCrN coatings," *Surf. Coatings Technol.*, vol. 201, no. 8, pp. 4505–4511, 2007.

[13] K. Bobzin, E. Lugscheider, R. Nickel, N. Bagcivan, and A. Krämer, "Wear behavior of Cr1−xAlxN PVD-coatings in dry running conditions," *Wear*, vol. 263, no. 7, pp. 1274–1280, 2007.

[14] S. Ruppi, "Deposition, microstructure and properties of texture-controlled CVD α-Al2O3 coatings," *Int. J. Refract. Met. Hard Mater.*, vol. 23, no. 4-6 SPEC. ISS., pp. 306–316, 2005.

[15] C. Mitterer, "2.16 - PVD and CVD Hard Coatings," in *Comprehensive Hard Materials*, V. K. Sarin, Ed. Oxford: Elsevier, 2014, pp. 449–467.

[16] S. Sheikh *et al.*, "Fracture toughness of cemented carbides: Testing method and microstructural effects," *Int. J. Refract. Met. Hard Mater.*, vol. 49, no. 1, pp. 153–160, 2015.

[17] M. Shaw, *Metal cutting principles*, 2°. New York: Oxford Unversity Press, 2005.

[18] J. Xiong, Z. Guo, M. Yang, W. Wan, and G. Dong, "Tool life and wear of WC–

TiC–Co ultrafine cemented carbide during dry cutting of AISI H13 steel," *Ceram. Int.*, vol. 39, no. 1, pp. 337–346, 2013.

[19] J. García, V. C. Ciprés, A. Blomqvist, and B. Kaplan, "Cemented carbide microstructures: a review," *Int. J. Refract. Met. Hard Mater.*, vol. 80, pp. 40–68, 2019.

[20] P. Montenegro, J. Gomes, R. Rego, and A. Borille, "Potential of niobium carbide application as the hard phase in cutting tool substrate," *Int. J. Refract. Met. Hard Mater.*, vol. 70, pp. 116–123, 2018.

[21] R. M. Genga, G. Akdogan, J. E. Westraadt, and L. A. Cornish, "Microstructure and material properties of PECS manufactured WC-NbC-CO and WC-TiC-Ni cemented carbides," *Int. J. Refract. Met. Hard Mater.*, vol. 49, pp. 240–248, 2015.

[22] E. Uhlmann, I. Dethlefs, F. Faltin, and L. Schweitzer, "Cutting and Drilling of Metals and Other Materials: A Comparison," in *Reference Module in Materials Science and Materials Engineering*, Elsevier, 2016.

[23] G. Fox-Rabinovich and G. E. Totten, *Self-organization During Friction - Advanced Surface-Engineered Materials and Systems Design*, 1st ed. Boca Raton: CRC Press, 2006.

[24] G. Q. Yu *et al.*, "Effects of N ion energy on titanium nitride films deposited by ion assisted filtered cathodic vacuum arc," *Chem. Phys. Lett.*, vol. 374, no. 3, pp. 264–270, 2003.

[25] A. Osada, E. Nakamura, H. Homma, T. Hayahi, and T. Oshika, "Wear mechanism of thermally transformed CVD Al2O3 layer," *Int. J. Refract. Met. Hard Mater.*, vol. 24, no. 5, pp. 387–391, 2006.

[26] V. Dehnavi, X. Y. Liu, B. L. Luan, D. W. Shoesmith, and S. Rohani, "Phase

transformation in plasma electrolytic oxidation coatings on 6061 aluminum alloy," *Surf. Coatings Technol.*, vol. 251, pp. 106–114, 2014.

[27]   W. Qiu, Y. Liu, J. Ye, H. Fan, and Y. Qiu, "Effects of (Ti,Ta,Nb,W)(C,N) on the microstructure, mechanical properties and corrosion behaviors of WC-Co cemented carbides," *Ceram. Int.*, vol. 43, no. 3, pp. 2918–2926, 2017.

[28]   A. Leyland and A. Matthews, "On the significance of the H/E ratio in wear control: a nanocomposite coating approach to optimised tribological behaviour," *Wear*, vol. 246, no. 1, pp. 1–11, 2000.

[29]   G. S. Fox-Rabinovich, S. C. Veldhuis, V. N. Scvortsov, L. S. Shuster, G. K. Dosbaeva, and M. S. Migranov, "Elastic and plastic work of indentation as a characteristic of wear behavior for cutting tools with nitride PVD coatings," *Thin Solid Films*, vol. 469–470, pp. 505–512, 2004.

[30]   E. O. Correa, J. N. Santos, and A. N. Klein, "Microstructure and mechanical properties of WC Ni–Si based cemented carbides developed by powder metallurgy," *Int. J. Refract. Met. Hard Mater.*, vol. 28, no. 5, pp. 572–575, 2010.

[31]   H. Zhang and Z. Z. Fang, "Characterization of quasi-plastic deformation of WC–Co composite using Hertzian indentation technique," *Int. J. Refract. Met. Hard Mater.*, vol. 26, no. 2, pp. 106–114, 2008.

[32]   H. Zhang, Z. Z. Fang, and J. D. Belnap, "Quasi-Plastic Deformation of WC-Co Composites Loaded with a Spherical Indenter," *Metall. Mater. Trans. A*, vol. 38, no. 3, pp. 552–561, Mar. 2007.

[33]   A. Góez *et al.*, "Contact damage and residual strength in hardmetals," *Int. J. Refract. Met. Hard Mater.*, vol. 30, no. 1, pp. 121–127, 2012.

[34]   A. E. Diniz, Á. R. Machado, and J. G. Corrêa, "Tool wear mechanisms in the

machining of steels and stainless steels," *Int. J. Adv. Manuf. Technol.*, vol. 87, no. 9, pp. 3157–3168, Dec. 2016.

[35] A. Biksa *et al.*, "Tribology International Wear behavior of adaptive nano-multilayered AlTiN / Me x N PVD coatings during machining of aerospace alloys," *Tribiology Int.*, vol. 43, no. 8, pp. 1491–1499, 2010.

[36] K. Bobzin, E. Lugscheider, O. Knotek, M. Maes, P. Immich, and C. Piñero, "Development of multilayer TiAlN + γ-Al2O3 coatings for difficult machining operations," in *Materials Research Society Symposium Proceedings*, 2006, vol. 890, pp. 27–32.

[37] E. M. Trent and P. K. Wright, *Metal Cutting*. 2000.

[38] R. M'Saoubi and L. Ryde, "Application of the EBSD technique for the characterisation of deformation zones in metal cutting," *Mater. Sci. Eng. A*, vol. 405, no. 1, pp. 339–349, 2005.

[39] R. Bejjani, M. Balazinski, H. Attia, P. Plamondon, and G. L'Éspérance, "Chip formation and microstructure evolution in the adiabatic shear band when machining titanium metal matrix composites," *Int. J. Mach. Tools Manuf.*, vol. 109, pp. 137–146, 2016.

Chapter 3: Study of wear performance and tribological characterization of AlTiN PVD coatings with different Al/Ti ratios during ultra-high speed turning of stainless steel 304

Qianxi He[1], Jose M. Paiva[1,2,*], Joern Kohlscheen[3], Ben D. Beake[4], and Stephen C. Veldhuis[1]

1- McMaster Manufacturing Research Institute, McMaster University, Hamilton, L8S4L8, Canada

2- Engineering Graduate Program – PPGEM, Pontificia Universidade Católica do Paraná, Curitiba, 80215901, Brazil

3- Kennametal Shared Services Gmbh, Altweiherstr 27-31, 91320, Ebermannstadt, Germany

4- Micro Materials Ltd., Willow House, Yale Business Village, Ellice Way, Wrexham, LL13 7YL, UK

* Corresponding author: paivajj@mcmaster.ca (Jose M. Paiva).

Author's Contribution

Qianxi He	Designed and conducted the experiments
	Analyzed the results.
	Wrote the manuscript.
Jose M. Paiva	Assisted with designing the research methodology.
	Assisted with writing and editing the manuscript.
Joern Kohlscheen	Deposited the coating.
Ben D. Beake	Assisted with data collection for micro-scratch tests
Stephen C. Veldhuis	Supervised the project.

Abstract

AlTiN coatings with different Al/Ti ratios (50/50, 60/40, 67/33, 70/30 and 73/27) deposited by cathodic arc PVD are investigated in this paper. An ultra-high speed of 420 m/min was applied during the finish turning tests of stainless steel 304 (SS304). The coating structure was characterized by SEM and XRD techniques. Assorted mechanical properties such as elastic modulus, coating adhesion, hardness and micro-scratch fracture toughness were assessed using nano-indentation and scratch testing. Chip characterization was performed to evaluate the tribological characteristics of the tool/chip interface. The wear performance study showed that cratering was the main wear mechanism. Tool life results have shown that the Al60Ti40 coating featured the longest tool life due to its favorable combination of tribological and micro-mechanical properties.

Keywords

3.1. Introduction

Austenitic stainless steels are considered hard-to-machine materials owing to their apparent tendency to work-harden during machining as well as adhesion [1,2]. Furthermore, due to this alloy's low thermal conductivity, a considerable amount of heat produced during cutting will be transferred to the tool, which degrades the substrate material, negatively impacting the cutting performance [3]. The application of hard films by physical vapor deposition (PVD) is an efficient way of improving cutting tools' wear resistance during machining of stainless steels. Titanium based coatings with their outstanding properties including high hardness, good wear resistance, and excellent corrosion resistance, have been commonly used to protect inserts in numerous challenging working conditions [4,5]. However, the oxidation resistance of TiN coating is still worse than other coating compositions such as AlTiN. TiN coatings will oxidize quickly at temperatures over 500 °C, with the creation of a brittle and loose TiO_2 layer [6]. The addition of aluminum in AlTiN coatings enhances their hardness, wear resistance and especially oxidation resistance at high temperatures (to a maximum of 1000 °C) [7-9]. Furthermore, AlTiN coatings have higher fatigue fracture resistance than TiN [9,10].

The mechanical properties and crystal structure of AlTiN coatings are known to be positively correlated to their Al content. For instance, the hardness of the coating increases up to a certain value and then decreases after that. The reduction of the hardness corresponds to the phase transformation when the hexagonal wurtzite AlN is preferred over the TiN's typical face-centered cubic (fcc) phase [11]. It was reported that AlTiN coatings feature a predominantly cubic structure when the Al content is slightly lower than 67 at. % (metal fraction of the nitride compound), a mixed cubic-

wurtzite structure at an Al content slightly above 67 at. % and finally a single hexagonal structure typical for AlN at the higher Al content [6,11].

Endrino et al. [1] studied four different AlCrN and AlTiN based PVD coating compositions with high Al content for austenitic stainless-steel machining. Within the stable wear stage, the nano crystalline AlTiN coated tools surpassed fine grained AlTiN variants, with almost double the life of the tool. Fox-Rabinovich et al. [12] compared the structural characteristics, wear performance, oxidation resistance, and mechanical properties of AlTiN and TiAlCrN coatings applied for hard-to-cut materials. The findings demonstrated the impacts of the coating structure and composition on the oxidation behaviour of $Al_{0.3}Cr_{0.7}N$ based coatings. In addition, modified aluminium-rich AlCrN coatings were found to have improved oxidation resistance [13].

The machining process of stainless steel 304 (SS304) at high cutting speed conditions involves elevated temperature in the cutting zone (at the interface between workpiece and tool) resulting in chemical transformation of the associated materials. Since Al is a very active metal, increasing the amount of Al in the coatings contributes to increased chemical reactivity. Owing to the difficulty of oxygen penetration into the contact zone, the active chemical reactions between the AlTiN coating and the workpiece tend to cause adhesive wear [14]. Several studies investigated the effect of high Al content in different coating chemical compositions. However, the performance of AlTiN PVD coatings with different Al/Ti ratios during ultra-high speed machining of SS304 was not investigated in literature up to the moment. In order to provide a better coating solution for the aforementioned process, it is vital to understand the surface modification of AlTiN coatings that benefit tool tribological performance during ultra-high speed turning of stainless steels. Therefore, a detailed analysis of five different

Al/Ti ratios of 50/50, 60/40, 67/33, 70/30 and 73/27, is presented in this paper. The variation in Al content alters the mechanical properties and different dominating wear mechanisms of the corresponding AlTiN coatings during ultra-high speed machining of SS304 with carbide inserts. Studies of tribological performance were emphasized through assessment of the frictional conditions of the cutting process mainly depend on the chip characteristics (including the chip compression ratio, metal flow descriptions, and shear bands observation, etc.). The main purpose of this paper is to study the tribological characteristics of the coated cutting tools since it shows the friction conditions at the contact face of tool, chip and workpiece and this leads to a better understanding of the tool wear performance.

3.2. Experimental procedure

An industrial-scale cathodic arc ion plating facility attached with four circular shaped evaporators was used to deposit PVD AlTiN coatings. Cutting inserts and top polished coupons made of WC with 6 wt. % of Co binder were used for analyses and testing. Source materials ("targets" with a diameter of 120 mm) with five different Al/Ti ratios (50/50, 60/40, 67/33, 70/30, and 73/27) were used for the deposition of different monolayer coatings. The PVD cycle consisted of heating, plasma etching, coating, and cooling. All substrates were plasma etch cleaned for 30 min using Ar ions at a substrate bias voltage of - 200 V and a pressure of 0.2 Pa. The chamber temperature was maintained at 500 °C during the deposition with the samples being rotated three times. The nitrogen flow rate was controlled to maintain a pressure of 3.5 Pa without using any noble gas. Deposition time was set to 180 min, resulting in a typical coating thickness of around 4 μm.

CNGG120408-FS (Kennametal, substrate K313) cutting inserts were used for

testing. The microstructure of SS304 is shown in Table 3.1. The chemical composition

as well as mechanical properties of this workpiece material are also outlined below.

Table 3.1. Microstructure, chemical composition, and mechanical properties of SS304 [15]

Element	Weight (%)	Yield strength (MPa)	Tensile strength (MPa)	Elongation (% in 50 mm)	Hardness	
					Rockwell B (HR B) max	Brinell (HB) max
Cr	18 - 20	205	515	40	92	201
Ni	8 - 10.5					
Mn	< 2					
Si	< 0.75					
N	< 0.1					
C	< 0.08					
P	< 0.045					
S	< 0.03					
Fe	Balance					
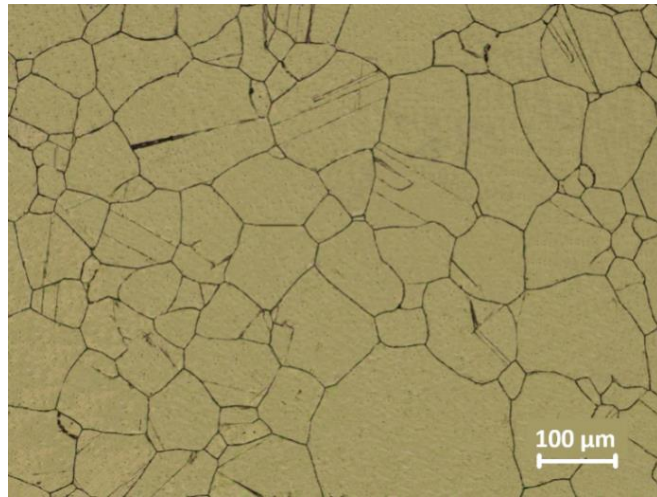
Single point turning was used to conduct the cutting tests using a φ = 150 mm and

L = 200 mm SS304 bar. For the cutting tests, a high-precision CNC lathe (Nakamura

Tome SC 450) was manipulated. All turning tests were performed under an ultra-high

speed of 420 m/min, a cut depth of 0.5 mm, and a feed rate of 0.15 mm/rev. A 5 %

concentration of semi-synthetic coolant was applied during the cutting tests. These

cutting conditions were selected to approach a novel ultra-high speed machining process

of stainless steels poorly explored so far. During the turning process, cutting forces were

collected at the first pass for each coated cutting tool tested in this work. A LabVIEW

professional development system (National Instruments, US) was used for this

measurement. According to ISO 3685, the tool life criterion adopted in this work was set to be cumulative flank wear of 300 μm. The tool wear on the cutting inserts was examined with the use of an optical microscope (Keyence VHX). Wear data was extracted a 95 % accuracy from an average of three tests.

To understand how different Al/Ti ratios in AlTiN PVD coatings affect cutting tool performance, the coating micro-structure needs to be analyzed. Scanning electron microscopy, SEM (VEGA, Tescan) identified the architecture, morphology and thickness of the coating. To determine the phase composition and transformation of these coatings, an X-ray diffractometer (D6 Discover, Bruker) was used. Each study was performed to classify the crystal phases from a source of Cu K alpha radiation in a standard configuration of 20-90° angular range. The diffraction configuration in this measurement was Bragg-Brentano (decoupled 2θ, α=5°).

A nano-indentation tester (NHT3, Anton Paar) was used to test the micro-mechanical characteristics of the coatings (hardness and young's modulus). During the tests the load applied was 20 mN using a geometry of the Vickers indenter. A matrix of 8 x 5 indentations was used to collect sufficient data. An average of these indentation values quantified the coatings' hardness and elastic modulus. To study the adhesion performance of the coatings on the carbide, micro-scratch tests were conducted by a Micro-scratch Tester (CORE, Micro Materials). For the three-scan, multi-pass topography-scratch-topography micro-scratch tests, a 25 μm end radius diamond conical shape indenter was used. After a 100 m levelling distance, the load with 175 mN/s was stepped up to a maximum of 7.5 N in the ramped scratch pass. The speed for scratch was 20 μm/s, while the scratch was 1 mm long. The contact load was set at 1 mN for both the pre-scratch and post-scratch topographic scans, as well as the initial

100 μm of the ramped scratch. Moreover, a scratch tester (Revetest, Anton Paar) coupled with a 200 μm radius Rockwell diamond indenter was employed for macro-scratch analysis on these coatings under an increasing load from 0.5 to 100 N (distance 3 mm). The fracture toughness of the coatings was measured using the same scratch tester (Revetest, Anton Paar) with a Vickers indenter under a constant 150 N load at a single location. Three repetitions were performed for each coating to yield the results of adhesion and fracture toughness.

Finally, to understand the performance of the coatings and the functional surfaces, cutting tests were developed to evaluate the wear performance improvement achieved by the different surface treatment techniques. 3D evaluation of cutting tools' wear volume and chips' undersurface morphology were performed by confocal microscopy (Infinity Focus G, Alicona) to determine to wear performance and chip character during cutting process. All examined chips had a 3 mm length and 2 mm width. Wear patterns of the used tools were assessed pre and post the underwent etching process to remove any adherent workpiece material. The etching solution consisted of a 2:1 solution of hydrochloric and nitric acids, respectively. The cutting tools were immersed in this solution for a period of 20 minutes. SEM, paired with Energy Dispersive Spectroscopy (EDS), was then used to assess the worn areas to confirm the chemical composition. This instrument was also used for chip characterization.

3.3. Results and discussion

3.3.1. Substrate and Coating characterizations

A micro-grain cemented carbide was used as the cutting tool's substrate in this work, as shown in Table 3.2. The main cemented carbide phases were 94 wt. % hard grains of WC and 6 wt. % of a significantly softer Co binder phase [15]. This has led to

a relatively abrasion resistant compound in the range of ISO K5-K10 carbide, which is known to be suitable for demanding cutting applications [16]. Additionally, with the high melting points, the carbide materials still preserve their hardness at very high manufacturing temperatures. Given the extremely fine distribution, the binder process softens at significantly higher temperatures compared to the tool material of high-speed steels [17,18]. These characteristics lead to an improvement of the cutting tool's mechanical properties, which then strengthens the carbide alloy's resistance to abrasion wear and chipping on the cutting edges [19,20]. The mechanical properties of the substrate are shown in Table 3.2.

Table 3.2. Micro-mechanical characteristics of the carbide substrate

Hardness (GPa)	Grain size (μm)	Density (g/cm^3)	Fracture toughness (MPa m$^{1/2}$)	Elastic modulus (GPa)	H/E
22.8±3.5	1.225	14.9	14.3±1.2	550±28	0.0414

Fig. 3.1 shows the SEM image of typical AlTiN PVD coating's cross-section. The thickness of the AlTiN PVD coating was about 4-5 μm, and the coating had a uniform and dense microstructure. In addition, it reveals nodular and flake defects of various sizes and shapes occurring on top surfaces, typical of droplet defects found in arc PVD. With Al content intensifying, the coatings showed a more nano-crystalline structure. This behavior was also previously reported [21,22]. As can be seen in the the image, AlTiN coating has a columnar structure. This is because in the process of nucleation during PVD, grains with energetically favorable orientations may grow upwards and outwards, which results in a strong crystallographic texture present within the material, leading to columnar growth structures [23]. It has been demonstrated in literature that

the main advantage of this structure is its superior tolerance against straining and thermal shock, which helps extend the tool's life time [24].
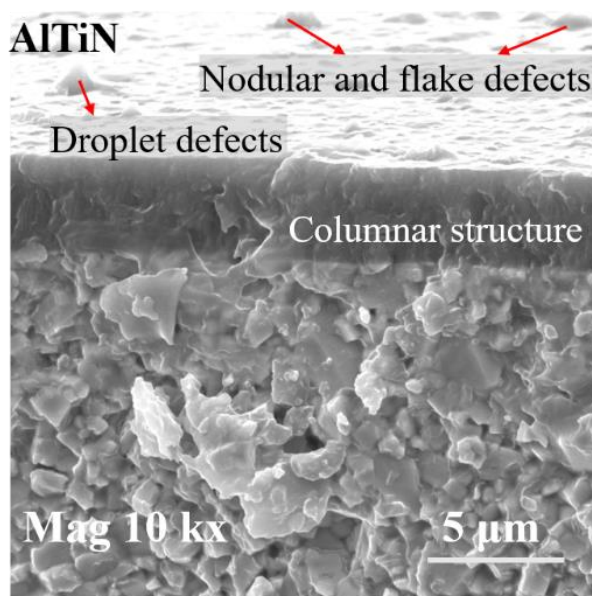
Fig. 3.1. Coating cross-section SEM image showing the microstructure of typical AlTiN PVD coating.

Fig. 3.2 shows the XRD patterns of various Al/Ti ratio PVD coatings deposited on the cemented carbide substrate material. All five coatings exhibited an intense peak with a preferred cubic crystal orientation (200) and another peak with a less intense cubic orientation (111) according to JCPDS 00-037-1140. In addition, Al/Ti 50/50, 60/40, 67/33 and 70/30 exhibited low intensity peaks of cubic phase orientation (220), whereas a peak of cubic phase oriented (201) was found in Al/Ti 73/27. In addition, the XRD scan showed a change of the peak positions to a higher diffraction angle with an increased amount of Al. This displacement happened because of a change in parameter of the lattice. The addition of an atom with a small atomic radius to a crystal structure gradually decreases the parameter of the lattice and a raising of the angle of diffraction

[25]. As aluminum is smaller than titanium, the cubic lattice gets distorted, stressed and the lattice parameter decreases. Moreover, the XRD spectrum in Fig. 3.2 showed the AlTiN coatings' strongest (200) orientation, reflecting the lowest surface and strain energies during the coating deposition process. The coating thus develops after deposition with the lowest surface energy between the crystal planes [26]. A reduction of signal intensity and broadening of the peaks had taken place in Al70Ti30 and even more so in the Al73Ti27 coating. Some new reflections around 50, 60, and 80 degree were detected that are very likely associated with the AlN wurtzite structure. There may even be amorphous phase contents in the Al73Ti27 coating as described in [21].
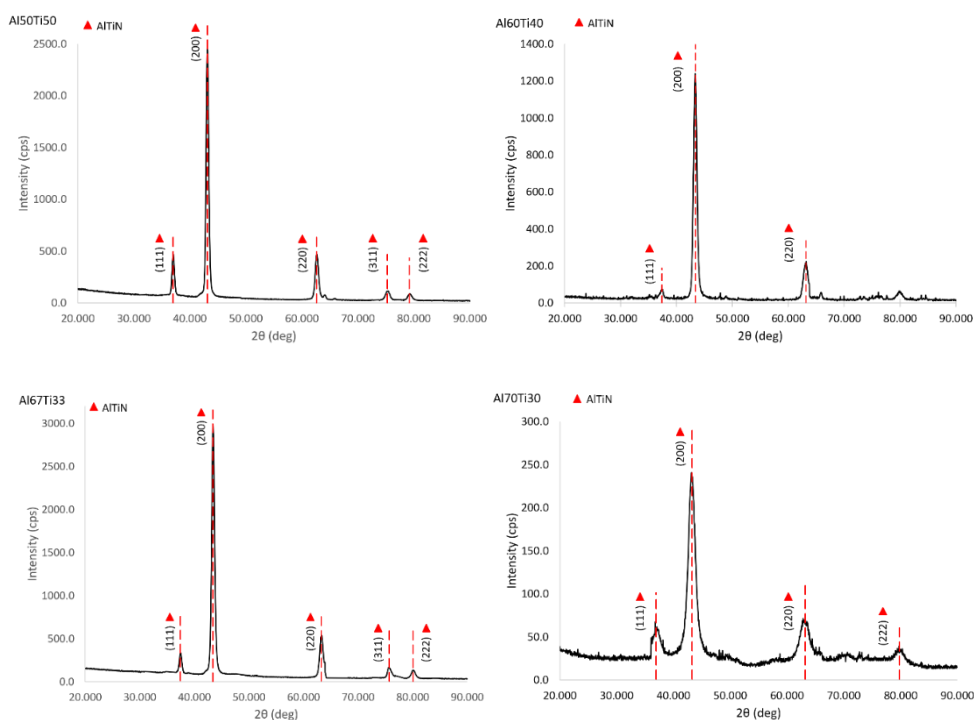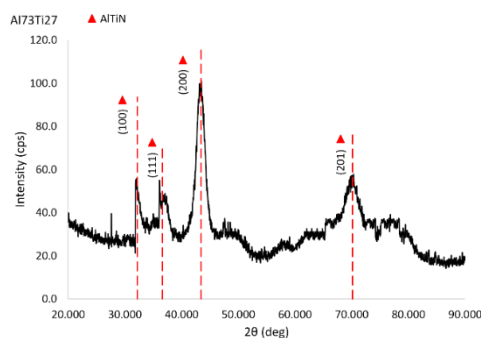
Fig. 3.2. XRD patterns of coated cutting tools: Al50Ti50; Al60Ti40; Al67Ti33; Al70Ti30; Al73Ti27.

Surface morphology of the coating's top surface are shown in Fig. 3.3. In general, all coatings featured a smooth surface with a surface average (Sa) value of under 0.17 μm. However, it can be seen that the Al50Ti50 coating had the lowest Sa value (0.1385 μm) compared to Al60Ti40, which had a relatively rougher surface (Sa = 0.1693 μm). Due to the defects during the deposition process, some spherical particles with low adhesion were formed on the coating surface. An unavoidable characteristic of the cathodic arc deposition process is the presence of droplets or macro-particles [27]. These coatings are super-finished under certain application areas, to create a smooth surface. However, contamination may be present inside the chamber during the deposition process with small particles from the fixtures and the walls being co-deposited, thereby affecting the coating's Sa. Although the coatings' rough surface may affect frictional conditions at the tool-chip interface [3], it was reported in our previous study that those imperfections might not significantly affect the machining process since they were all in the same low range with minor differences between them.
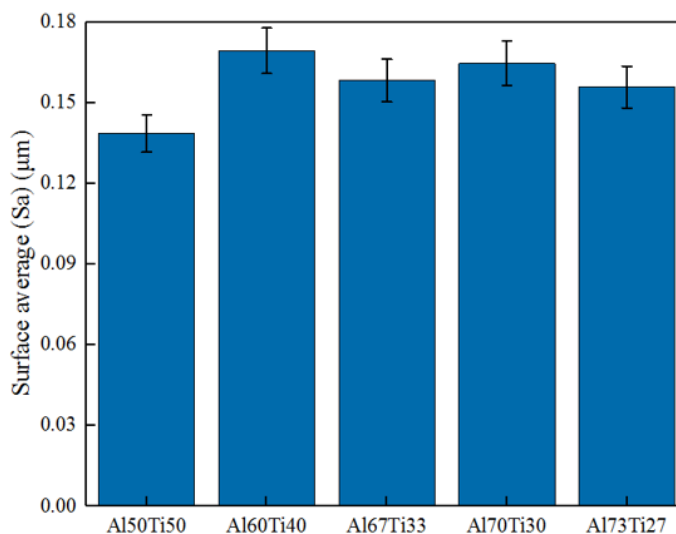
Fig. 3.3. Surface average of different Al/Ti ratio PVD coatings.

Table 3.3 displays the considered PVD AlTiN coatings' mechanical properties. The microhardness and elastic modulus of the AlTiN coatings as a function of the different ratios of Al/Ti, confirmed that the Al/Ti 50/50 coating exhibited the highest hardness and elastic modulus out of all the tested coatings. This could be partially explained by low Aluminum concentration in its chemical composition, which results in the formation of different microstructures. Hardness and modulus reduced significantly below 30 GPa and 400 GPa, respectively, at higher Al contents (Al > 67), which indicates a very likely presence of a softer hexagonal phase [6]. The importance of H/E ratio (elastic strain to failure) was outlined [24] and fracture toughness was found to enhance the tribological behavior for a specific substrate carbide and coating system [15]. In this case, Al50Ti50 and Al60Ti40 had a H/E value lower than 0.06 due to their high elastic modulus. Researchers [28] showed that the H/E ratio correlates with wear resistance, but in cutting tests longer tool life for an optimum H/E reported which varies with the type of test, the material being machined, and cutting speed, etc. In this

application, a coating system with a low H/E ratio improves the longevity of the tool [15,28]. Energy generated during machining due to work hardening of the workpiece material could be dissipated through plastic deformation. Coating system with a lower H/E ratio showed more plasticity and had the ability to dissipate more energy generated and consequently change the wear mechanism associated with the machining of SS304 at an ultra-high speed.

Table 3.3. Mechanical characteristics for the AlTiN coatings with different Al/Ti ratios.

PVD coating layer	Al50Ti50	Al60Ti40	Al67Ti33	Al70Ti30	Al73Ti27
Hardness (GPa)	37.4 ± 1.87	35.2 ± 1.76	29.8 ± 1.49	26.7 ± 1.33	23.7 ± 1.18
Elastic modulus (GPa)	663.2 ± 33	592.9 ± 27	495.8 ± 24	381.5 ± 21	334.7 ± 23
H/E	0.056	0.059	0.061	0.069	0.071
Fracture toughness (MPa m$^{1/2}$)	0.228 ± 0.011	0.234 ± 0.012	0.258 ± 0.013	0.301 ± 0.015	no cracks observed
Macro-scratch Lc1 (N)	47.3 ± 0.24	45.8 ± 0.23	45.6 ± 0.23	45.1 ± 0.22	44.4 ± 0.22
Macro-scratch Lc2 (N)	54.1 ± 0.27	53.7 ± 0.27	53.1 ± 0.26	52.2 ± 0.26	51.6 ± 0.25
Micro-scratch Lc1 (N)	4.2 ± 0.3	4.3 ± 0.1	4.9 ± 0.2	4.7 ± 0.3	4.2 ± 0.3
Micro-scratch Lc2 (N)	5.4 ± 0.2	5.6 ± 0.2	5.7 ± 0.1	5.4 ± 0.2	5.5 ± 0.3
Scratch toughness (N^2)	5.0 ± 0.5	5.7 ± 0.9	3.6 ± 1.4	3.3 ± 0.7	5.2 ± 1.5

Scratch testing was conducted to determine the coatings' adhesion to the substrate. It can be seen from Table 3.3 that, Al/Ti 50/50 and 60/40 coating showed slightly similar critical loads measured for macro-scratch Lc2, and then the high values for these two coatings presented a stronger adhesion to the substrate, compared with other coatings. This is also proved by the SEM image of the scratch tracks, as shown in Fig. 3.4. It is easy to find that all the coatings tested possessed cohesive failure, and tensile cracking was the predominant mechanical failure mode on the nitride specimen, which was also stated in [29]. The onset of coating delamination occurred at a similar position on the

scratch test line for Al50Ti50, Al60Ti40, Al67Ti33 and Al70Ti30 whereas the Al73Ti27 coating flaked off at a later position since it is the softest and most ductile of all the coatings. No cracks were observed during the fracture toughness test on the Al73Ti27 coating (as shown in Table 3.3), demonstrating the high toughness of this coating. This is due to the highest ductility and elastic deformation of the coating under a high load. The initial delamination seemed to be very similar in coatings with a high Al content, with large pieces flaking off without evidential cracking. This was attributed to their relative softness and consequent higher ductility [30]. Although the Al50Ti50 and Al60Ti40 variant exhibited lateral cracking at the beginning of their respective track, both coating systems had adequate adhesion to the substrate, only flaking of smaller areas occurs initially. According to the ISO standard (ISO 27307:2015), the coating characterized by this kind of crack indicates a strong interaction of the coating with the substrate, which results in improved adhesion. On the other hand, at a higher Al content (Al > 67), coatings had more vacancy in atom arrangement due to the smaller lattice parameter of Al than Ti. This leads to a relatively sparse microstructure that contributes to both more delamination and spallation of the coating [31]. In general, spalling and buckling are correlated with the adherence of the coating to the substrate [32]. In this case, with more dense microstructures, Al/Ti 50/50 and 60/40 coatings had better adhesion, which resulted in less spallation along the scratch trace.
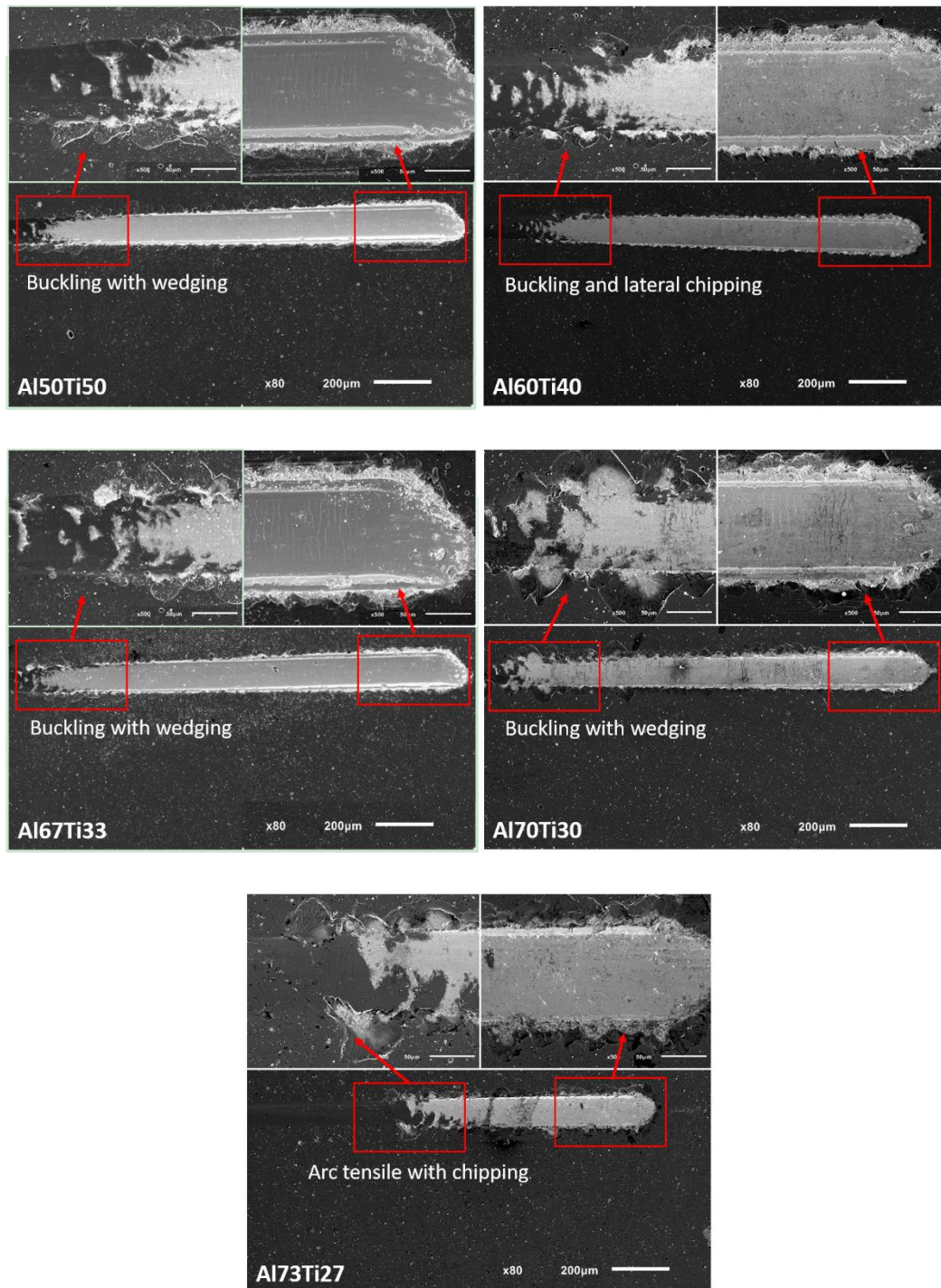
Fig. 3.4. SEM images of scratch tracks: Al50Ti50; Al60Ti40; Al67Ti33; Al70Ti30; Al73Ti27.

Micro-scratch tests results of critical loads are shown in Table 3.3 and the indenter displacement versus indenter depth over the surface is shown in Fig. 3.5. As shown in

Table 3.3, the coatings displayed almost identical micro-critical loads in Lc2. The differences in micro-scratch Lc1 were considerably higher in Al/Ti 67/33 and 70/30 coatings. Zabinski and Voevodin recommended that the lower critical load in a scratch test will provide fracture toughness evaluation [33]. This definition was later established by Zhang and coworkers who equated Lc1 with the resistance to crack initiation and (Lc2-Lc1) as a crack propagation measure (Lc2 = total coating failure load) [34,35]. They demonstrated a parameter (later labelled "scratch toughness") describing a combined initiation and propagation resistance to crack: *scratch toughness = Lc1(Lc2-Lc1)*. In this case, the scratch toughness was highest in the Al/Ti 60/40 coating. The Al/Ti 73/27 and 70/30 coatings exhibited a sharper (more abrupt) depth change at failure than the other coatings. The final on-load scratch depth was greater in these coatings. The micro-scratch depth data (Fig. 3.5) and the SEM image (Fig. 3.4) both showed changing deformation for 70/30 and 73/27. In the SEM lateral chipping extends further from the scratch track consistent with the more abrupt depth changes in the micro-scratch. The lower chipping on the Al/Ti 50/50 and 60/40 coating is consistent with more gradual deformation.
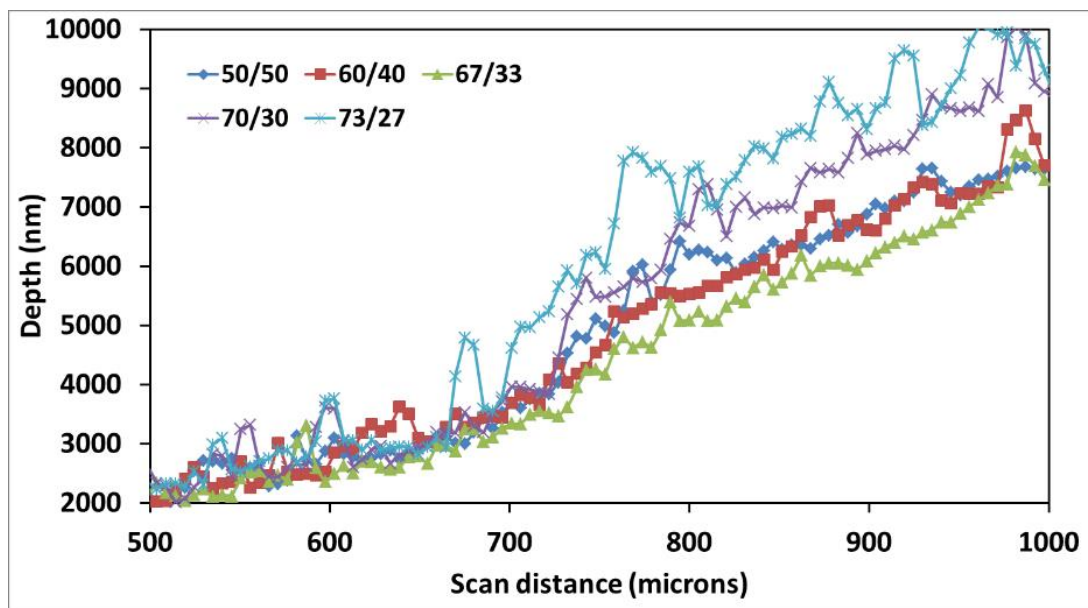
Fig. 3.5. Micro-scratch tests of different Al/Ti ratio coatings: the indenter displacement versus indenter depth over the surface.

3.3.2. Ultra-high speed cutting tests

Fig. 3.6 demonstrates the evolution of flank wear versus cutting length during a test conducted under a 420 m/min cutting speed and coolant. 3D optical images are showing the inserts' progress wear. In general, the main failure mechanism was a combination of abrasion on the flank face and adhesion on the rake face, with intensive built-up-edge (BUE) formation on the tool rake surface contributing to intensive chipping, as can be seen in the 3D images. The insert coated with Al73Ti27 failed shortly after 800 m with the most severe tool wear. The severely damaged flank signified that the coating layer had worn out as a result of direct adhesive interaction between the carbide tool and stainless steel, which resulted in tool failure. In contrast, the insert coated with Al60Ti40 had the longest tool life in this turning test. It also exhibited a different wear mode in comparison with the other tested tools. Crater wear was the predominant wear mode, which indicates that the coating could protect the area

around the crater and the cutting edge for a substantially longer time. As such, the Al60Ti40 coating featured the best performance as a result of not only its hardness, but also lower brittleness and better adhesion.
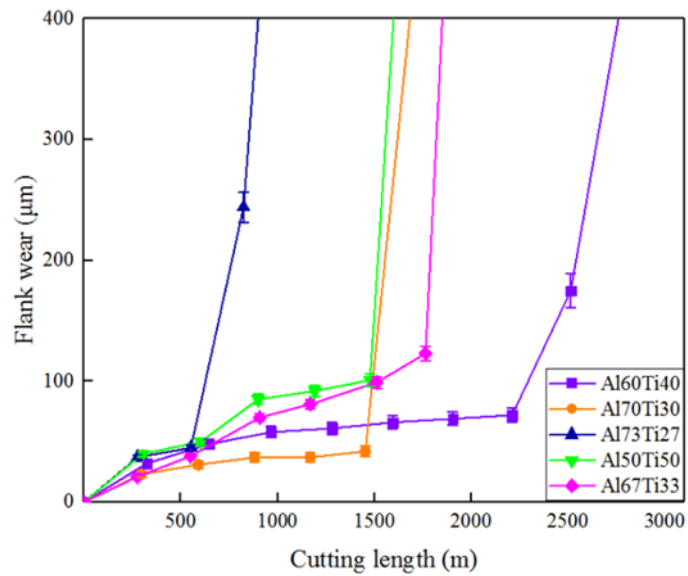
a) Tool life curve of five different Al/Ti ratio coated inserts: flank wear vs. cutting length.

| 600m (2nd pass) | 1500m (5th pass) | 2800m (9th pass) |
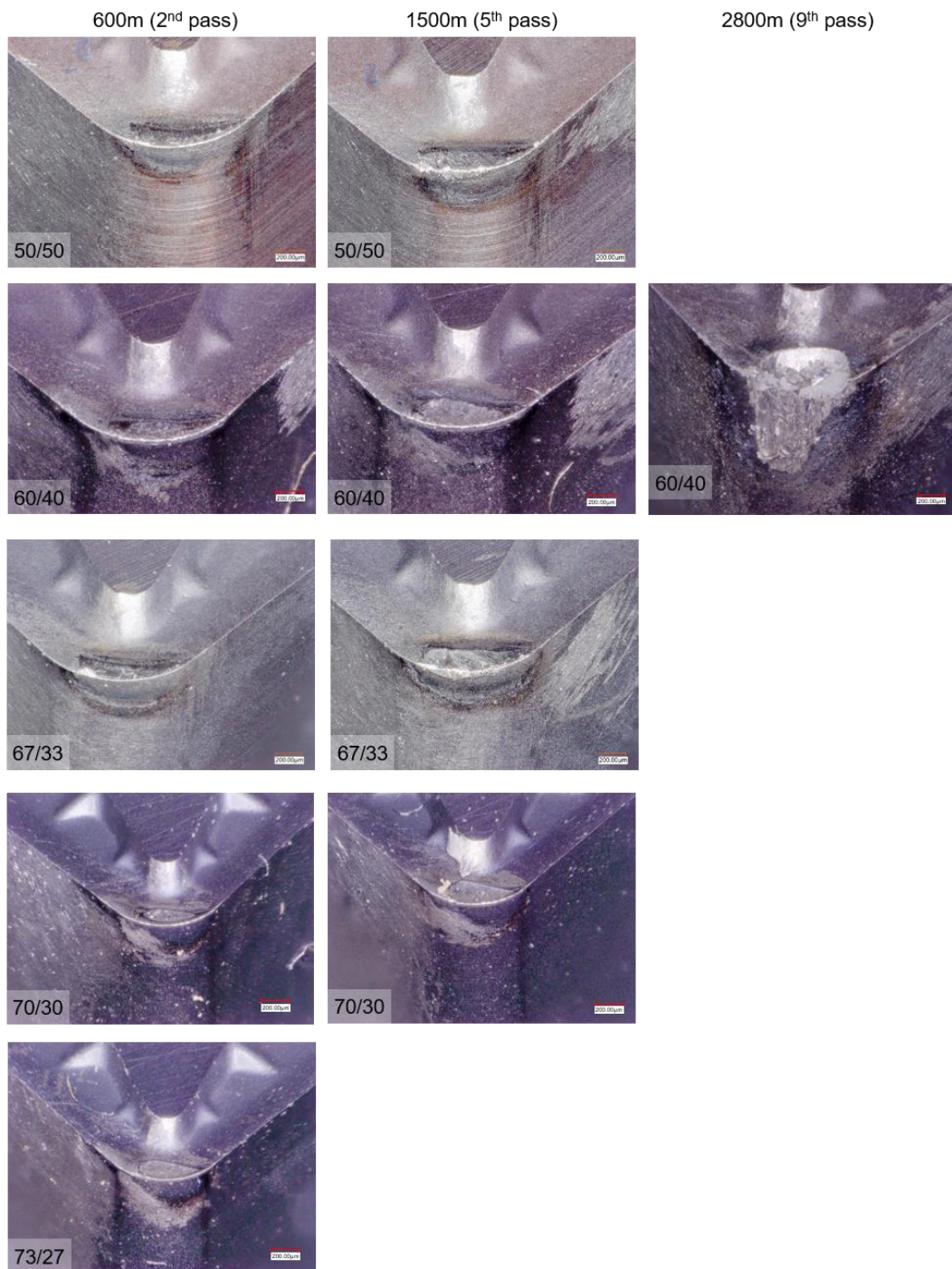
b) Keyence 3D optical images of tools' progress wear modes during machining.

Fig. 3.6. Cutting test results for coated tools with different Al/Ti ratios: 50/50, 60/40, 67/33, 70/30 and 73/27.

The cutting force curve patterns of different Al/Ti ratio coated tools are presented

in Fig. 3.7. All data was obtained over the same period under a relatively stable turning process. The Al60Ti40 coated tool emitted the most stable cutting force signals with a very reduced numbers of peaks and valleys during SS304 machining. However, the vibration amplitude of the cutting force was high in the other inserts. The rest of the Al/Ti ratio tools (especially those with Al content over 67) frequently reached either peaks or valleys during turning. This behavior confirms that high loads applied on a low hardness coating, combined with high cutting temperature, contribute to coating deformation [36]. As the coating begins to deform, material accumulation will drastically alter material flow during cutting, facilitating the generation of BUE. BUE formation at the tool's tip has a direct impact on the cutting force [37,38], since intense BUE at the contact interface of tool and workpiece increases friction at the cutting zone, reflecting in higher forces to produce the cutting process.
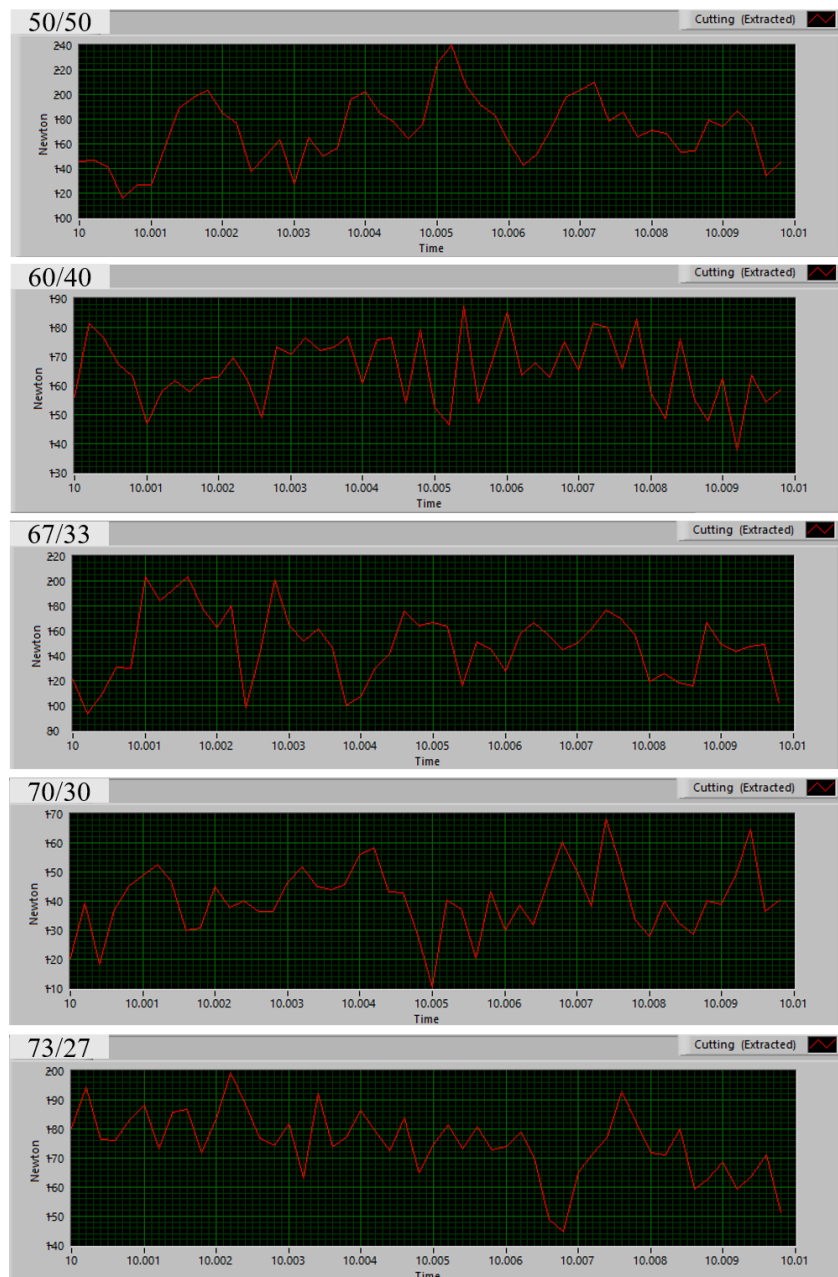
Fig. 3.7. Cutting forces collected for five coated tools during the first pass at a steady state.

3.3.3. Wear mechanism

To understand the wear mechanism which occurs during the ultra-high speed machining of SS304, the best and the worst tool performance were selected to perform a consistent analysis throughout SEM characterization. SEM images of the worn Al/Ti

60/40 and 73/27 cutting tools before and after etching are shown in Fig. 3.8. Machining of austenitic stainless steel under high cutting speeds promoted various interactions within the cutting zone between the tool surface, chip, and workpiece, causing intense tool wear due to both extreme thermal and mechanical loads. In this case, the wear mechanism was a complex combination of abrasion, attrition and diffusion wear for all the tested cutting tools. Literature indicates that unstable attrition wear plays a crucial role during the machining of austenitic stainless steel, resulting in material adhesion and subsequent extreme BUE formation and sharp cutting edges chipping [39]. A high cutting speed should be applied to reduce the intensity of the BUE, by accelerating the material removal rate. As mentioned above, the standard method for determining cutting edge wear resistance is to measure the resulting wear mark width below the main cutting edge on the tool flank face. However, at a high cutting speed, the crater wear on the rake face needs to be considered and quantified as well. Cratering takes place inside a zone in which the chip actually contacts with the cutting insert during machining, which leads to intensive heat generation and extreme shear forces [40]. As shown in Fig. 3.8, crater wear predominates over flank wear during high-speed machining of stainless steel in causing ultimate tool failure. In all cases, the coating has been removed at an initial stage of the cutting test and the exposed surface of the substrate was affected by a combination of abrasive, diffusion, and chemical wear. Consequently, the cobalt binder in the cemented carbide is subject to thermal softening due to the intense temperature in the cutting zone and was thus removed at a higher rate during the cutting process [41]. As confirmed in Fig. 3.8, the Al73Ti27 coated insert exhibited the most intense chipping. Because of the strong adhesion of the workpiece on the tool, chipping wear was attributed to BUE formation. In this case, the relatively soft coating is prone to

delamination (scratch test result) and as such, could not sustain the heavy loads and high temperatures present within the cutting zone. It started to fail as soon as fragments of the tool edge were carried away by the detaching BUE, which resulted in substrate exposure and subsequent severe crater wear.

On the other hand, the insert coated with Al60Ti40 exhibited a uniform circular shaped crater wear. Although the moderate Al content could not provide the best oxidation resistance, this was far outweighed by the higher hardness compared to the coatings with a higher Al content. The Al60Ti40 coating system was found to provide an overall optimal balance between hardness, oxidation resistance and good adhesion, which improved the wear resistance and has led to the best tool life.
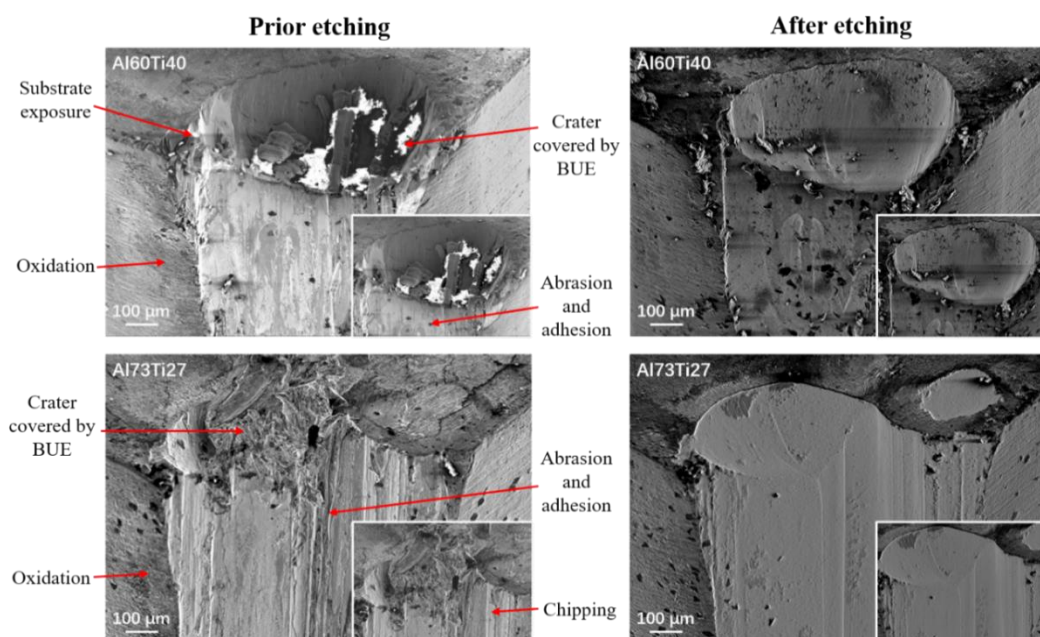
Fig. 3.8. SEM images of tool wear at the end of tool life prior to and after the etching process: Al60Ti40 (cutting length 2800 m) and Al73Ti27 (cutting length 1000 m).

Fig. 3.9 shows the EDS element map data of the worn tools at the end of tool life.

The element maps obtained from all AlTiN PVD coated tools indicated that a significant amount of workpiece (stainless steel) has adhered to both the flank and the rake surface of the tool (see Fe and Cr signals). The presence of Fe and Cr also suggested the formation of iron and chromium oxides along the flank wear of the tool. Such oxides are composites that are naturally contained in BUE structures [15]. It is worth mentioning that the strong signal of Fe/Cr above the tool rake face in the Al/Ti 73/27 insert provided evidence for a large amount of workpiece adhesion, which caused intensive BUE to form and consequently detach, in turn leading to chipping on the tool flank face. The image also indicated substrate exposure because of the Al signal absence (from AlTiN coating) but a strong W signal (WC substrate). This finding is in a strong agreement with experimental observations of the tool wear, which showed that the coating detached from the chip/tool interface as the tungsten carbide substrate became visible. However, a weaker W signal compared to that of Fe/Cr, has proven that the exposed substrate was rapidly covered by a BUE due to strong metal flow over the substrate, which resulted in severe adhesion.
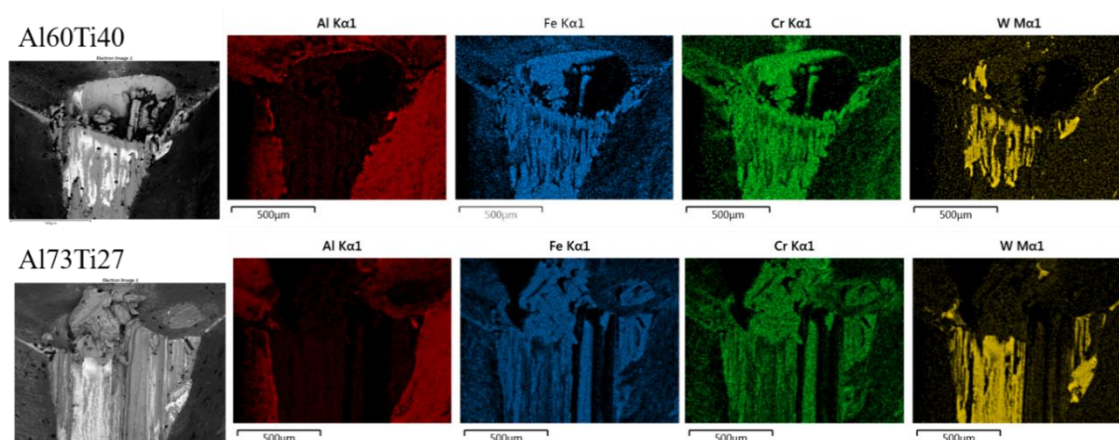
Fig. 3.9. EDS elemental maps of worn areas at the end of tool life: Al60Ti40 (cutting length 2800 m) and Al73Ti27 (cutting length 1000 m).

To quantify the tool wear condition of the cutting inserts, Alicona was used to measure the BUE and worn volume after tool failure, before and after the etching of the worn tool, respectively. The minimum and maximum deviations of the unused reference tool obtained by Alicona in 3D tool wear statistics were measured with an accuracy of 95 %. These data confirm the minimal and maximal variation below and above the original plane. The size of BUE generated at the end of the tool life and total wear volume of each cutting tool after the etching are shown in Fig. 3.10. The Al50Ti50 coated tool had the highest BUE, followed by the Al73Ti27 tool. The other three insets exhibited a lower volume of BUE formation, with small deviation. The formation of an unstable built-up structure has resulted in its detachment and corresponding cutting-edge chipping. Fracture of the BUE also brought away pieces of the cutting edge from the insert, which exacerbated chipping on the tool cutting edge. On the other hand, as can be seen from the wear damage on the cutting edge, Al60Ti40 exhibited a significantly lower wear volume as compared to the other four inserts. Numerical wear statistics data confirmed that the tool edge failure of the Al60Ti40 coated tool was lower than that of the other four studied coatings. This coating is therefore proven to have the superior and more effective tool performance during ultra-high speed turning of SS304.
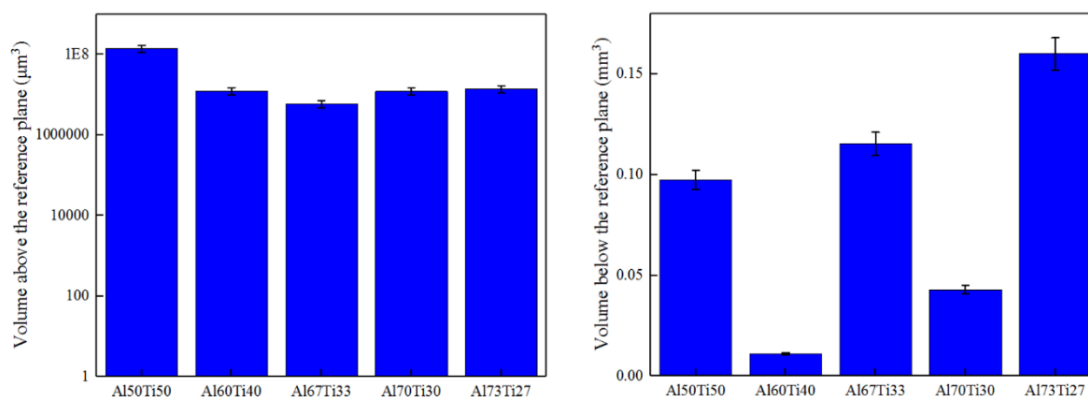
Fig. 3.10. The deviations of BUE and wear volume with the unworn reference plane.

3.3.4. Tribological characterization

One of the major ways of evaluating the tribological conditions during the cutting process is through the chip formation process. The chip flow process can reveal the tribological characteristics of the deformed workpiece material for assessing the frictional characteristics at the tool/chip interface [3]. In this study, chips were collected at the initiation stage of the cutting length of 5 m. The SEM images of the general chip shapes, undersurface morphology and shear band are shown in Fig. 3.11. The Al60Ti40 chip and Al70Ti30 chip had the most curled shape out of the five studied chips. However, the chips produced by Al/Ti 60/40 coated tools had a smoother undersurface. This means that the chip flow in the cutting zone is hastened since there is the lowest friction at the rake surface of the tool [39]. All the other four chips, by comparison, showed readily evident intense chip sticking to the tool, resulting in tearing at the chips' undersurface and subsequent intense friction. Such tearing thus suggests that the metal flow at the interface between tool and chip is strongly arrested.

In addition, the chips' shear band images (Fig. 3.11) show that the curved segments in each insert were slightly different. While all of the chips studied had a conventional

lamellar structure, as a result of the extreme friction conditions at the tool-chip interface, the spacing on the chip shear band between the segments is inconsistent for Al/Ti 50/50, 70/30 and 73/27 chips. In contrast, chips produced by Al60Ti40 and Al67Ti33 coated tools generally exhibited a similar and regular lamellar structural pattern and spacing between the adjacent segments. Nevertheless, fracture patterns in the Al67Ti33 chip were obviously showed on the entire surface of the lamellar chip shear band, due to the combined effect of high-speed sliding and friction conditions between the tool and the chip.
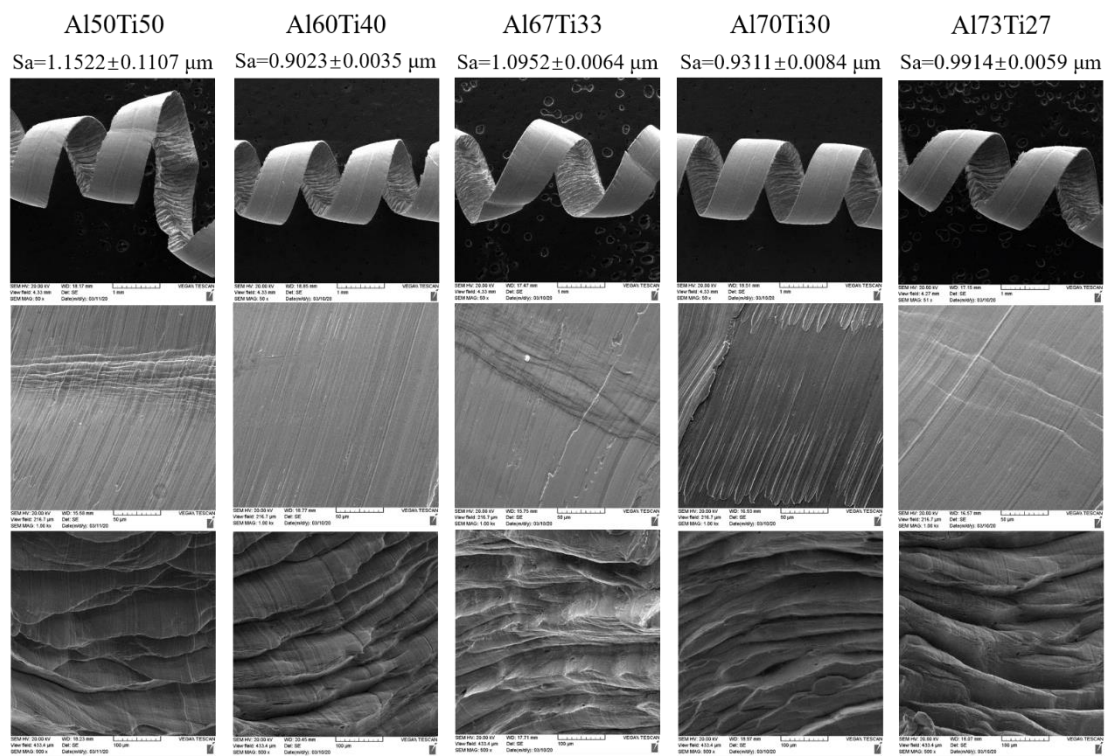
Fig. 3.11. Chip characteristics: generation shape, undersurface, shear band and surface average of the chips.

Cutting forces were obtained during all cutting tests to determine the specific energy and friction coefficient for the cutting. This was done to provide an

understanding of the tribological features of the interface between tool and workpiece [42]. Fig. 3.12 provides a general relation of the Al/Ti ratio with the friction coefficient and specific cutting energy with all of the various AlTiN PVD coatings. The results indicated that there was a substantial enhancement of the friction conditions at the tool/chip/workpiece interface after the Al/Ti 60/40 coated tool was used for machining since it had the lowest friction coefficient μ. The specific cutting energy is defined as the total energy required to cut a unit volume of material from the workpiece [43]. It is considered an important index of the machinability of the material and allows to get a greater understanding of the whole cutting process. Apart from the lowest and most stable cutting force (as shown in Fig. 3.7), Al60Ti40 coated tool also had the lowest specific cutting energy. Moreover, Fig. 3.12 illustrates that the actual tool-chip contact length (TCCL) is also determined by the friction conditions in the cutting zone. Under all tested conditions, the Al/Ti 60/40 coating had a minimal contact length which greatly reduced wear on the tool. One more crucial aspect is that in the Al60Ti40 sample the chip sliding velocity had raised, suggesting that this coating speeded up the process of metal flow.

The reason for this outstanding friction performance of the Al60Ti40 tool can be ascribed to the optimal combination of its mechanical properties. Since this coating system has a good balance of H/E, it is capable of better dissipating the specific cutting energy generated during machining. Thus, the Al60Ti40 coating was able to better protect the insert and postpone the substrate exposure, leading to an extension of the tool life. In addition, with a suitable Al/Ti ratio, this coating was capable of generating lubricious tribo-films with balanced Al and Ti oxides, which provided superior oxidation resistance [44,45]. Moreover, intense heat generated during ultra-high speed

machining results in strong diffusion wear, and therefore, a high hot hardness is needed to sustain the coating's mechanical properties at such high temperatures. In this case, the suitable chemical composition with the favorable mechanical properties of the Al/Ti 60/40 coating enhance its hot hardness property, which affects the tribological characteristics during cutting, providing a good balance of wear resistance and oxidation resistance, then resulting in the longest tool life.
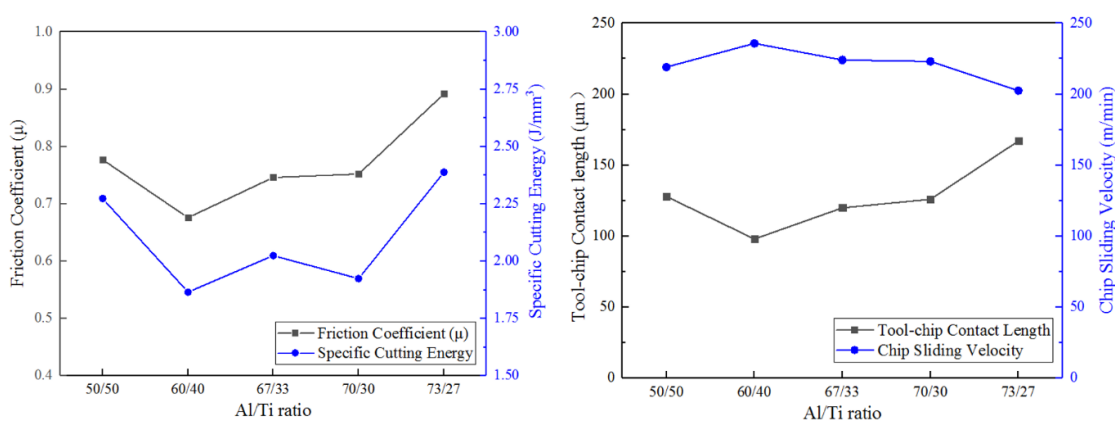
Fig. 3.12. Tribological characteristics of different Al/Ti ratio coatings in the cutting zone: friction coefficient μ and specific cutting energy; TCCL and chip sliding velocity.

Table 3.4 summarizes data regarding chip characteristic studies for different Al/Ti ratios coatings, such as chip thickness, chip compression ratio, chip shear angle, chip sliding velocity and friction coefficient μ. Based on the numerical analysis, chip compression ratio (CCR closer to 1), shear angle (closer to 45°) and chip sliding velocity of the Al/Ti 60/40 coating were all superior to those of the other studied coatings. All data obtained from both SEM photographs and comparative trends show that the chip characteristics with the Al60Ti40 coated tool machining were improved.

Table 3.4. Results of the chip characteristic studies for different Al/Ti ratios coatings.

Al/Ti ratio	Chip thickness (mm)	Tool-chip Contact Length (mm)	Chip Compression Ratio - CCR	Φ - Shear Angle (°)	β - Friction Angle (°)	ϒ - Shear Strain	Chip Sliding Velocity (m/min)	Friction Coefficient (μ)
50/50	0.286	0.128	0.522	28.57	21.43	1.68	219.15	0.777
60/40	0.266	0.098	0.562	30.47	19.53	1.53	235.88	0.676
67/33	0.280	0.120	0.534	29.14	20.86	1.64	224.12	0.746
70/30	0.281	0.126	0.531	29.02	20.98	1.65	223.10	0.752
73/27	0.310	0.167	0.482	26.63	23.37	1.85	202.53	0.892

Based on this analysis, both undersurface and shear band image (Fig. 3.11) confirmed that Al60Ti40 chip has the smoothest undersurface morphology. This illustrates that during the chip flow, the Al60Ti40 chip can be formed under a high shear level which improves chip development through accelerating the chip deformation process. Therefore, it can be concluded that the Al60Ti40 coated tool minimised friction and dramatically improved overall tool life (as shown in Fig. 3.6).

3.4. Conclusions

In this paper, five different compositions of arc PVD AlTiN coatings with different Al/Ti ratios (50/50, 60/40, 67/33, 70/30 and 73/27) were investigated during ultra-high speed machining (420 m/min) of stainless steel 304. It was found that superior tool life as well as tribological and wear performance were achieved by the Al60Ti40 coating whose Al content is well below the threshold composition required for the formation of the hexagonal wurtzite phase. In addition, the beneficial combination of hot hardness and mechanical properties of Al60Ti40 made it well suited for this application. As such, the following conclusions from this analysis can be drawn:

1. Analysis of wear performance showed that intensive crater wear has led to tool failure instead of regularly observed flank wear as a result of intense temperatures generated on the tool rake face under ultra-high cutting speeds, which causes diffusion and consequent intensive chemical wear. The Al60Ti40 coated tool exhibited the longest tool life.

2. An excess of Al composition in AlTiN coatings has led to a significant reduction of the hardness values from about 37 GPa to below 25 GPa. This in turn, resulted in poor performance of the AlTiN coatings with an Al/Ti ratio of 67/33, 70/30 and 73/27 during ultra-high speed turning of adhesive material (high shear force and heat generation).

3. Expected high oxidation resistance of the coating layer along with the high Al content (over 67) was not a decisive factor under the considered conditions. On the other hand, the optimal combination of superior substrate adhesion and high hardness, the Al60Ti40 coating rendered capable of stabilizing the worn area around the crater. Therefore, the crater's depth could grow evenly with moderate flank wear, resulting in the longest tool life.

4. Chip characterization of the Al/Ti 60/40 coating showed the smoothest chip undersurface with the lowest surface average. The uniformed lamellar shear band confirmed that this chip was formed by accelerating the deformation within the chip during the chip flow. This is an indication of a lower intensity of friction between the tool/chip interface being achieved by the enhanced mechanical properties of the Al60Ti40 coating. The superior tool life of this coating can be attributed to these properties.

Based on the results of this turning test, the AlTiN coatings are suitable for ultra-

high speed turning of stainless steel if an optimal compositional balance between hardness and adhesion is reached.

3.5. References

[1]   J.L. Endrino, G.S. Fox-rabinovich, C. Gey, Hard AlTiN , AlCrN PVD coatings for machining of austenitic stainless steel, 200 (2006) 6840–6845. https://doi.org/10.1016/j.surfcoat.2005.10.030.

[2]   A.M. K. Holmberg, Chapter 5 Coating Characterization and Evaluation, in: K. Holmberg, A. Matthews (Eds.), Coat. Tribol. Princ. Tech. Appl. Surf. Eng., Elsevier, 1994: pp. 257–308. https://doi.org/https://doi.org/10.1016/S0167-8922(08)70755-7.

[3]   E.M. Trent, P.K. Wright, Metal Cutting, 2000. https://doi.org/10.1016/B978-075067069-2/50012-7.

[4]   Q.F.T. Wang, Y.L.Z. Wu, T. Zhang, T. Li, Microstructure and Corrosion Resistance of the AlTiN Coating Deposited by Arc Ion Plating, Acta Metall. Sin. (English Lett. 29 (2016) 1119–1126. https://doi.org/10.1007/s40195-016-0497-8.

[5]   X. Wang, P.Y. Kwon, D. Schrock, D. (Dae-W. Kim, Friction coefficient and sliding wear of AlTiN coating under various lubrication conditions, Wear. 304 (2013) 67–76. https://doi.org/https://doi.org/10.1016/j.wear.2013.03.050.

[6]   L. Chen, J. Paulitsch, Y. Du, P.H. Mayrhofer, Thermal stability and oxidation resistance of Ti–Al–N coatings, Surf. Coatings Technol. 206 (2012) 2954–2960. https://doi.org/https://doi.org/10.1016/j.surfcoat.2011.12.028.

[7]   J. Peng, D. Su, C. Wang, Combined Effect of Aluminum Content and Layer Structure on the Oxidation Performance of Ti1−xAlxN Based Coatings, J. Mater. Sci.   Technol.   30   (2014)   803–807. https://doi.org/https://doi.org/10.1016/j.jmst.2014.03.020.

[8]   T. Polcar, A. Cavaleiro, High temperature properties of CrAlN, CrAlSiN and AlCrSiN coatings – Structure and oxidation, Mater. Chem. Phys. 129 (2011) 195–201. https://doi.org/https://doi.org/10.1016/j.matchemphys.2011.03.078.

[9]   B.D. Beake, J.F. Smith, A. Gray, G.S. Fox-rabinovich, S.C. Veldhuis, J.L. Endrino, Investigating the correlation between nano-impact fracture resistance and hardness / modulus ratio from nanoindentation at 25 – 500 ° C and the fracture resistance and lifetime of cutting tools with Ti 1 − x Al x N (x = 0 . 5 and 0 . 67) PVD coatings in, 201 (2007) 4585–4593. https://doi.org/10.1016/j.surfcoat.2006.09.118.

[10]   G.S. Fox-Rabinovich, B.D. Beake, J.L. Endrino, S.C. Veldhuis, R. Parkinson, L.S. Shuster, M.S. Migranov, Effect of mechanical properties measured at room and elevated temperatures on the wear resistance of cutting tools with TiAlN and AlCrN coatings, Surf. Coatings Technol. 200 (2006) 5738–5742. https://doi.org/https://doi.org/10.1016/j.surfcoat.2005.08.132.

[11]   C. He, J. Zhang, G. Song, G. Ma, Z. Du, J. Wang, D. Zhao, Microstructure and mechanical properties of reactive sputtered nanocrystalline (Ti,Al)N films, Thin Solid Films. 584 (2015) 192–197. https://doi.org/https://doi.org/10.1016/j.tsf.2014.12.027.

[12]   G.S. Fox-Rabinovich, A.I. Kovalev, M.H. Aguirre, B.D. Beake, K. Yamamoto, S.C. Veldhuis, J.L. Endrino, D.L. Wainstein, A.Y. Rashkovskiy, Design and performance of AlTiN and TiAlCrN PVD coatings for machining of hard to cut materials, Surf. Coatings Technol. 204 (2009) 489–496. https://doi.org/10.1016/j.surfcoat.2009.08.021.

[13]   J.L. Endrino, G.S. Fox-Rabinovich, A. Reiter, S. V Veldhuis, R.E. Galindo, J.M.

Albella, J.F. Marco, Oxidation tuning in AlCrN coatings, Surf. Coatings Technol. 201 (2007) 4505–4511. https://doi.org/https://doi.org/10.1016/j.surfcoat.2006.09.089.

[14] L. Aihua, D. Jianxin, C. Haibing, C. Yangyang, Z. Jun, Friction and wear properties of TiN, TiAlN, AlTiN and CrAlN PVD nitride coatings, Int. J. Refract. Met. Hard Mater. 31 (2012) 82–88. https://doi.org/https://doi.org/10.1016/j.ijrmhm.2011.09.010.

[15] Q. He, J.M. Paiva, J. Kohlscheen, B.D. Beake, S.C. Veldhuis, An integrative approach to coating / carbide substrate design of CVD and PVD coated cutting tools during the machining of austenitic stainless steel, 46 (2020) 5149–5158. https://doi.org/10.1016/j.ceramint.2019.10.259.

[16] J. Xiong, Z. Guo, M. Yang, W. Wan, G. Dong, Tool life and wear of WC–TiC–Co ultrafine cemented carbide during dry cutting of AISI H13 steel, Ceram. Int. 39 (2013) 337–346. https://doi.org/https://doi.org/10.1016/j.ceramint.2012.06.031.

[17] G. Östberg, K. Buss, M. Christensen, S. Norgren, H.-O. Andrén, D. Mari, G. Wahnström, I. Reineck, Mechanisms of plastic deformation of WC–Co and Ti(C, N)–WC–Co, Int. J. Refract. Met. Hard Mater. 24 (2006) 135–144. https://doi.org/https://doi.org/10.1016/j.ijrmhm.2005.04.009.

[18] S. Luyckx, The Hardness of Tungsten Carbide-Cobalt Hardmetal, in: Handb. Ceram. Hard Mater., John Wiley & Sons, Ltd, 2008: pp. 946–964. https://doi.org/10.1002/9783527618217.ch23.

[19] ISO 4499-2:2008, Hardmetals — Metallographic determination of microstructure — Part 2: Measurement of WC grain size, (n.d.).

[20] J. García, V.C. Ciprés, A. Blomqvist, B. Kaplan, Cemented carbide microstructures: a review, Int. J. Refract. Met. Hard Mater. 80 (2019) 40–68. https://doi.org/https://doi.org/10.1016/j.ijrmhm.2018.12.004.

[21] T. Ishigaki, S. Tatsuoka, K. Sato, K. Yanagisawa, K. Yamaguchi, S. Nishida, Influence of the Al content on mechanical properties of CVD aluminum titanium nitride coatings, Int. J. Refract. Met. Hard Mater. 71 (2018) 227–231. https://doi.org/https://doi.org/10.1016/j.ijrmhm.2017.11.028.

[22] P. Panjan, M. Cekada, Growth defects in PVD hard coatings Growth defects in PVD hard coatings, Vaccum. 84 (2009) 209–214. https://doi.org/10.1016/j.vacuum.2009.05.018.

[23] Z.H. Barber, The Structure of Vapor-Deposited Materials, in: Ref. Modul. Mater. Sci. Mater. Eng., Elsevier, 2016. https://doi.org/https://doi.org/10.1016/B978-0-12-803581-8.03333-6.

[24] M. Peters, B. Saruhan-Brings, U. Schulz, Advanced Coatings for rotating Aero Engines, in: 2009.

[25] K. Bobzin, T. Brögelmann, C. Kalscheuer, T. Liang, Post-annealing of (Ti,Al,Si)N coatings deposited by high speed physical vapor deposition (HS-PVD), Surf. Coatings Technol. 375 (2019) 752–762. https://doi.org/https://doi.org/10.1016/j.surfcoat.2019.06.100.

[26] G.Q. Yu, B.K. Tay, S.P. Lau, K. Prasad, L.K. Pan, J.W. Chai, D. Lai, Effects of N ion energy on titanium nitride films deposited by ion assisted filtered cathodic vacuum arc, Chem. Phys. Lett. 374 (2003) 264–270. https://doi.org/https://doi.org/10.1016/S0009-2614(03)00719-X.

[27] M. Falsafein, F. Ashrafizadeh, A. Kheirandish, Influence of thickness on

adhesion of nanostructured multilayer CrN/CrAlN coatings to stainless steel substrate, Surfaces and Interfaces. 13 (2018) 178–185. https://doi.org/https://doi.org/10.1016/j.surfin.2018.09.009.

[28] A. Leyland, A. Matthews, On the significance of the H/E ratio in wear control: a nanocomposite coating approach to optimised tribological behaviour, Wear. 246 (2000) 1–11. https://doi.org/https://doi.org/10.1016/S0043-1648(00)00488-9.

[29] L.A. Espitia, H. Dong, X.-Y. Li, C.E. Pinedo, A.P. Tschiptschin, Scratch test of active screen low temperature plasma nitrided AISI 410 martensitic stainless steel, Wear. 376–377 (2017) 30–36. https://doi.org/https://doi.org/10.1016/j.wear.2017.01.091.

[30] T. Li, M. Li, Y. Zhou, Phase segregation and its effect on the adhesion of Cr–Al–N coatings on K38G alloy prepared by magnetron sputtering method, Surf. Coatings Technol. 201 (2007) 7692–7698. https://doi.org/https://doi.org/10.1016/j.surfcoat.2007.02.044.

[31] B.-J. Xiao, Y. Chen, W. Dai, K.-Y. Kwork, T.-F. Zhang, Q.-M. Wang, C.-Y. Wang, K.H. Kim, Microstructure, mechanical properties and cutting performance of AlTiN coatings prepared via arc ion plating using the arc splitting technique, Surf. Coatings Technol. 311 (2017) 98–103. https://doi.org/https://doi.org/10.1016/j.surfcoat.2016.12.074.

[32] A. Kleinbichler, M.J. Pfeifenberger, J. Zechner, S. Wöhlert, M.J. Cordill, Scratch induced thin film buckling for quantitative adhesion measurements, Mater. Des. 155 (2018) 203–211. https://doi.org/https://doi.org/10.1016/j.matdes.2018.05.062.

[33] A.A. Voevodin, J.S. Zabinski, Load-adaptive crystalline–amorphous

nanocomposites, J. Mater. Sci. 33 (1998) 319–327. https://doi.org/10.1023/A:1004307426887.

[34] S. Zhang, D. Sun, Y. Fu, H. Du, Effect of sputtering target power on microstructure and mechanical properties of nanocomposite nc-TiN/a-SiNx thin films, Thin Solid Films. 447–448 (2004) 462–467. https://doi.org/https://doi.org/10.1016/S0040-6090(03)01125-8.

[35] Y.X. Wang, S. Zhang, Toward hard yet tough ceramic coatings, Surf. Coatings Technol. 258 (2014) 1–16. https://doi.org/https://doi.org/10.1016/j.surfcoat.2014.07.007.

[36] A.M. El-Tamimi, T.M. El-Hossainy, Investigating the Tool Life, Cutting Force Components, and Surface Roughness of AISI 302 Stainless Steel Material Under Oblique Machining, Mater. Manuf. Process. 23 (2008) 427–438. https://doi.org/10.1080/10426910801974846.

[37] S. Sukvittayawong, I. Inasaki, Detection of built-up edge in turning process, Int. J. Mach. Tools Manuf. 34 (1994) 829–840. https://doi.org/https://doi.org/10.1016/0890-6955(94)90062-0.

[38] V. Sivaraman, S. Sankaran, L. Vijayaraghavan, The Effect of Cutting Parameters on Cutting Force During Turning Multiphase Microalloyed Steel, 4 (2012) 157–160. https://doi.org/10.1016/j.procir.2012.10.028.

[39] A. Biksa, K. Yamamoto, G. Dosbaeva, S.C. Veldhuis, G.S. Fox-rabinovich, A. Elfizy, T. Wagg, L.S. Shuster, Tribology International Wear behavior of adaptive nano-multilayered AlTiN / Me x N PVD coatings during machining of aerospace alloys, Tribiology Int. 43 (2010) 1491–1499. https://doi.org/10.1016/j.triboint.2010.02.008.

[40]   J. Kohlscheen, C. Bareiss, Effect of Hexagonal Phase Content on Wear Behaviour of AlTiN Arc PVD Coatings, (2018). https://doi.org/10.3390/coatings8020072.

[41]   D. Jianxin, Z. Jiantou, Z. Hui, Y. Pei, Wear mechanisms of cemented carbide tools in dry cutting of precipitation hardening semi-austenitic stainless steels, Wear. 270 (2011) 520–527. https://doi.org/https://doi.org/10.1016/j.wear.2011.01.006.

[42]   M. Shaw, Metal cutting principles, 2°, Oxford Unversity Press, New York, 2005.

[43]   W. Polini, S. Turchetta, Force and specific energy in stone cutting by diamond mill, Int. J. Mach. Tools Manuf. 44 (2004) 1189–1196. https://doi.org/https://doi.org/10.1016/j.ijmachtools.2004.04.001.

[44]   J.L. Mo, M.H. Zhu, Tribological oxidation behaviour of PVD hard coatings, Tribol. Int. 42 (2009) 1758–1764. https://doi.org/https://doi.org/10.1016/j.triboint.2009.04.026.

[45]   Q. Zhang, Y. Xu, T. Zhang, Z. Wu, Q. Wang, Tribological properties, oxidation resistance and turning performance of AlTiN/AlCrSiN multilayer coatings by arc ion plating, Surf. Coatings Technol. 356 (2018) 1–10. https://doi.org/https://doi.org/10.1016/j.surfcoat.2018.09.027.

Chapter 4: Analysis of the performance of PVD AlTiN coating with five different Al/Ti ratios during the high-speed turning of stainless steel 304 under dry and wet cooling conditions

Qianxi He[1], Jose M. Paiva[1,2], Joern Kohlscheen[3], and Stephen C. Veldhuis[1]

1- McMaster Manufacturing Research Institute, McMaster University, Hamilton, L8S4L8, Canada

2- Engineering Graduate Program – PPGEM, Pontificia Universidade Católica do Paraná, Curitiba, 80215901, Brazil

3- Kennametal Shared Services Gmbh, Altweiherstr 27-31, 91320, Ebermannstadt, Germany

∗ Corresponding author: paivajj@mcmaster.ca (Jose M. Paiva).

Author's Contribution

Qianxi He	Designed and conducted the experiments
	Analyzed the results.
	Wrote the manuscript.
Jose M. Paiva	Assisted with designing the research methodology.
	Assisted with writing and editing the manuscript.
Joern Kohlscheen	Deposited the coating.
Stephen C. Veldhuis	Supervised the project.

Abstract

High-speed machining of austenitic stainless steel normally causes significant tool damage and generates reduced tool life. In this paper, five AlTiN PVD coatings with different Al/Ti atomic ratios (50/50, 60/40, 67/33, 70/30 and 73/27) which deposited on cemented carbide inserts were used to conduct high-speed of 370 m/min finish turning tests. The experiments were carried out under different cooling conditions (dry and wet) on SS304 to study the tribological behavior of the AlTiN coatings with different Al/Ti ratios and the effect of the coolant under such aggressive cutting conditions. During the experiments, tool life, cutting force, wear mechanism, friction condition and surface integrity of machined workpiece were investigated. Crater wear was found to be the predominant wear mode during the cutting test, while the complex combination of oxidation, abrasion/attrition, adhesion, and chipping contributed to the tool failure. Given the machining conditions proposed in this study, the results revealed that all coated inserts possessed an improved friction behavior in the wet cutting condition. Compared to the dry machining, all five coatings had exhibited 2-3 times longer tool life. The AlTiN coated insert (Al/Ti = 60/40), in particular, exhibited a cutting length of almost 7,000 m, compared to 1,000 m for the AlTiN coated insert (Al/Ti = 73/27).

Keywords

4.1. Introduction

The excellent corrosion resistance of austenitic stainless steels makes them ideal for chemical, mechanical and medical industrial applications [1]. However, due to their high Ni and Cr content, the machining of austenitic stainless steel tends to be carried out under excessive temperatures and cutting forces [2], and has a high tendency to produce work-hardening [3,4]. As a result of the workpiece material adhering to the tool cutting edge during cutting operations, the high cutting forces and temperatures generated normally lead to an unpredictable tool wear performance [5]. One of the most prevalently used materials for industrial cutting tool is cemented carbide (WC – Co). Inserts made from this material are resistant to the high temperatures and forces produced during traditional cutting operations [6]. AlTiN coatings are well known for their superior wear performance [7] and advanced oxidation resistance under high temperature conditions [8,9]. These metastable hard coatings generate an Al_2O_3 top layer during the machining process [10], which provides high oxidation resistance and thermal stability at temperatures in excess of 800 °C [11,12]. The amount of Al in AlTiN coatings tends to affect their mechanical properties and crystalline structure. As the concentration of Al in the AlTiN coating is increased, the transition from the cubic structure to the mixed cubic wurtzite structure takes place. A reduction of hardness occurs when the hexagonal AlN begins to predominate over the face-centered cubic TiN phase [13,14].

On the other hand, using cutting fluids during machining process were shown to have significant effects on the cutting tools' lives since it is possible to reduce the temperature at the tool/workpiece interface in the cutting zone [15,16]. Also, the use of coolant could provide lubrication to tool and workpiece, which in turn leads to a longer

tool life [17]. Nevertheless, due to the problems such as environmental pollution, human health, and manufacturing costs, dry machining in some cases could be an optimal solution, to acquire acceptable machining accuracy [18–20]. However, it is difficult to determine the optimal cooling process for certain tool coatings and special workpiece materials, since machining with/without coolant always has their advantages and drawbacks [21].

There are some studies in the literature that concerns the optimization of cutting parameters [22], analysis of tool wear patterns and cutting insert treatments during machining of various stainless steels [20,23]. In addition, some researchers studied the wear mechanism of coated tools under low cutting speed conditions at a range of 100-200 m/min [2,24]. However, there is no research regarding the high-speed machining (over 300 m/min) of stainless steels by AlTiN coated cemented carbide inserts, under wet and dry conditions. In addition to that, a fundamental tribological study is still needed to be performed in order to understand the tribological characteristics of AlTiN PVD coatings with different Al/Ti ratios under different cooling conditions during the high-speed turning of stainless steels. In this study, the authors provided a significant comprehension of the wear performance and the tribological behavior of the different AlTiN PVD coatings applied under harsh conditions. This is the major novelty presented in this work. In order to supplement the aforementioned research gaps, high-speed turning (370 m/min) of austenitic stainless-steel grade 304 (SS304) under both wet and dry process conditions was conducted in this work. An AlTiN coating with five miscellaneous Al/Ti ratios (50/50, 60/40, 67/33, 70/30 and 73/27) was deposited on the cemented carbide (WC – Co) insert separately by an arc ion plating PVD method. The tool life curve and wear performance of different AlTiN coated tools were studied under

two separate cooling conditions, and the tribological characteristics were evaluated in terms of the properties of chip formation. Furthermore, the hardness and microstructure of chip cross-sections, as well as the surface integrity of the machined workpiece were assessed. This contributes to the study of the machinability of stainless steel 304.

The aim of this study is to better understand the wear mechanism of AlTiN coated tools under wet and dry conditions during the high-speed turning of austenitic stainless steel. An analysis of tribological characteristics gives us an insight into the friction conditions between the cutting insert, the chip and the workpiece interfaces within the cutting zone. This is correlated with the tool wear performance and ultimately, the tool life. Moreover, a comparison of the five separate Al/Ti ratios in PVD AlTiN coatings provides a guideline for selecting coatings to be used in further industrial applications.

4.2. Experimental procedure

Five different PVD monolayer AlTiN coatings (with Al/Ti ratio of 50/50, 60/40, 67/33, 70/30, and 73/27) were deposited on a cemented carbide (WC – 6 wt. % Co) substrate using the cathodic arc ion method. The coating deposition process included four stages as follows: heating, ion etching, depositing, and cooling. Argon ion etching was conducted to clean the substrate for 30 minutes at a -200 V bias voltage and a 0.2 Pa pressure. During the deposition process, the temperature of the substrate was 500 °C, the nitrogen flow rate was 3.5 Pa and the deposition time was 3 hours. The turntable can provide up to threefold rotation of the substrates during PVD deposition. The final coating thickness was around 3-4 microns. All of the studied inserts were provided by Kennametal with an ISO catalog number CNGG120408FS and a K313 substrate grade. The basic coating/substrate properties are shown in Table 4.1 [25].

Table 4.1. Properties of AlTiN coated inserts with five different Al/Ti ratios.

AlTiN coated inserts	Al/Ti=50/50	Al/Ti=60/40	Al/Ti=67/33	Al/Ti=70/30	Al/Ti=73/27
Coating thickness (μm)	3.2	3.6	3.4	3.8	4.0
Surface roughness (μm)	0.14	0.16	0.15	0.16	0.15
Hardness (GPa)	37.4	35.2	29.8	26.7	23.7
Cemented carbide Substrate					
Grain size (μm)			1.23		
Hardness (GPa)			22.8		
Density (g/cm3)			14.9		

High-speed turning tests were conducted on an austenitic stainless steel 304 bar, on Nakamura-Tome model SC-450, a high-precision CNC lathe. Cutting parameters are shown in Table 4.2.

Table 4.2. High-speed turning parameters.

Cutting speed, v (m/min)	370
Feed rate, f (mm/rev)	0.15
Depth of cut (mm)	0.5
Cutting operation	Finish
Cutting condition	Wet (7 % semi-synthetic coolant) and Dry
Workpiece material	SS304 bar with Φ 150 mm and L 200 mm

A LabVIEW professional development system (National Instruments, US) was used to collect cutting forces during the machining processes, whose sensor was connected to the tool holder in the lathe. All the cutting forces were collected during the

first pass, which provides a relatively stable environment for all of the inserts during the same cutting period cycle.

3D and flank face optical images of the inserts were taken under a VHX-950F model digital optical microscope (Keyence, Japan) after each pass to catalogue the progress of tool wear. The wear depth on the insert flank face was examined and recorded by the same instrument until it reached 300 μm, which is a tool failure criterion, according to ISO 3685.

The tool wear pattern and the chemical composition at the worn areas were determined after the tool failure. This was detected by a model 6610LV SEM (JEOL, Japan) and EDS (Oxford Instruments, UK). Volumes of tool wear and built-up-edge (BUE) adhering to the tool surface were identified under an Infinite Focus G5 white light interferometry microscope (Alicona, Austria). Laboratory Measurement Module was used to scan the worn tool geometry under 5x magnification and compare it with the new tool geometry. This process was able to generate 3D data and conduct quantitative differences analysis. The etching process was conducted to reveal the extent of cratering on the insert that was found by both SEM and Alicona microscopes. A 2:1 liquid mixture of hydrochloric and nitric acids (HCL and HNO_3) was used for the etching process. All of the worn inserts were put inside the container with this solution for around 20 min to remove the BUE.

Chips cut by each tool were collected during the first pass to appraise the tribological characteristics at the tool/workpiece interface and to assess tool performance during high-speed turning operations. SEM (VEGA, Tescan) images depicted the general chip curl, the undersurface and morphology of the shear band, also the chip cross-section microstructure. In addition, a chip cross-section analysis was

conducted to determine the micro-hardness, chip thickness and to obtain relevant numerical data. Chips were mounted vertically in epoxy resin and polished by an auto-polisher which used #1200 and #2400 SiC sandpaper, followed by water-free 9 μm, 6 μm, 3 μm and 1 μm diamond grinding suspension. Kalling's 2 reagent was used to etch the chip cross-section. A nano-indentation tester (NHT3, Anton Paar) paired with a Vickers indenter was used to measure the micro-hardness of the chip cross-section. A maximum linear load of 5 mN, with a loading/unloading rate of 10 mN/min and a 5 second creep time was applied. An average of the hardness measurements on the tip, middle and edge of the chips was obtained, respectively.

Finally, a surface integrity study was conducted on the machined workpiece after the first turning path. Surface topography and average roughness are the two important indices to characterize the surface integrity of the machined SS304. The length of the sample was 10 mm on the SS304 bar for each cutting tool and cooling condition. The Alicona microscope was also used to measure the machined workpiece surface average roughness and to show the surface texture. SEM (VEGA, Tescan) was used to identify the workpiece surface topography. The area of the examined workpiece material was a 3 mm x 3 mm square, with a data accuracy of 95 percent.

4.3. Results and discussion

4.3.1. High-speed cutting tests

Fig. 4.1 depicts the tool life curve with the growth of flank wear during the turning tests in wet and dry conditions. The tool wear pattern at the end of life can be viewed in the Alicona 3D image. In general, all AlTiN PVD coated tools underwent a catastrophic failure, and the wear mechanism was identified to be a combination of abrasion, attrition and adhesion with an intensive formation of BUE. The latter ended up causing chipping

on the tool flank face [26], as can be seen in the Alicona image. The AlTiN coated insert (Al/Ti = 60/40) exhibited the maximum tool life in both cutting conditions, whereas the AlTiN coated insert (Al/Ti = 73/27) featured the worst wear performance. A favorable balance between mechanical properties and chemical composition of the AlTiN coating (Al/Ti = 60/40) is considered to be the main reason for its superior wear resistance under the intense temperatures of high-speed machining, which had resulted in the longest tool life [25].

Another important observation is that all of the coated tools experienced a significant improvement in cutting length in the wet condition during machining, of at least twice as long as in the dry condition. It is worth noting that the AlTiN coated insert (Al/Ti = 60/40) featured the longest tool life in either case: a cutting length of almost 7,000 m with coolant and around 2,500 m without.
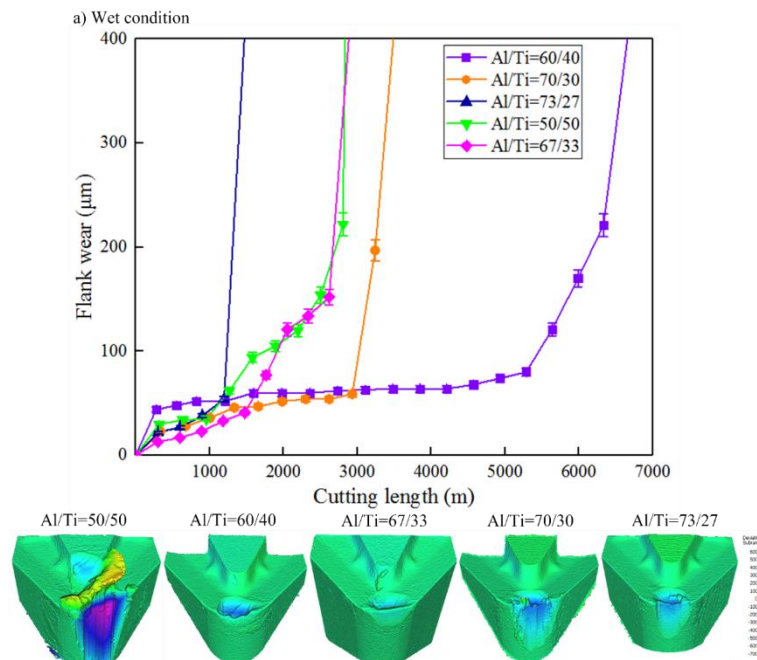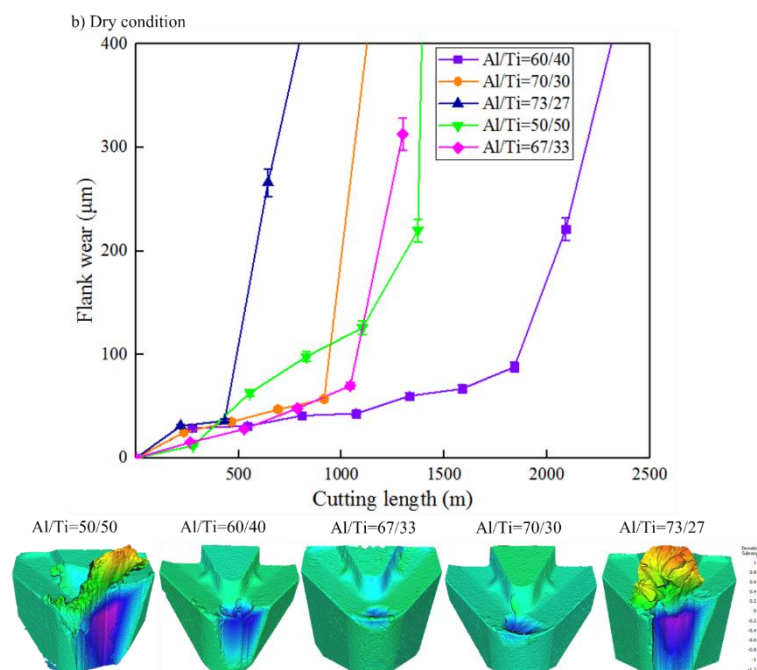
Fig. 4.1. The cutting length curve and Alicona 3D images of worn inserts (at the end of tool life) coated with AlTiN coatings with five different Al/Ti ratios. Performance tests were performed under a) wet and b) dry conditions.

The cutting forces experienced by inserts coated with AlTiN coatings with five different Al/Ti atomic ratios and performed under wet and dry conditions are shown in Fig. 4.2. In general, the cutting forces under the dry condition were lower than those under the wet condition. During dry machining, temperature generated at the cutting zone was higher than in the wet condition. In this case, an Al_2O_3 layer had rapidly formed to protect the tool, which stabilized the cutting environment during the first pass [12,27] and resulted in a relatively lower cutting force.

In addition, the lowest cutting force exhibited by the AlTiN coated insert (Al/Ti = 60/40) could be partially attributed to its stable chemical composition which provided a balance of hot hardness and oxidation resistance. By the time the coating begins to deform under the high temperature and heavy load, the accumulation of material has

altered the metal flow during cutting, accelerating the BUE formation [28] and thereby directly affecting the cutting force [29,30]. The preferable balance of the AlTiN (Al/Ti = 60/40) coating system's mechanical properties contributed to a reduction of BUE formation as well as the cutting force value.
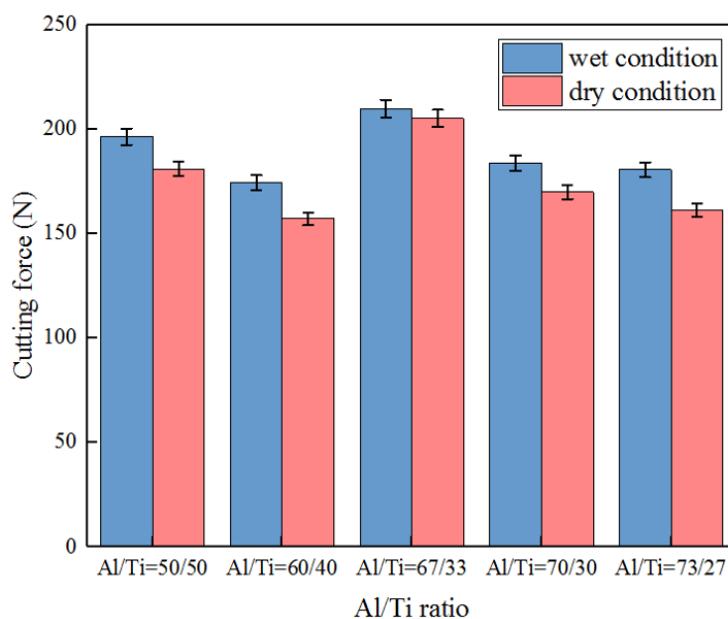
Fig. 4.2. The cutting force of AlTiN coated inserts with five different Al/Ti ratios during the first pass under wet and dry conditions.

4.3.2. Tool wear mechanism

Optical images of the tool wear progress in Fig. 4.3 help provide a better understanding of tool performance under the two different cutting conditions. In both cases, crater wear had occurred first on the rake face of each tool and then proceeded to grow in dimensions. The crater wear was identified as the predominant wear mode during the turning process. This is because, under high cutting speed, the temperature generated at the cutting zone was high, as Al was a highly active element, it was very easy to react with oxygen forming Al_2O_3 oxide layer at elevated temperature, which

caused oxidation and diffusion, leading to crater wear [31]. As crater wear grew, substrate exposure caused diffusion of the Co binder, which was thermal softening effect by reason of the excessive temperature at the cutting zone [32]. The hard particles form the substrate accelerated abrasion wear, leading to tool failure (as shown in Fig. 4.1). This was also observed in [25].

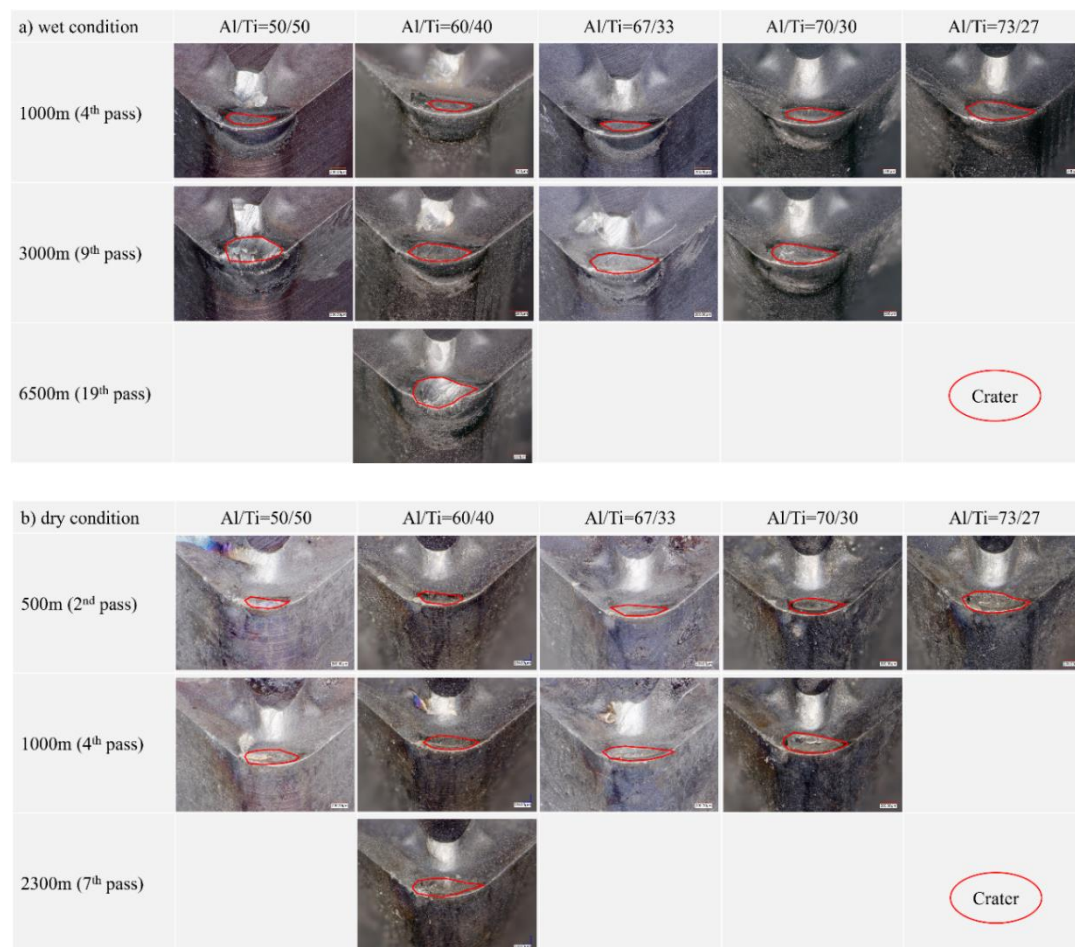Fig. 4.3. 3D Optical images showing the wear progress of AlTiN coated inserts with five different Al/Ti ratios under a) wet and b) dry conditions.

Fig. 4.4 shows the SEM images of five worn AlTiN coated inserts at the end of their tool life. The performance tests were conducted under wet and dry conditions. The tool failure wear mode was considered as a complex combination of the following wear

mechanism: abrasion, attrition, and oxidation, which in turn caused BUE formation, crater wear and substrate exposure. The combined tool failure wear patterns of high-speed SS304 turning were also observed during the ultra-high speed finishing process in Ref. [25]. Under such high-speed machining conditions of austenitic stainless steel, intense heat generated at the cutting zone as well as the heavy load affect the material deformation, promote various interactions between the workpiece, chip and cutting insert and ultimately result in a complicated wear mechanism. Although crater wear can be clearly observed on each of the five tools, the AlTiN coated inserts (Al/Ti = 50/50 and 73/27) featured a more intensive BUE, which had led to chipping on the tool edge. The unstable attrition wear contributed to the workpiece adhesion that caused extreme BUE formation when austenitic stainless steel was machined [27]. The main cause of this can be found in the mechanical properties of the coating system. The microstructure and mechanical properties of AlTiN coatings with five different Al/Ti ratios have been explored in considerable detail in our previous study [25]. The low wear resistance of the AlTiN coating (Al/Ti = 73/27) can be attributed to the softness and ductility provided by its greater Al content, which also reduced its adhesion to the substrate. This composition, however, cannot support a high load during machining as evidenced by coating detachment following BUE and chipping. Conversely, although the AlTiN coating (Al/Ti = 50/50) had a relatively high hardness to resist heavy loads, the brittleness of this hard material also causes BUE formation in some cases. In either situation, the severe BUE that formed had caused the coating to detach, which then resulted in chipping and consequent tool failure. The resulting chipping and tool failure were not favourable for high-speed machining.

The rest of the coatings however, featured relatively stable crater patterns on the

rake faces at the end of tool life. The chemical compositions as well as mechanical properties of the coating system were considered as somewhat balance that impacted the tool wear and oxidation resistance, which would provide a longer tool life under such high-speed machining process.
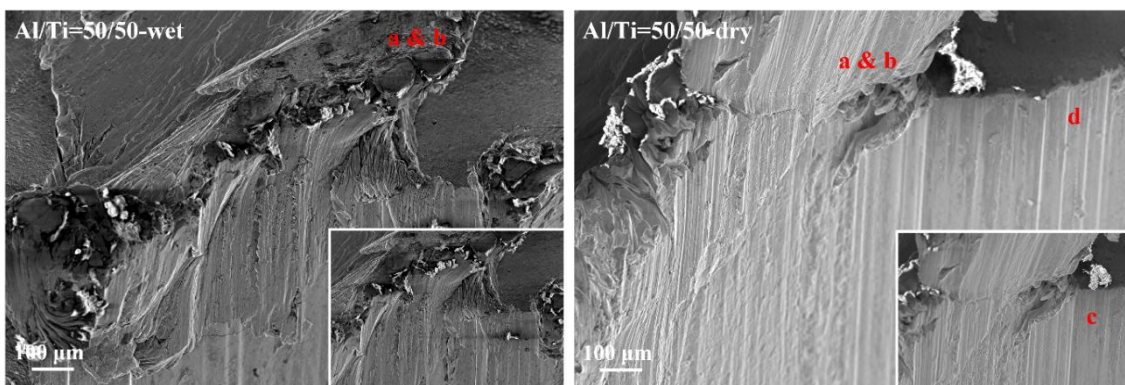
a. built-up-edge (BUE); b. crater wear; c. substrate exposure; d. abrasion and attrition
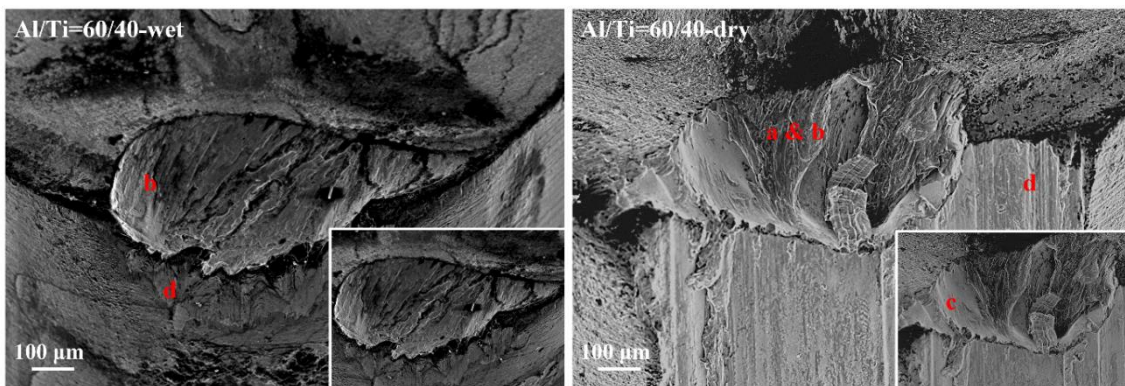
a. built-up-edge (BUE); b. crater wear; c. substrate exposure; d. abrasion and attrition

a. built-up-edge (BUE); b. crater wear; c. substrate exposure; d. abrasion and attrition

a. built-up-edge (BUE); b. crater wear; c. substrate exposure; d. abrasion and attrition
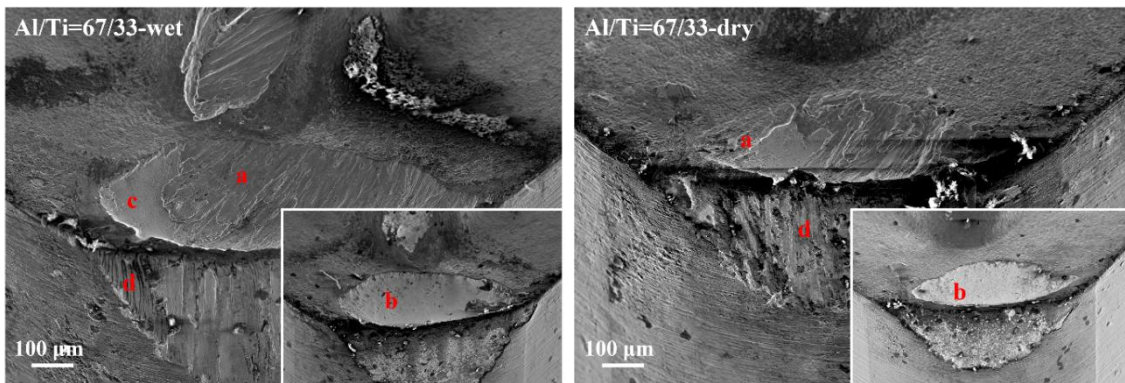
a. built-up-edge (BUE); b. crater wear; c. substrate exposure; d. abrasion and attrition
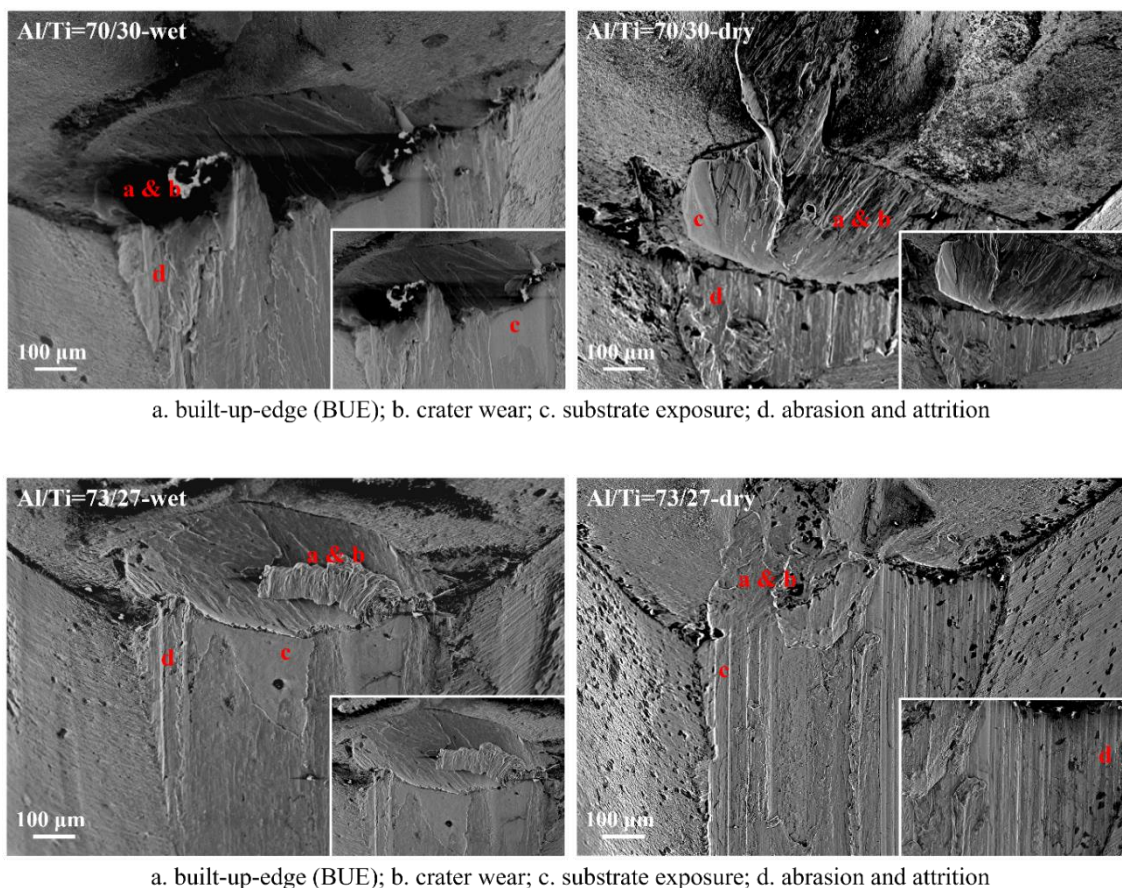
Fig. 4.4. SEM images of the failure wear patterns of the AlTiN coated inserts with five different Al/Ti ratios under wet and dry conditions.

The EDS element maps in Fig. 4.5 depicts the workpiece material adhesion at the end of tool life. The Al signal shows that the coating layer remained on the tool surface, whereas W, highlighted in yellow, indicates substrate exposure. According to the literature [33,34], the occurrence of W indicated the transition from combined diffusion-adhesion to diffusion wear mechanism. Due to the high temperature in the contact zone, plastic deformation happened to be conducive diffusion of components between the cutting insert and workpiece material. This is also partially confirmed by the wear mode shown in Fig. 4.4 (BUE and substrate exposure). In addition, the presence of Fe and Cr signals indicate that workpiece material (SS304) adhered to the tool rake/flank face,

causing BUE formation [35]. This clearly demonstrates that AlTiN coated inserts (Al/Ti = 50/50 and 73/27) experienced a large amount of BUE formation which resulted in chipping and tool substrate exposure (along with consequent tool failure). Furthermore, the Fe/Cr signal prevailing over the W signal on the tool rake faces indicates that substrate exposure was quickly covered by the workpiece material during machining, which can be clearly corroborated by the experimental results shown in Fig. 4.1 and Fig. 4.3.
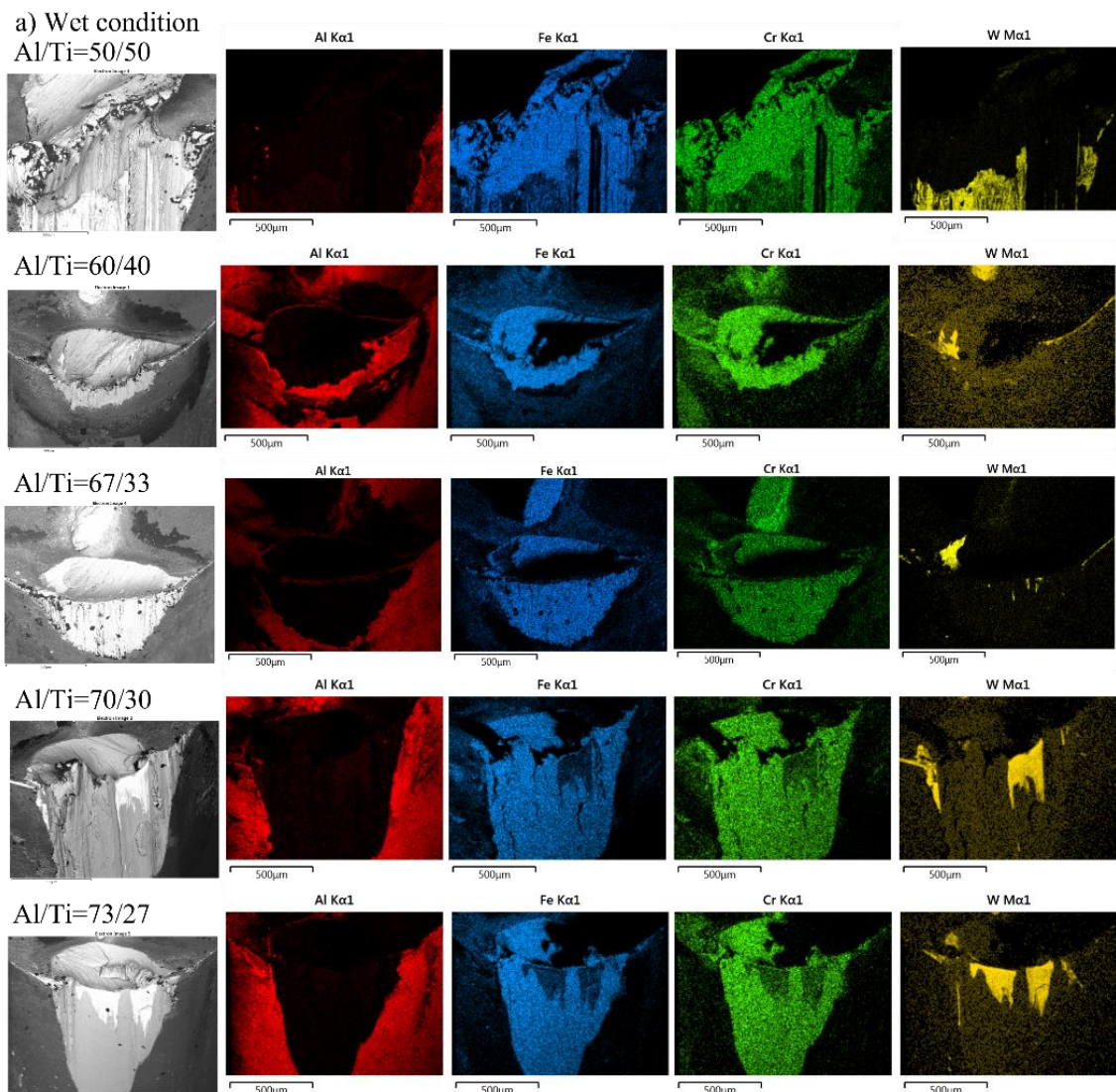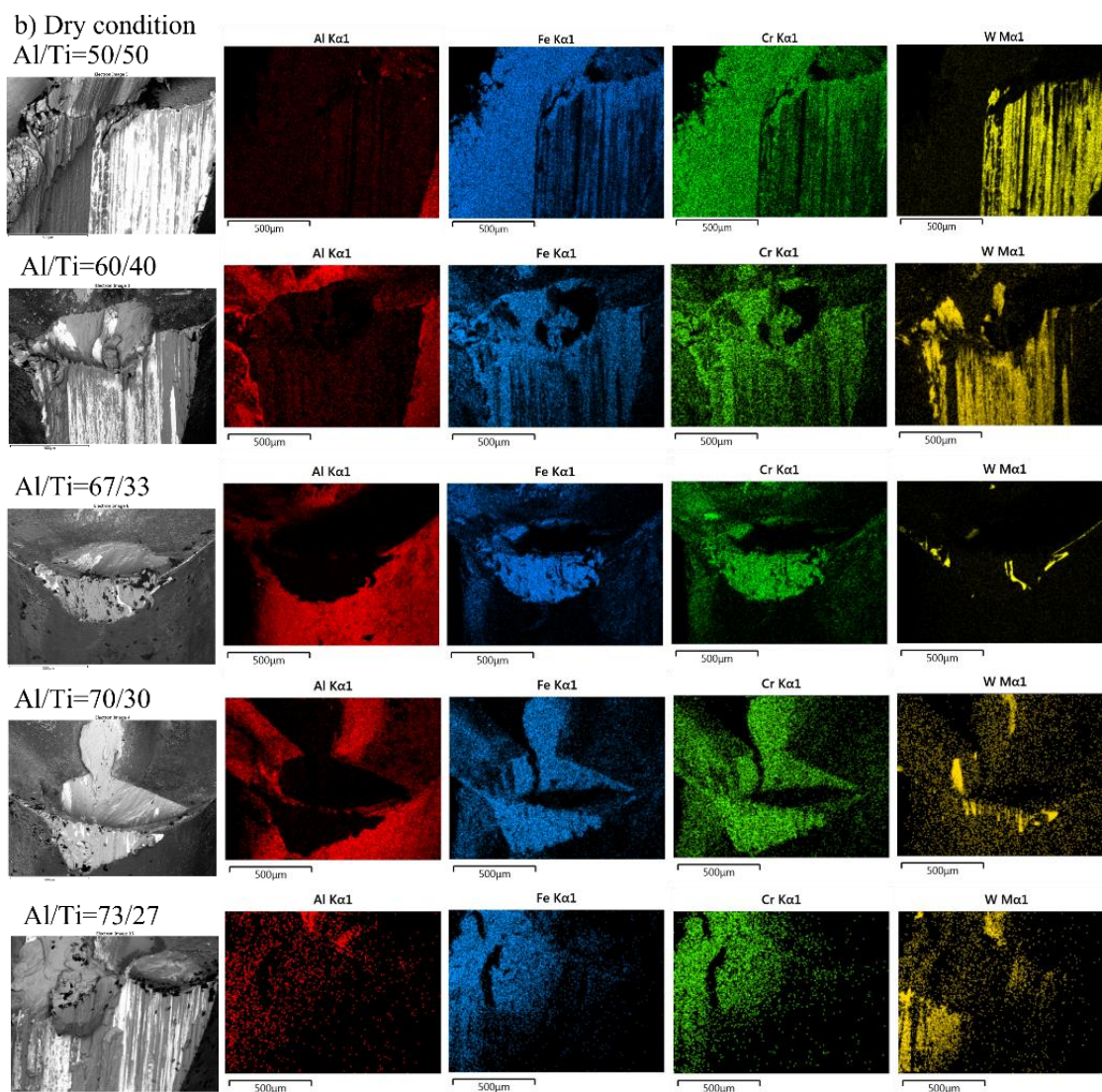
Fig. 4.5. EDS image identifying the chemical elements of AlTiN coated inserts with five different Al/Ti ratios at the end of tool life under the a) wet and b) dry conditions.

The wear volume (below the reference plane) and BUE volume (above the reference plane) of the worn tools at the end of cutting process are shown in Fig. 4.6. With an accuracy of 95 %, the maximum and minimum deviations from the unused reference tool obtained by Alicona from 3D tool wear were quantitatively evaluated. The AlTiN coated inserts (Al/Ti = 50/50 and 73/27) exhibit the largest deviation in either of the two figures, which confirms that these two tools presented the most intense BUE,

and then it peeled off with the coating causing chipping and substrate exposure, in turn leading to severe tool wear. In addition, it is worth noting that most tools featured a greater adhesive BUE volume in the dry condition rather than in the wet condition, which could be partially explained by higher temperatures concentrated at the cutting zone in absence of coolant, which promotes material deformation and results in significant BUE formation.

Differently, the AlTiN coated inserts (Al/Ti = 60/40 and 67/33) had relatively less BUE and wear at the end of the cutting operation. This could be attributed to their stable chemical composition and microstructure which ensured better hot hardness and oxidation resistance.
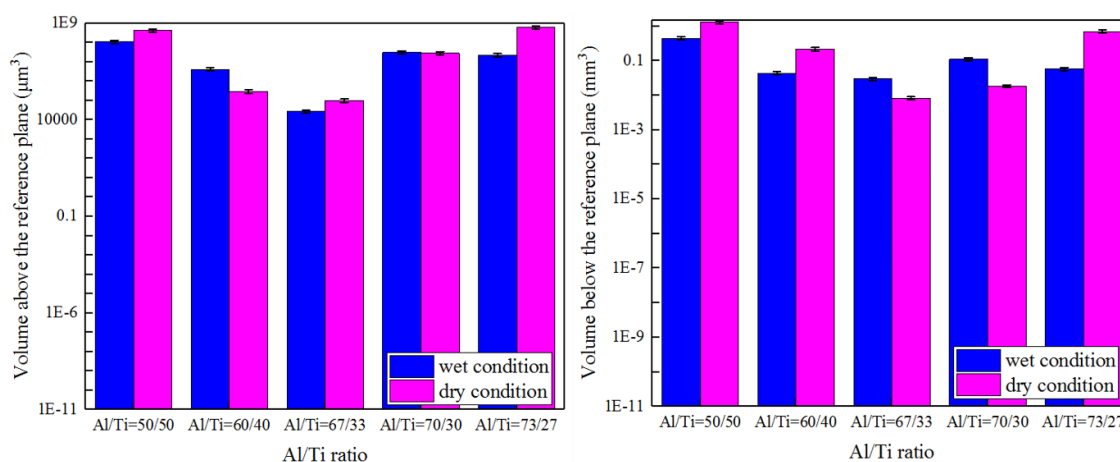
Fig. 4.6. Tool wear volume and BUE volume data of AlTiN coated inserts with five different Al/Ti ratios after machining under wet and dry conditions.

4.3.3. Tribological characteristics

Chip analysis is one of the most essential methods of determining the tribological characteristics during the high-speed turning process. Chip flow can be used to evaluate the friction circumstances at the workpiece-tool-chip interface, since the workpiece

material is in direct contact with the cutting tool and is deformed to generate chips during machining [36]. Table 4.3 shows the chip thickness, tool-chip contact length (tccl), chip compression ratio (ccr), friction angle and friction coefficient data. The original chip thickness data was measured on the chip cross-section from the average of 20 positions. The chip compression ratio (ccr), shear angle and friction coefficient were the most important parameters considered in this study. In general, chips collected under the wet condition exhibited better results than the ones obtained under the dry condition (a higher chip compression ratio nearer to 1, a larger shear angle towards 45° and a lower friction coefficient below 1). Furthermore, the chip produced by the AlTiN coated insert (Al/Ti = 60/40) performed best in both wet and dry cutting tests, whereas the chip produced by the AlTiN coated insert (Al/Ti = 73/27) featured the worst friction condition during machining. It should be remarked that the chip produced by the AlTiN coated insert (Al/Ti = 60/40) exhibited the significantly lowest friction coefficient (below 0.3) in the wet condition, indicating its recommended use for the high-speed turning of SS304.

Table 4.3. A summary of chip characterization data for AlTiN coatings with five different Al/Ti ratios under wet and dry conditions.

Al/Ti ratio	Cutting condition	Chip thickness (µm)	Tool-chip Contact Length (µm)	Chip Compression Ratio - CCR	Φ - Shear Angle (°)	β - Friction Angle (°)	ϒ - Shear Strain	Chip Sliding Velocity (m/min)	Friction Coefficient (µ)
50/50		282	165	0.53	29.0	21.0	1.65	196.1	0.76
60/40		190	122	0.79	40.1	9.9	0.97	291.1	0.26
67/33	Wet	281	164	0.53	29.1	21.0	1.64	196.8	0.75
70/30		254	164	0.59	31.7	18.3	1.45	217.7	0.62
73/27		306	182	0.49	26.9	23.1	1.83	180.6	0.87
50/50		298	171	0.50	27.5	22.5	1.77	185.3	0.84
60/40		246	131	0.61	32.5	17.5	1.39	224.4	0.57
67/33	Dry	301	166	0.49	27.3	22.7	1.79	183.7	0.85
70/30		273	168	0.55	29.8	20.2	1.59	202.5	0.71
73/27		311	188	0.48	26.5	23.5	1.86	177.7	0.89

Fig. 4.7 shows the trends of tool-chip contact length (tccl), chip sliding velocity, friction coefficient µ and specific cutting energy. The tool-chip contact length and chip sliding velocity were determined by the friction condition during the cutting tests. Due to its short tool-chip contact length, the chip cut by the AlTiN coated insert (Al/Ti = 60/40) was more deformed and had a greater curl compared to other chips. This means that the chip flow had a higher velocity and reduced period of contact with the tool. Instead of sticking to the tool, the chips flowed smoothly, which further reduced the wear-based friction on the tool rake face, thereby improving the overall tool performance.

Cutting forces were collected during the first pass of all the cutting tests to determine the specific cutting energy, which is defined as the total energy required to cut a unit volume of material from the workpiece [37]. It is one of the most fundamental

aspects of understanding the tribological characteristics at the tool-chip-workpiece interface [37,38]. Fig. 4.7 shows the specific cutting energy of AlTiN coated inserts with five different Al/Ti ratios under wet and dry cutting conditions. Unlike other data trends, the specific cutting energy of these tools in the dry condition was lower than those in the wet condition. This could be explained by the lower cutting forces in the dry condition during the first pass. The temperature was extremely high during dry cutting, which facilitated the formation of an oxidation layer on the surface of the cutting insert [39,40]. This oxidation coating layer lubricated the interface between the cutting tool and the workpiece, making the cutting process more stable and smoother, thereby reducing the specific cutting energy. In this study, although the AlTiN coating (Al/Ti = 73/27) was expected to generate the most Al-Oxide layers due to its greater Al content, the AlTiN coated insert (Al/Ti = 60/40) was found to instead have the lowest cutting forces and required the least energy to cut the unit material. This phenomenon can be explained by the AlTiN (Al/Ti = 60/40) coating's favorable balance of mechanical properties and microstructure [25].
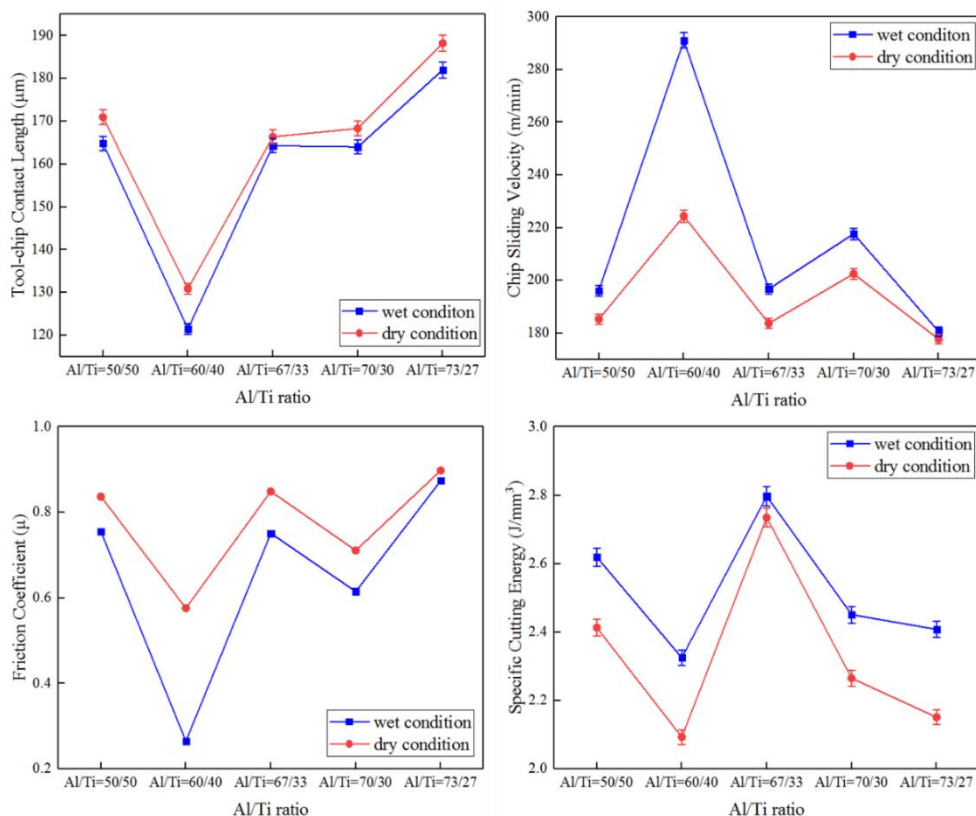
Fig. 4.7. Tribological characteristics at the tool/chip interface under wet and dry conditions based on chip analysis: tool-chip contact length, chip sliding velocity, friction coefficient, and specific cutting energy.

Apart from the above quantitative analyses, SEM images had also described the friction process at the tool-chip-workpiece contact zone during the high-speed turning of SS304. Fig. 4.8 shows the general curl, undersurface and shear band morphology of the chips cut by AlTiN coatings with five different Al/Ti ratios under both wet and dry conditions. It can be seen that the chip produced by the AlTiN coated insert (Al/Ti = 60/40) featured the greatest degree of curl compared with other chips under each condition. Furthermore, some chips such as the chips produced by the AlTiN coated insert (Al/Ti = 50/50 and 70/30) exhibited varying degrees of irregular curls. As can be seen in the image of its undersurface, the chip produced by the AlTiN coated insert

(Al/Ti = 60/40) had a relatively smooth morphology compared with other chips, which exhibited a greater amount of rough crease marks. This means that the chip produced by the AlTiN coated insert (Al/Ti = 60/40) smoothly flowed over the tool-chip interface, generating low friction and adhesion, whereas chips produced by the other coating compositions tended to stick to the tool, causing tearing and growth of friction [27]. All chips produced under the wet condition featured a better undersurface than the ones produced under the dry condition, as indicated by the difference in the number of evident tear marks on the chips. The liquid coolant had not only provided lubrication between the chip and the tool, but also reduced the temperature during high-speed machining [41]. In this case, the chips were not heavily intercepted at the tool-chip interface and to some extent, they were capable of being quickly flushed out from the tool-chip-workpiece interface under coolant pressure.

The chip shear bands in Fig. 4.8 reveal the chip flow and shear deformation of the material. For the chips produced by the AlTiN coated inserts (Al/Ti = 50/50, 67/33, 70/30 and 73/27), not only was the spacing between the segments different, but the deformed directions were also inconsistent. The shear bands of these chips showed clear marks which prevented fluent deformation in Fig. 4.8. In other words, the friction at the tool-chip interface was extremely high and the chip was incapable of smoothly sliding during the machining process. Conversely, the shear band (in both wet and dry conditions) of the chips produced by the AlTiN coated insert (Al/Ti = 60/40) demonstrated a much more regular slice structure and a uniform interval between the adjacent segments. Although all chips featured cracks on different levels, the chip produced by the AlTiN coated insert (Al/Ti = 60/40) had the smallest and fewest marks due to the low friction and high sliding velocity (also correspond Table 4.3 and Fig. 4.7).

This was the result of a combination of the mechanical properties and chemical composition of this coating, which was also reported in [25].
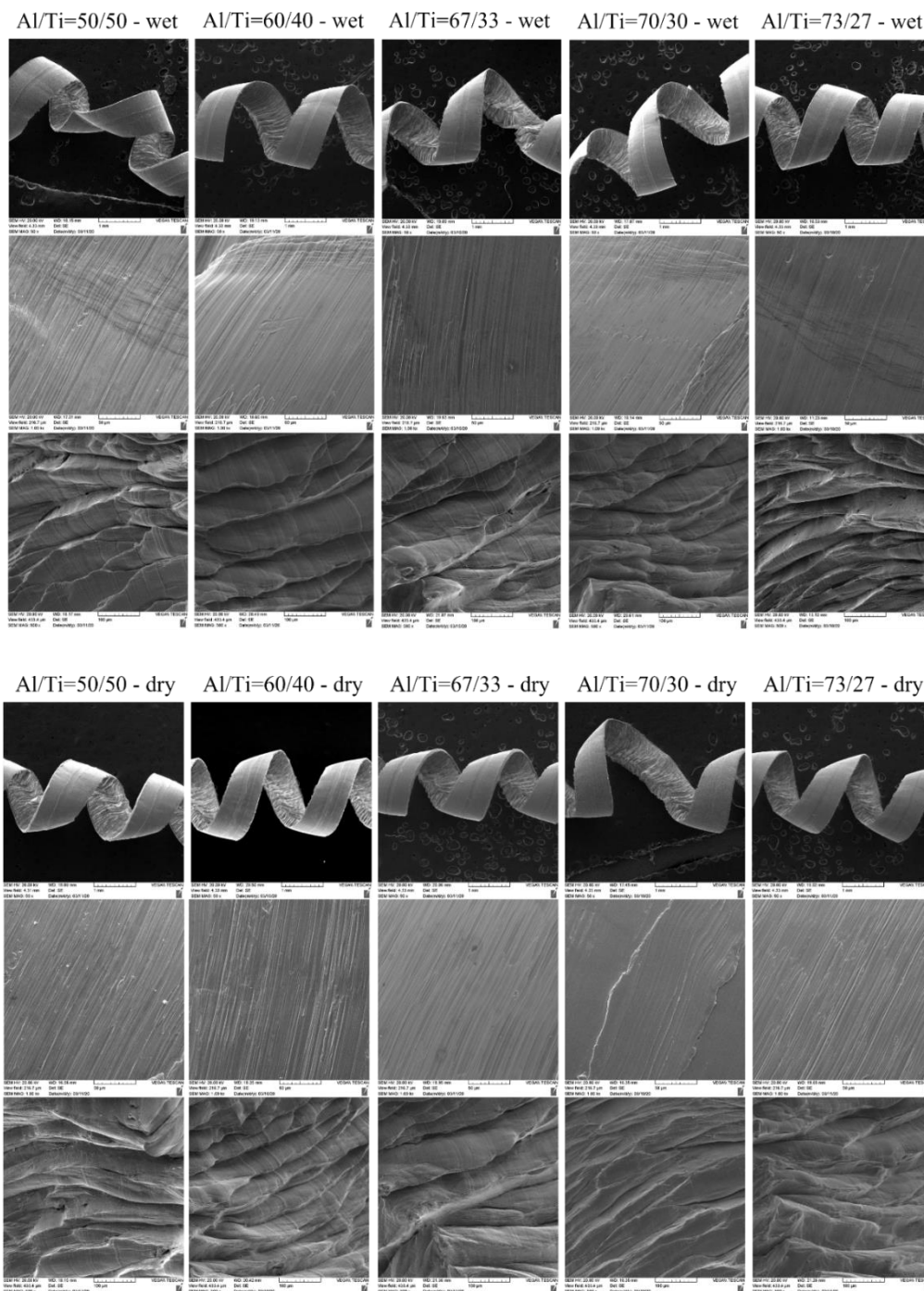

Fig. 4.8. SEM image of chip general position, chip undersurface, and chip shear band for AlTiN coatings with five different Al/Ti ratios under wet and dry conditions.

Based on the above tribological analysis, the friction condition at the interface of the AlTiN coated insert (Al/Ti =60/40) and SS304 workpiece material was the mildest in both wet and dry conditions. With the addition of coolant, this coated tool produced chips with a high sliding velocity and compression ratio, resulting in a high level of deformation. This kind of chip generation benefited from the insert coating's microstructure and mechanical properties [25], leading to the least amount of wear on the tool rake/flank face and the longest tool life out of all the tested coating compositions.

4.3.4. The studies of the chip cross section and the workpiece surface integrity

As previously discussed, AlTiN coated inserts (Al/Ti = 50/50, 67/33, and 70/30) had a relatively similar performance and chip characteristics throughout the tool life test. The AlTiN coated insert (Al/Ti = 50/50) was selected to explore the chip cross-section and workpiece surface integrity study since this chemical composition is commonly used in industrial applications. In addition, the AlTiN coated inserts (Al/Ti = 60/40 and 73/27) were chosen as well since they exhibited the longest and shortest tool life.

A chip cross-section study is helpful in understanding the material deformation mechanism which occurs in the primary deformation zone [42,43]. Saw-tooth chips were formed in this experiment, as shown in Fig. 4.9. The formation of this type of serrated chip is attributed to thermally assisted deformation due to the high temperatures of high-speed turning as confirmed in [42]. Hardness tests on the edge, middle and tip of the chip cross-section were conducted to identify the extent of strain-hardening. The results were obtained from the average hardness of three points on various chip samples, respectively. Fig. 4.9 shows the hardness measurements at different testing points at specific distances from the tool-chip interface. The hardness increased from the edge to

the tip throughout the primary shear zone of all the chips, which confirmed the strain-hardening effect. During high-speed turning of SS304, plastic deformation occurred due to metal flow at the tool-chip contact surface [35]. Chips produced in the wet condition generally performed better than those in the dry condition due to their significant variation in hardness from the edge to the tip. This can be explained by the accelerated metal flow and strain plastic deformation induced into the chip [35]. The presence of coolant reduced friction between the tool and the chip and accelerated the metal flow. In this case, chips under the wet condition were generated with a higher sliding velocity and therefore intensity strengthening presented within them.

When focusing on the hardness trend on the chips that produced under the wet condition, it can be seen the chip produced by the AlTiN coated insert (Al/Ti = 60/40) had the highest hardness which measured on the chip cross-section. This was attributed to its lowest friction angle and greater chip compression ratio (ccr) compared with the other chips (as shown in Table 4.3). During the high-speed turning process, shear stress induced different lattice stretching in the workpiece material, corresponding to various chip formation characteristics [35], and this was expressed in diverse cross-sectional hardness. Results confirmed severe plastic deformation in the chips produced by the AlTiN coated insert (Al/Ti = 60/40) in the wet condition, which accounts for their curliest shape and outstanding formation characteristics. The optimal mechanical properties and chemical composition of the AlTiN coating (Al/Ti = 60/40) are the chief reasons for its superior performance.
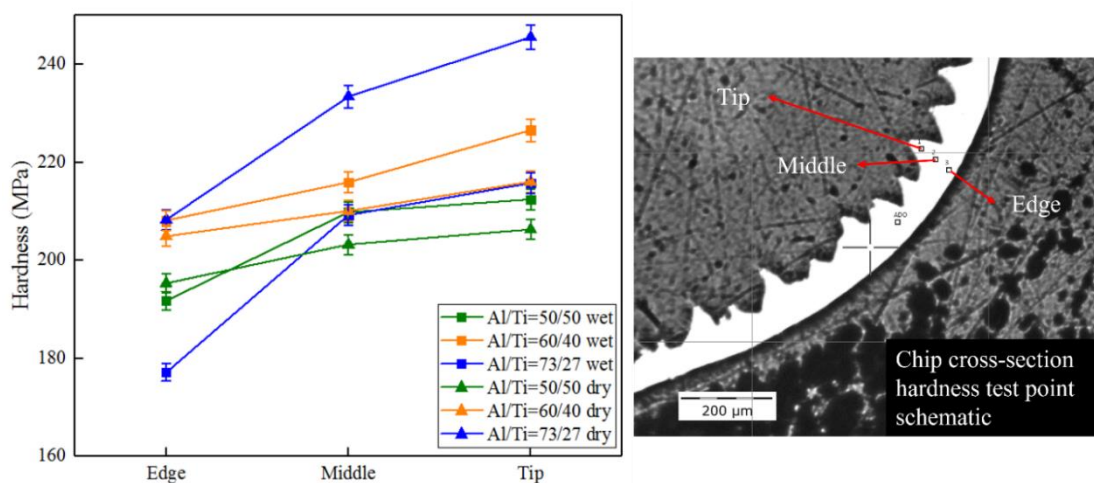
Fig. 4.9. Hardness on the cross-section of chips produced with inserts coated with different AlTiN coatings; the performance tests were conducted under wet and dry conditions.

Fig. 4.10 shows the cross-sectional SEM images of chip microstructures; the chips were produced by inserts protected with different AlTiN coatings, while the performance tests were conducted under wet and dry conditions. Plastic deformation is considered to promote phase transformation [44], which normally can be observed in stainless steel [45]. This heterogeneous region was recognized as strain-induced martensite. The chips generated under dry condition overall showed more and apparent marks which indicates the SS304 material squeezed together and impede the chip flow during the machining. Those results can be also proved by the cross-section hardness tests presented in Fig. 4.9. Furthermore, the chip produced by the AlTiN coated insert (Al/Ti = 60/40) demonstrated a significant smooth and uniform pattern of the metal flow, especially for that cut in the wet condition. This correlated to the previous analysis of chip characteristics, evidently proved to be the best results generated from the AlTiN coating with the Al/Ti ratio of 60/40.
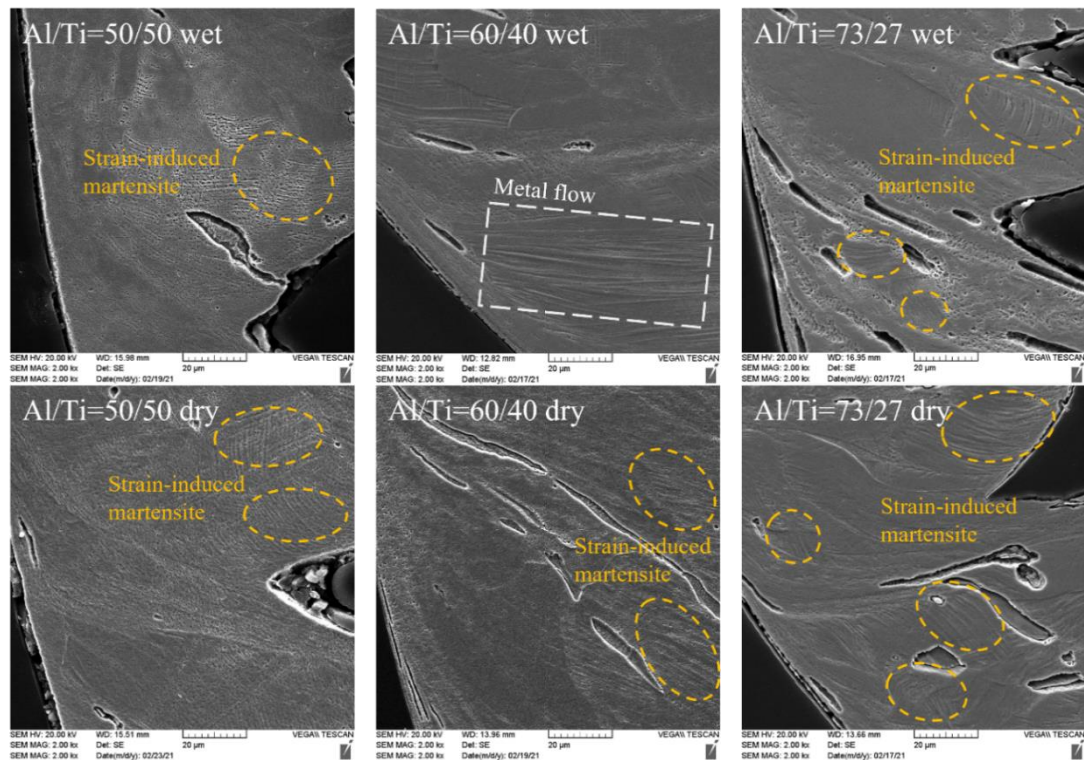
Fig. 4.10. Cross-sectional SEM image of chip microstructures; the chips were produced by different AlTiN coated inserts under wet and dry cutting conditions.

The surface integrity of the machined SS304 workpiece in this paper was analyzed through a study of workpiece surface morphology and surface average roughness. The SEM and Alicona images of the SS304 surface are shown in Fig. 4.11. All of the studied inserts generated a higher surface roughness on the SS304 workpiece material in the dry cutting condition than in the wet condition, which can be attributed to the change of friction conditions at the chip-tool-workpiece contact zone. The application of coolant during the cutting process reduced friction [46] and further improved the surface roughness of the machined workpiece. Moreover, the AlTiN coated insert (Al/Ti = 60/40) featured the best performance out of all the studied tools since the machined workpiece had the lowest Sa under both cooling conditions. The surface generated by the AlTiN coated insert (Al/Ti = 60/40) was generally smooth with minimum visible cracks and/or

adhesion marks. Conversely, the sliding and adhesion of chips on the workpiece surface machined by the AlTiN coated inserts (Al/Ti = 50/50 and 73/27) were one of the reasons for its high surface roughness. This was also closely linked to the chip undersurface morphology due to the presence of tearing and sticking marks on the chips shown in Fig. 4.8. During high-speed machining, the workpiece material had adhered to the tool, causing continuous growth of BUE until chips began to detach from the workpiece, which contributed to the latter's surface roughness [47,48]. Consequently, it affected the surface integrity of the machined workpiece. Furthermore, the BUE cannot sustain the heavy loads that taking place in the cutting zone, and naturally the BUE will flake off, resulting in the chipping. As a consequence of this phenomenon, the surface roughness was not favorable due to the melting of chips on the workpiece. This occasionally was observed when chipping had occurred on the AlTiN coated inserts (Al/Ti = 50/50 and 73/27). The relationship between tool wear performance and the surface integrity of the machined workpiece material was described in [49] as well.
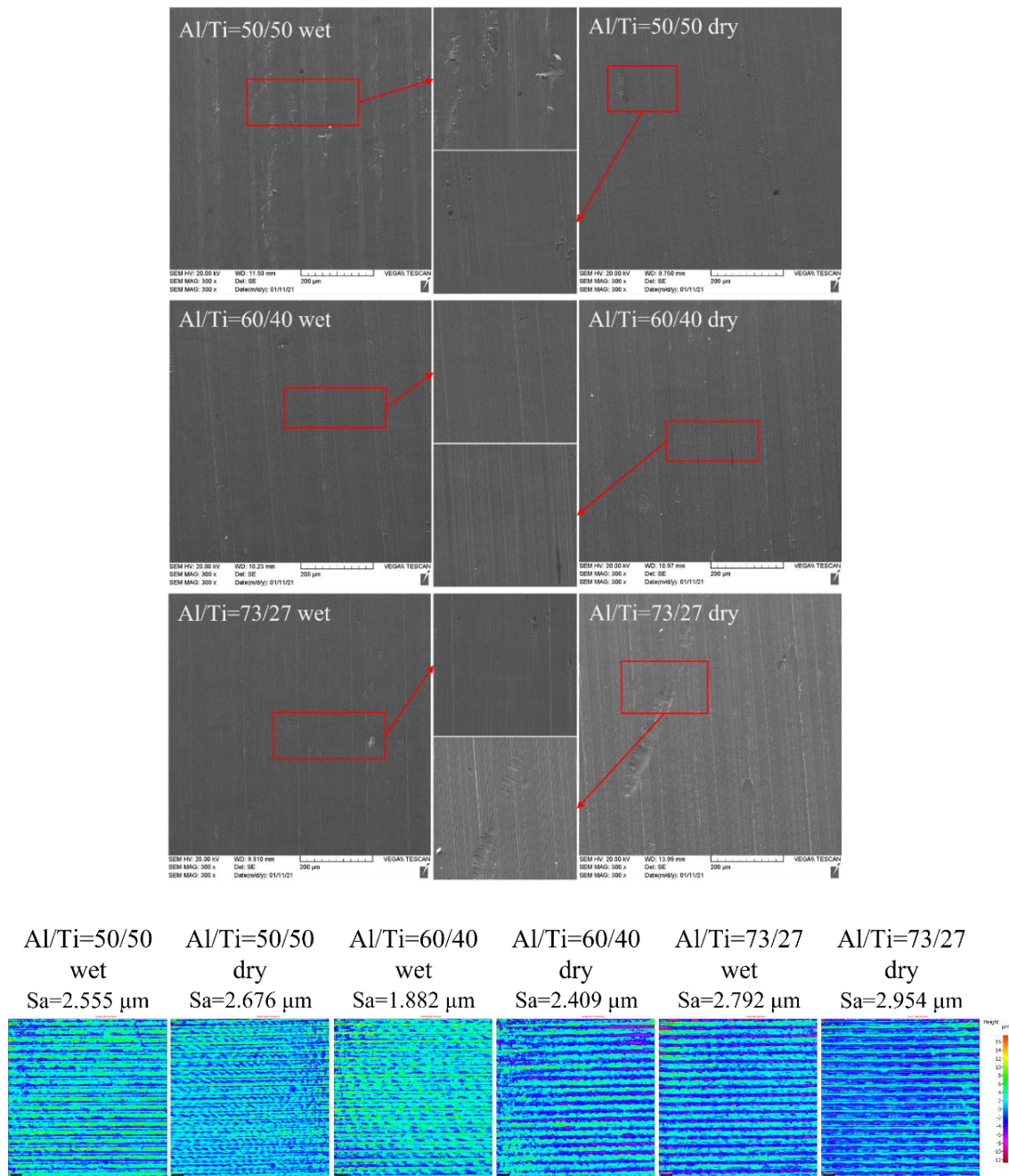
Fig. 4.11. Surface integrity results of SS304 cut with AlTiN coated inserts (Al/Ti = 50/50, 60/40, and 73/27) under wet and dry conditions.

4.4. Conclusions

This work presents a comprehensive study of wear behavior and tribological performance of AlTiN PVD coated inserts with five different Al/Ti ratios for high-speed

turning (370 m/min) of SS304 under harsh cutting conditions. Based on the experimental findings and detailed discussion, the following conclusions can be given:

i. Tool life results showed that all the inserts performed better in the presence of coolant for high-speed machining of SS304, with an extended cutting length by 2-3 times. Among them, the AlTiN coated insert (Al/Ti = 60/40) possessed the longest tool life of 7,000 m under the wet condition, and 2,500 m under the dry condition. Crater wear was confirmed to be dominant wear mode, in combination with BUE and chipping that contributed to the tool failure.

ii. Chip characteristics analysis revealed that the friction at the cutting zone was generally lower with the use of a coolant, but the coating systems had reduced the cutting forces under dry turning thanks to the formation of alumina at the first stage of the cutting process. The most rapid sliding velocity and the smoothest metal flow was observed in chips generated by the AlTiN coated insert (Al/Ti = 60/40).

iii. SS304 machined with the AlTiN coated insert (Al/Ti = 60/40) in the wet condition produced the best surface integrity, as corroborated by the minimum friction present at the tool-chip-workpiece interface. The optimal balance between the mechanical properties and chemical composition of this coating are the main reasons for this favorable outcome.

4.5. References

[1]   M. Nalbant, Y. Yildiz, Effect of cryogenic cooling in milling process of AISI 304 stainless steel, Trans. Nonferrous Met. Soc. China. 21 (2011) 72–79. https://doi.org/https://doi.org/10.1016/S1003-6326(11)60680-8.

[2]   N. Altan, A. Çiçek, M. Gülesin, O. Özbek, Effect of cutting conditions on wear performance of cryogenically treated tungsten carbide inserts in dry turning of stainless steel, Tribiology Int. 94 (2016) 223–233. https://doi.org/10.1016/j.triboint.2015.08.024.

[3]   I. Korkut, M. Kasap, I. Ciftci, U. Seker, Determination of optimum cutting parameters during machining of AISI 304 austenitic stainless steel, Mater. Des. 25 (2004) 303–305. https://doi.org/https://doi.org/10.1016/j.matdes.2003.10.011.

[4]   D. O'Sullivan, M. Cotterell, Machinability of austenitic stainless steel SS303, J. Mater. Process. Technol. 124 (2002) 153–159. https://doi.org/https://doi.org/10.1016/S0924-0136(02)00197-8.

[5]   A.I. Journal, B. Słodki, W. Zębala, G. Struzikiewicz, Correlation Between Cutting Data Selection and Chip Form in Stainless Steel Turning, 0344 (2015). https://doi.org/10.1080/10910344.2015.1018530.

[6]   S.S. Gill, J. Singh, H. Singh, R. Singh, Metallurgical and mechanical characteristics of cryogenically treated tungsten carbide (WC–Co), Int. J. Adv. Manuf. Technol. 58 (2012) 119–131. https://doi.org/10.1007/s00170-011-3369-4.

[7]   J.L. Endrino, G.S. Fox-rabinovich, C. Gey, Hard AlTiN , AlCrN PVD coatings for machining of austenitic stainless steel, Surf. Coatings Technol. 200 (2006) 6840–6845. https://doi.org/10.1016/j.surfcoat.2005.10.030.

[8]   P. Sahoo, K. Patra, V.K. Singh, M.K. Gupta, Q. Song, M. Mia, D.Y. Pimenov, Influences of TiAlN coating and limiting angles of flutes on prediction of cutting forces and dynamic stability in micro milling of die steel (P-20), J. Mater. Process. Technol. 278 (2020) 116500. https://doi.org/https://doi.org/10.1016/j.jmatprotec.2019.116500.

[9]   H. Çalışkan, M. Küçükköse, The effect of aCN/TiAlN coating on tool wear, cutting force, surface finish and chip morphology in face milling of Ti6Al4V superalloy, Int. J. Refract. Met. Hard Mater. 50 (2015) 304–312. https://doi.org/https://doi.org/10.1016/j.ijrmhm.2015.02.012.

[10]   M. Arndt, T. Kacsich, Performance of new AlTiN coatings in dry and high speed cutting, Surf. Coatings Technol. 163–164 (2003) 674–680. https://doi.org/https://doi.org/10.1016/S0257-8972(02)00694-1.

[11]   M. Witthaut, R. Cremer, A. von Richthofen, D. Neuschütz, Improvement of the oxidation behavior of Ti1-xAlxN hard coatings by optimization of the Ti/Al ratio, Fresenius. J. Anal. Chem. 361 (1998) 639–641. https://doi.org/10.1007/s002160050976.

[12]   J.-E. Desaigues, C. Lescalier, A. Bomont-Arzur, D. Dudzinski, O. Bomont, Experimental study of Built-Up Layer formation during machining of high strength free-cutting steel, J. Mater. Process. Technol. 236 (2016) 204–215. https://doi.org/https://doi.org/10.1016/j.jmatprotec.2016.05.016.

[13]   C. He, J. Zhang, G. Song, G. Ma, Z. Du, J. Wang, D. Zhao, Microstructure and mechanical properties of reactive sputtered nanocrystalline (Ti,Al)N films, Thin Solid Films. 584 (2015) 192–197. https://doi.org/https://doi.org/10.1016/j.tsf.2014.12.027.

[14] L. Chen, J. Paulitsch, Y. Du, P.H. Mayrhofer, Thermal stability and oxidation resistance of Ti–Al–N coatings, Surf. Coatings Technol. 206 (2012) 2954–2960. https://doi.org/https://doi.org/10.1016/j.surfcoat.2011.12.028.

[15] M.Z.A. Yazid, C.H. Che Hassan, A.G. Jaharah, A.I. Gusri, M.S. Ahmad Yasir, Tool Wear of PVD Coated Carbide Tool when Finish Turning Inconel 718 under High Speed Machining, Adv. Mater. Res. 129–131 (2010) 1004–1008. https://doi.org/10.4028/www.scientific.net/AMR.129-131.1004.

[16] R.W. Maruda, G.M. Krolczyk, P. Nieslony, S. Wojciechowski, M. Michalski, S. Legutko, The influence of the cooling conditions on the cutting tool wear and the chip formation mechanism, J. Manuf. Process. 24 (2016) 107–115. https://doi.org/10.1016/j.jmapro.2016.08.006.

[17] S. Paul, N.R. Dhar, A.B. Chattopadhyay, Beneficial effects of cryogenic cooling over dry and wet machining on tool wear and surface finish in turning AISI 1060 steel, J. Mater. Process. Technol. 116 (2001) 44–48. https://doi.org/https://doi.org/10.1016/S0924-0136(01)00839-1.

[18] J. Kundrák, G. Varga, Possibility of Reducing Environmental Load in Hard Machining, in: Precis. Mach. VI, Trans Tech Publications Ltd, 2012: pp. 205–210. https://doi.org/10.4028/www.scientific.net/KEM.496.205.

[19] J. Sharma, B.S. Sidhu, Investigation of effects of dry and near dry machining on AISI D2 steel using vegetable oil, J. Clean. Prod. 66 (2014) 619–623. https://doi.org/https://doi.org/10.1016/j.jclepro.2013.11.042.

[20] M. Handawi, S. Elmunafi, M.Y. Noordin, D. Kurniawan, Tool Life of Coated Carbide Cutting Tool when Turning Hardened Stainless Steel under Minimum Quantity Lubricant using Castor Oil, Procedia Manuf. 2 (2015) 563–567.

https://doi.org/10.1016/j.promfg.2015.07.097.

[21] T. Leppert, Effect of cooling and lubrication conditions on surface topography and turning process of C45 steel, Int. J. Mach. Tools Manuf. 51 (2011) 120–126. https://doi.org/https://doi.org/10.1016/j.ijmachtools.2010.11.001.

[22] S.A. Bagaber, A.R. Yusoff, Multi-objective optimization of cutting parameters to minimize power consumption in dry turning of stainless steel 316, J. Clean. Prod. 157 (2017) 30–46. https://doi.org/10.1016/j.jclepro.2017.03.231.

[23] G.M. Krolczyk, P. Nieslony, S. Legutko, Determination of tool life and research wear during duplex stainless steel turning, Arch. Civ. Mech. Eng. 15 (2015) 347–354. https://doi.org/https://doi.org/10.1016/j.acme.2014.05.001.

[24] R.W. Maruda, G.M. Krolczyk, P. Nies, J.B. Krolczyk, S. Legutko, Chip formation zone analysis during the turning of austenitic stainless steel 316L under MQCL cooling condition, 149 (2016) 297–304. https://doi.org/10.1016/j.proeng.2016.06.670.

[25] Q. He, J.M. Paiva, J. Kohlscheen, B.D. Beake, S.C. Veldhuis, Study of wear performance and tribological characterization of AlTiN PVD coatings with different Al/Ti ratios during ultra-high speed turning of stainless steel 304, Int. J. Refract. Met. Hard Mater. (2021) 105488. https://doi.org/https://doi.org/10.1016/j.ijrmhm.2021.105488.

[26] A.E. Diniz, Á.R. Machado, J.G. Corrêa, Tool wear mechanisms in the machining of steels and stainless steels, Int. J. Adv. Manuf. Technol. 87 (2016) 3157–3168. https://doi.org/10.1007/s00170-016-8704-3.

[27] A. Biksa, K. Yamamoto, G. Dosbaeva, S.C. Veldhuis, G.S. Fox-Rabinovich, A. Elfizy, T. Wagg, L.S. Shuster, Wear behavior of adaptive nano-multilayered

AlTiN/MexN PVD coatings during machining of aerospace alloys, Tribol. Int. 43 (2010) 1491–1499. https://doi.org/https://doi.org/10.1016/j.triboint.2010.02.008.

[28] S. Sukvittayawong, I. Inasaki, Detection of built-up edge in turning process, Int. J. Mach. Tools Manuf. 34 (1994) 829–840. https://doi.org/https://doi.org/10.1016/0890-6955(94)90062-0.

[29] A.M. El-Tamimi, T.M. El-Hossainy, Investigating the Tool Life, Cutting Force Components, and Surface Roughness of AISI 302 Stainless Steel Material Under Oblique Machining, Mater. Manuf. Process. 23 (2008) 427–438. https://doi.org/10.1080/10426910801974846.

[30] V. Sivaraman, S. Sankaran, L. Vijayaraghavan, The Effect of Cutting Parameters on Cutting Force During Turning Multiphase Microalloyed Steel, 4 (2012) 157–160. https://doi.org/10.1016/j.procir.2012.10.028.

[31] J. Kohlscheen, C. Bareiss, Effect of Hexagonal Phase Content on Wear Behaviour of AlTiN Arc PVD Coatings, (2018). https://doi.org/10.3390/coatings8020072.

[32] D. Jianxin, Z. Jiantou, Z. Hui, Y. Pei, Wear mechanisms of cemented carbide tools in dry cutting of precipitation hardening semi-austenitic stainless steels, Wear. 270 (2011) 520–527. https://doi.org/https://doi.org/10.1016/j.wear.2011.01.006.

[33] D. V Suetin, N.I. Medvedeva, Structural, electronic and magnetic properties of η-carbides M3W3C (M = Ti, V, Cr, Mn, Fe, Co, Ni), J. Alloys Compd. 681 (2016) 508–515. https://doi.org/https://doi.org/10.1016/j.jallcom.2016.04.279.

[34] R.W. Maruda, G.M. Krolczyk, E. Feldshtein, P. Nieslony, B. Tyliszczak, F.

Pusavec, Tool wear characterizations in finish turning of AISI 1045 carbon steel for MQCL conditions, Wear. 372–373 (2017) 54–67. https://doi.org/https://doi.org/10.1016/j.wear.2016.12.006.

[35] Q. He, J.M. Paiva, J. Kohlscheen, B.D. Beake, S.C. Veldhuis, An integrative approach to coating / carbide substrate design of CVD and PVD coated cutting tools during the machining of austenitic stainless steel, 46 (2020) 5149–5158. https://doi.org/10.1016/j.ceramint.2019.10.259.

[36] E.M. Trent, P.K. Wright, Metal Cutting, 2000. https://doi.org/10.1016/B978-075067069-2/50012-7.

[37] W. Polini, S. Turchetta, Force and specific energy in stone cutting by diamond mill, Int. J. Mach. Tools Manuf. 44 (2004) 1189–1196. https://doi.org/https://doi.org/10.1016/j.ijmachtools.2004.04.001.

[38] M. Shaw, Metal cutting principles, 2°, Oxford Unversity Press, New York, 2005.

[39] J. Peng, D. Su, C. Wang, Combined Effect of Aluminum Content and Layer Structure on the Oxidation Performance of Ti1−xAlxN Based Coatings, J. Mater. Sci. Technol. 30 (2014) 803–807. https://doi.org/https://doi.org/10.1016/j.jmst.2014.03.020.

[40] J.L. Mo, M.H. Zhu, Tribological oxidation behaviour of PVD hard coatings, Tribol. Int. 42 (2009) 1758–1764. https://doi.org/https://doi.org/10.1016/j.triboint.2009.04.026.

[41] J.S. Dureja, R. Singh, T. Singh, P. Singh, M. Dogra, M.S. Bhatti, Performance Evaluation of Coated Carbide Tool in Machining of Stainless Steel (AISI 202) under Minimum Quantity Lubrication (MQL), 2 (2015) 123–129. https://doi.org/10.1007/s40684-015-0016-9.

[42] A.I. Journal, R.S. Pawade, S.S. Joshi, MECHANISM OF CHIP FORMATION IN HIGH-SPEED TURNING OF INCONEL 718, 0344 (2011). https://doi.org/10.1080/10910344.2011.557974.

[43] J. Nomani, A. Pramanik, T. Hilditch, G. Littlefair, Chip formation mechanism and machinability of wrought duplex stainless steel alloys, (2015) 1127–1135. https://doi.org/10.1007/s00170-015-7113-3.

[44] J.M.F. d. Paiva, R.D. Torres, F.L. Amorim, D. Covelli, M. Tauhiduzzaman, S. Veldhuis, G. Dosbaeva, G. Fox-Rabinovich, Frictional and wear performance of hard coatings during machining of superduplex stainless steel, Int. J. Adv. Manuf. Technol. 92 (2017) 423–432. https://doi.org/10.1007/s00170-017-0141-4.

[45] P.K. Chiu, K.L. Weng, S.H. Wang, J.R. Yang, Y.S. Huang, J. Fang, Low-cycle fatigue-induced martensitic transformation in SAF 2205 duplex stainless steel, Mater. Sci. Eng. A. 398 (2005) 349–359. https://doi.org/https://doi.org/10.1016/j.msea.2005.03.096.

[46] G. Krolczyk, P. Nieslony, S. Legutko, Microhardness and Surface Integrity in Turning Process of Duplex Stainless Steel (DSS) for Different Cutting Conditions, 23 (2014) 859–866. https://doi.org/10.1007/s11665-013-0832-4.

[47] Y.S. Ahmed, G. Fox-Rabinovich, J.M. Paiva, T. Wagg, S.C. Veldhuis, Effect of Built-Up Edge Formation during Stable State of Wear in AISI 304 Stainless Steel on Machining Performance and Surface Integrity of the Machined Part, Mater. (Basel, Switzerland). 10 (2017) 1230. https://doi.org/10.3390/ma10111230.

[48] A. Devillez, G. Le Coz, S. Dominiak, D. Dudzinski, Dry machining of Inconel 718, workpiece surface integrity, J. Mater. Process. Technol. 211 (2011) 1590–1598. https://doi.org/https://doi.org/10.1016/j.jmatprotec.2011.04.011.

[49]   M.A. Xavior, M. Adithan, Determining the influence of cutting fluids on tool wear and surface roughness during turning of AISI 304 austenitic stainless steel, J.   Mater.   Process.   Technol.   209   (2009)   900–909. https://doi.org/https://doi.org/10.1016/j.jmatprotec.2008.02.068.

Chapter 5: A study of mechanical and tribological properties as well as wear performance of a multifunctional bilayer AlTiN PVD coatings during the ultra-high-speed turning of 304 austenitic stainless steel

Q. He[1], J.M. DePaiva[1,2,*], J. Kohlscheen[3], and S.C. Veldhuis[1]

1- McMaster Manufacturing Research Institute, McMaster University, Hamilton, L8S4L8, Canada

2- Engineering Graduate Program – PPGEM, Pontificia Universidade Católica do Paraná, Curitiba, 80215901, Brazil

3- Kennametal GmbH, Altweiherstr 27-31, 91320, Ebermannstadt, Germany

∗ Corresponding author: paivajj@mcmaster.ca (J.M. DePaiva).

Author's Contribution

Qianxi He	Designed and conducted the experiments
	Analyzed the results.
	Wrote the manuscript.
Jose M. DePaiva	Assisted with designing the research methodology.
	Assisted with writing and editing the manuscript.
Joern Kohlscheen	Deposited the coating.
Stephen C. Veldhuis	Supervised the project.

Abstract

In this study, a novel bi-layer AlTiN PVD coating was deposited on a tungsten carbide substrate. The bi-layer coating, with a total thickness of 3.5 microns consists of a 1.0 μm $Al_{60}Ti_{40}N$ top layer and a 2.5 μm $Al_{50}Ti_{50}N$ sublayer. Monolayer $Al_{60}Ti_{40}N$ and $Al_{50}Ti_{50}N$ coatings (each around 3.5 μm) were used as benchmarks. All the studied coatings were deposited by an industrial cathodic arc PVD coater. The ultra-high-speed finish turning of austenitic stainless steel 304 (SS304) was performed under a cutting speed of 420 m/min. The coatings' mechanical properties (hardness, elastic modulus, toughness, and adhesion) were evaluated using nano-indentation and scratch methods. The obtained data illustrated the influence of the mechanical properties of the coatings on tool wear performance. Cutting tests showed that the longest tool life was achieved by the bi-layer coated tool. Wear morphology studies had revealed that a combination of oxidation/diffusion wear mechanisms resulted in cratering whereas abrasion/attrition led to flank wear. An investigation of tribological characteristics had shown that the bi-layer coated tool produced improved chips. This indicates an optimal frictional condition at the cutting zone. Finally, a chip cross-section analysis was performed to verify the microstructure variations and work-hardening effect in the chips.

Keywords

5.1. Introduction

Austenitic stainless steel 304 (SS304) is commonly used as a workpiece material for many applications including aerospace, vehicle accessories, medical equipment and ship parts [1]. This material has a beneficial combination of corrosion resistance and mechanical properties as a result of its chemical composition. The steel has high chromium (Cr) and nickel (Ni) content. In addition to the corrosion resistance provided by Cr, the heat resistance of Ni is responsible for the low thermal conductivity of this material [2,3]. This makes SS304 difficult to machine due to the concentration of heat flow within the cutting zone [4–6]. New generations of PVD coatings have been developed to improve the cutting process [7,8]. The major characteristics that these new coatings need to possess are a low friction coefficient during cutting as well as the ability to sustain the high temperatures and loads present at the cutting zone [9,10]. Therefore, PVD AlTiN coatings present a potent alternative to address the aforementioned issues on account of their high oxidation and wear resistance [11–14]. Nevertheless, the right balance between Al/Ti needs to be strictly determined to guarantee that the coating system can withstand the issues that manifest during cutting [15,16]. In our previous study, five different compositions of a monolayer AlTiN PVD coating with various Al/Ti ratios (73/27, 70/30, 67/33, 50/50, and 60/40) were investigated during the high-speed turning of SS304. A coated insert with an Al/Ti ratio of 60/40 was found to have the best balance of tribological and mechanical properties, which consequently resulted in the longest tool life [17].

However, our previous study had also shown that addressing the various wear mechanisms during the cutting of SS304 which result in different wear patterns (such as flank wear and crater wear), would require a multifunctional coating layer. Some of

the monolayers, such as $Al_{50}Ti_{50}N$ have improved hardness and loading support, combined with high adhesion to the substrate, others have better tribological characteristics, such as $Al_{60}Ti_{40}N$. None of the studied monolayer AlTiN coatings with various Al/Ti ratios were capable of fully addressing the observed wear mechanisms. In the present research, this has been achieved through the combination of an $Al_{50}Ti_{50}N$ under layer and an $Al_{60}Ti_{40}N$ upper layer in a corresponding bilayer coating.

5.2. Experimental procedure

AlTiN coatings were deposited by an industrial scale PVD method (a cathodic arc ion plating system), equipped with four circular-shaped evaporators. Cemented carbide (WC with 6 wt. % Co binder) was used in this study as the substrate. To deposit monolayer coatings with different Al contents, source materials with two different Al/Ti ratios ($Al_{50}Ti_{50}N$ and $Al_{60}Ti_{40}N$) were used. The whole PVD cycle included heating, plasma etching, coating and cooling. All the substrates underwent plasma etching before deposition, which supplied Ar ions at a bias voltage of -200 V with a pressure of 0.2 Pa for half an hour. During the deposition, the chamber was kept under a constant temperature of 500 °C. A pressure of 3.5 Pa was maintained by controlling the Nitrogen flow rate. No additional noble gas was used. The deposition time was around 3 h. Residual stress of the coating surface was measured by the X-ray diffraction (XRD) technique, on the top surface of each coating. Set up parameters were as following: the target was Ti (Kα avg 2.7497 Å), under the target power of 30kV and 20 mA; X-Ray Elastic Constant was 12,200 ksi, and Bragg Angle (2θ) was 80º. The crystallographic plane in this measurement was {200}.

Cutting tool inserts with the code CNGG120408-FS (Kennametal, substrate K313) were used for ultra-high-speed, single point turning tests. All the inserts were performed

edge preparation following the industrial standard parameters, without other special edge preparation that might affect experimental results. The workpiece material in this work was an austenitic stainless steel 304 round bar (150 mm diameter and 200 mm length). Table 5.1 summarizes the chemical composition and mechanical properties of this material.

Table 5.1. The chemical composition and basic mechanical properties of SS304 [18]

Element	Cr	Ni	Mn	Si	N	C	P	S	Fe
Weight (%)	18 - 20	8 - 10.5	< 2	< 0.75	< 0.1	< 0.08	< 0.045	< 0.03	Balance

Yield strength (MPa)	Tensile strength (MPa)	Elongation (% in 50 mm)	Rockwell B hardness (HR B) max	Brinell hardness (HB) max
205	515	40	92	201

All cutting tests were performed on a high precision CNC lathe (Nakamura Tome SC 450). The turning parameters were: 420 m/min speed, 0.15 mm/rev feed rate and 0.5 mm depth of cut. The cutting fluid was a semi-synthetic coolant with a concentration of 5 %. These cutting conditions were the same as in the authors' previous study. The cutting forces were measured by a LabVIEW professional development system. The tool life criterion (ISO 3685) in this work was set as maximum flank wear of 0.3 mm. A digital optical microscope (Keyence, Japan) was used to investigate the progressive tool wear, thereby evaluating the wear performance of the cutting tools during the turning process. Using ANOVA analysis, the wear data had been acquired from an average of three tests for each variant, which led to a data set error of 5 %.

The micro-mechanical characteristics (hardness and elastic modulus) of the

coatings were measured by a nano-indentation test (NHT3, Anton Paar). The standard procedure was based on Oliver–Pharr method (ISO 14577), which was a typical loading-unloading experiment. The applied load during the tests was 20 mN using Vickers indenter geometry. To collect enough data, an 8 x 5 indentation matrix was used in this measurement. An average of the obtained indentation values was used to assess the hardness and elastic modulus of the coatings. Scratch experiments were carried out by a scratch tester (Revetest, Anton Paar) to investigate the adhesion of the coatings to the WC substrate. This was conducted under an increasing load from 0.5 to 100 N, with a total distance of 3 mm on the track. A Rockwell diamond indenter with a radius of 200 μm was used. Moreover, the same scratch tester equipped with a Vickers indenter was also used for the toughness measurement of the coatings. This was based on the Palmqvist toughness test method (ISO 28079:2009). The load for this test was a constant 150 N, applied at a single point. Three repeated tests were performed for each coating for both the adhesion and toughness studies. The crack length at the corners of the indentations was used to calculate the toughness value.

A scanning electron microscope (SEM) coupled with energy dispersive spectroscopy (EDS) (VEGA, Tescan) was used to analyze the coating/substrate system and the tool wear mechanism. A 3D confocal microscope (Infinity Focus G, Alicona) measured the adhesion (built-up-edge, BUE) and wear volume of the failed inserts. Inserts at the end of tool life were 3D scanned to measure the volume of BUE adhered during the machining. Subsequently, they were cleaned through an etching process in order to determine the actual wear areas. The etching solution for this process was aqua regia, which was HCl and HNO_3 with a volume ratio of 3:1. The Alicona instrument was also used to measure the coating and chip surface average (Sa). The chip formation

characteristics were studied to assess the tribological condition of the tool, chip, and workpiece contact surfaces. The chip undersurfaces, shear band and cross-section microstructures were observed by a SEM (VEGA, Tescan). A Kalling's No.2 reagent was used for the etching process specifically prepared for this test. A chip cross section hardness test was conducted by a nano-indentation tester (NHT3, Anton Paar), with the linear load set to be 5 mN and a loading/unloading rate of 10 mN/min. All of the above numerical tests were conducted at least 3 times, with the average of each result recorded with an accuracy of 95 %.

5.3. Results and discussion

5.3.1. Substrate and coating characterizations

The SEM image of the cross-section of the coating/substrate system is shown in Fig. 5.1. The total thickness of each coating was around 3 to 3.5 microns. The thickness of the $Al_{60}Ti_{40}N$ top layer in the bi-layer coating was 1 μm and that of the $Al_{50}Ti_{50}N$ sublayer was around 2.5 μm. The chemical composition was detected to confirm the atomic ratio of Al/Ti in all three coatings. The cutting tool substrate used in this study was a micro-grain cemented carbide (ISO M5-M10 grade) containing 94 wt. % of hard WC grains and 6 wt. % of soft Co binder in the phase [19]. The grain size of the substrate was 1.225 μm. Usually, fine grain size of WC (between 0.8 μm to 1.3 μm) [20] has beneficial impact on the mechanical properties of the cutting tool by improving the abrasion resistance of the carbide and chipping wear of the cutting edges [21].
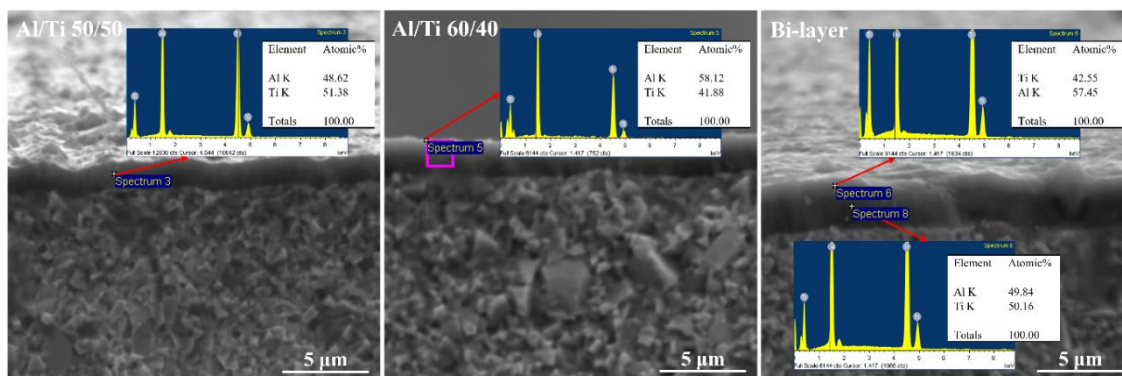
Fig. 5.1. Cross-section microstructure and chemical composition of three coatings.

The physical and mechanical properties of the studied PVD coatings are given in Table 5.2. The $Al_{50}Ti_{50}N$ coating had the highest hardness and elastic modulus on account of its high degree of crystallinity with the cubic phase [17]. The $Al_{60}Ti_{40}N$ coating exhibited the highest toughness, followed by the $Al_{50}Ti_{50}N$ coating. At higher Al concentrations, the coatings possessed greater ductility and elastic deformation. This observation accorded with the hardness/elastic modulus tests. On the other hand, the hardness and elastic modulus of the Al/Ti 60/40+50/50 bi-layer coating was between those of the two component monolayers, indicating the beneficial combination of its mechanical properties. The bi-layer coating featured elevated hardness from the supporting $Al_{50}Ti_{50}N$ coating and improved toughness of the upper $Al_{60}Ti_{40}N$ layer.

The compressive residual stress of $Al_{60}Ti_{40}N$ coating was lower than that of $Al_{50}Ti_{50}N$ coating, as shown in Table 5.2. This was affected by the deposition parameters such as temperature, pressure, bias voltage, and deposition time [22]. Also, the composition of the coating layer contributed to this result. Since the amount of Al and Ti differ, the stability of the cubic AlTiN phase, given the different quantity of atoms of Al also influenced the residual stress. The bi-layer coating obtained almost the same residual stress as the $Al_{60}Ti_{40}N$ coating since the top layer chemical composition was

the same as the $Al_{60}Ti_{40}N$ coating surface.

Table 5.2. Physical and mechanical properties of three AlTiN PVD coatings.

PVD coatings	Bi-layer	Al/Ti 50/50	Al/Ti 60/40
L_C1 (N)	59.2±0.30	47.3±0.24	45.8±0.23
L_C2 (N)	69.9±0.35	54.1±0.27	53.7±0.27
Hardness (GPa)	36.4±1.82	37.4±1.87	35.2±1.76
Elastic modulus (GPa)	638.9±32	663.2±33	592.9±27
H/E	0.057	0.056	0.059
Toughness (N/μm)	1.86±0.093	1.74±0.087	1.95±0.097
Residual stress (MPa)	-1651±40	-2853±124	-1632±39
Surface average, Sa (μm)	0.23±0.011	0.14±0.007	0.17±0.009

Scratch testing was performed to evaluate the adhesion of the coatings to the substrate. As can be seen in Table 5.2, the $Al_{50}Ti_{50}N$ and $Al_{60}Ti_{40}N$ monolayers had relatively similar critical loads in both Lc1 and Lc2. However, the bi-layer Al/Ti 60/40+50/50 coating had a significantly greater critical load due to the microstructure of the coatings and the bonding force generated by their subsequent deposition. In the monolayers, adhesion was directly related to the degree of bonding between the coating and substrate. However, in the bi-layer coating, the scratch indenter needs to apply a greater amount of force to overcome the bonds present between the two coating layers as well as those of the Al/Ti 50/50 sublayer to the substrate. This had resulted in greater critical loads and better adhesion of the bi-layer coating to the substrate.

The scratch track profiles are depicted in Fig. 5.2. In general, only small flaking areas were initially observed on these three coatings. This kind of crack formation was directly related to the strong bonding interactions between the coating and the substrate (ISO 27307:2015). The onset of coating delamination occurred at a similar load for

Al$_{50}$Ti$_{50}$N and Al$_{60}$Ti$_{40}$N. These two coatings exhibited lateral cracking at the beginning of the track, which was identified as buckling with wedging. Although the bi-layer coating also featured buckling cracks at the initial stage, the delamination areas (white spots in Fig. 5.2a) were significantly smaller than in the monolayers. This bi-layer coating seemed to have a strong bonding between the two coating layers instead of the substrate being directly exposed at the beginning (white spots), which was also correlated to the critical loads shown in Table 5.2. All of the studied coatings exhibited spallation and chipping shape at the end of the track, but the bi-layer coating apparently had fewer amount and smaller cracks than the monolayers (Fig. 5.2, a and b-c). A. Kleinbichler, et al. [23] had described how the adhesion of the coating to the substrate is associated with spalling and buckling. In our case, the bi-layer coating with improved adhesion featured less spallation along the tracks (Fig. 5.2a).
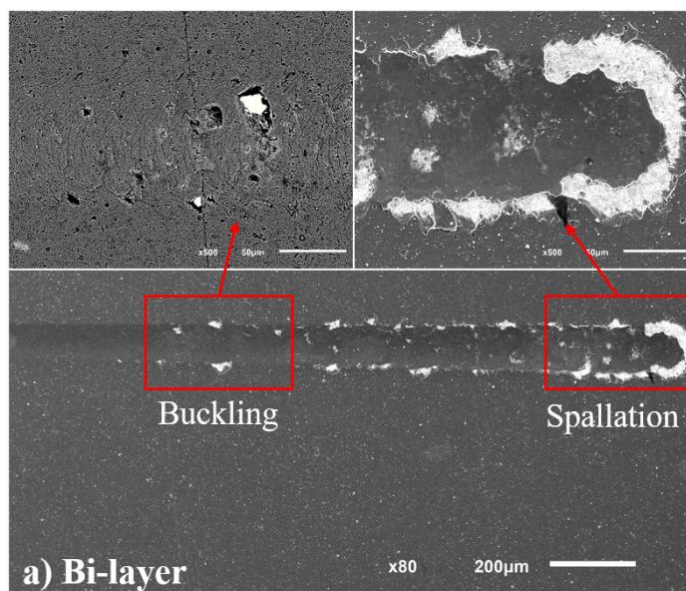
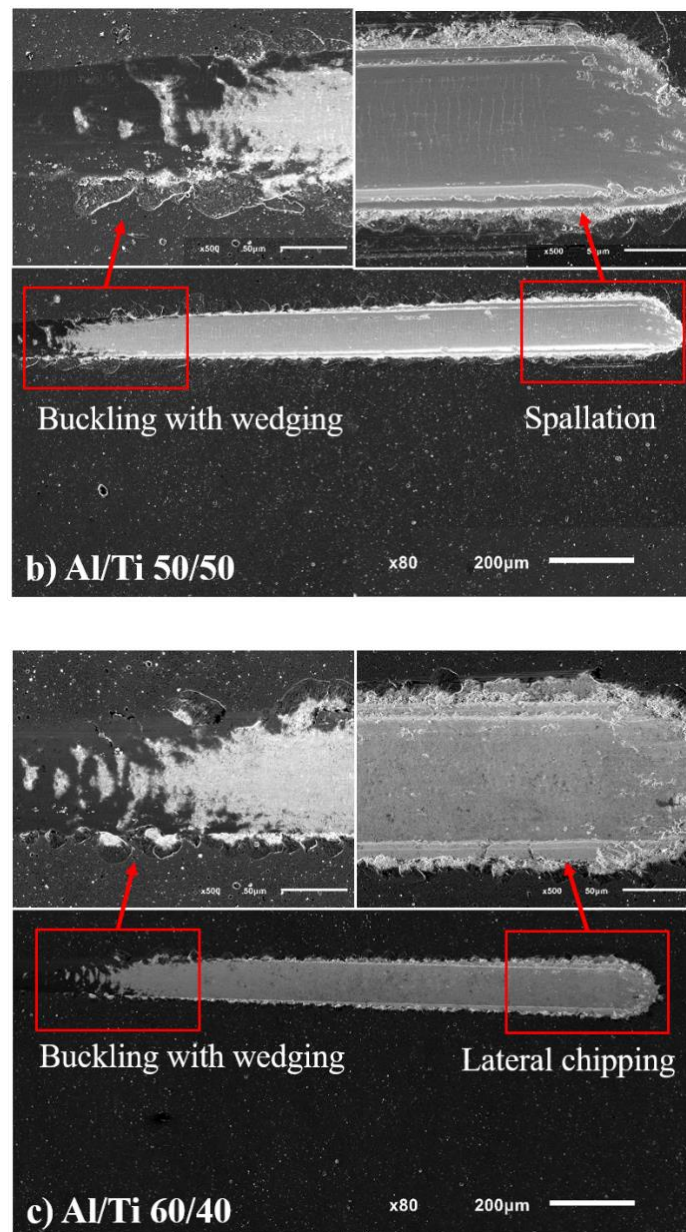Fig. 5.2. SEM image of scratch tracks on the coatings: a) Bi-layer coating, b) monolayer Al/Ti 50/50, and c) monolayer Al/Ti 60/40.

5.3.2. Cutting test results

Fig. 5.3 shows the cutting test results of SS304 following ultra-high-speed (420 m/min) finish turning using three different inserts with Al/Ti 50/50 and Al/Ti 60/40 monolayer coatings and an Al/Ti 60/40+50/50 bi-layer coating. In general, all of the

coated inserts reached abrupt failure. The $Al_{50}Ti_{50}N$ coated tool exhibited the shortest

tool life and failed after 1500 m, whereas the $Al_{60}Ti_{40}N$ insert had a significantly longer

tool life of around 2800 m. The tool with bi-layer coating had the longest tool life of

over 3700 m. The latter's tool life was more than 1.3 times greater than that of the best

monolayer coating. This can be attributed to the outstanding mechanical properties

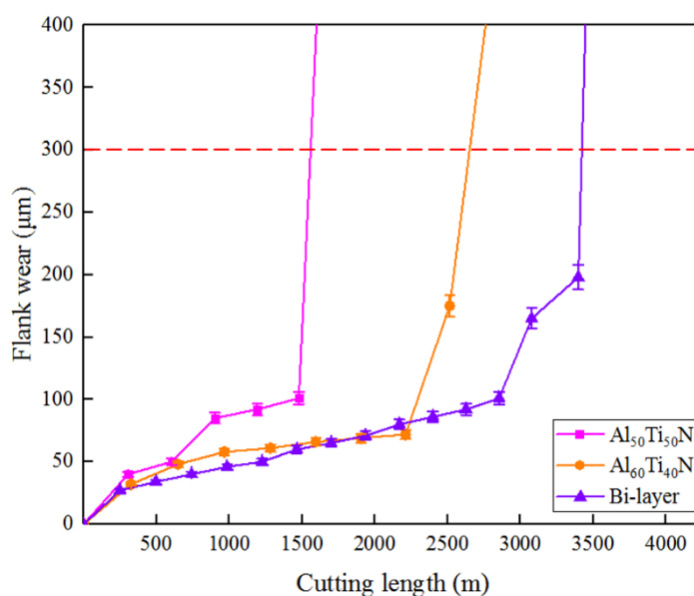provided by the bi-layer coating system.

Fig. 5.3. Cutting tests results: flank wear versus cutting length.

Cutting forces were collected at the initial stage of the cut (around 5 m) for each

tool during the turning process. The cutting force average value is recorded in Fig. 5.4.

In all of the tests, the results are plotted with a specific error line of 5 %. Although the

$Al_{60}Ti_{40}N$ coated tool had the lowest cutting force, given the error margins of cutting

force data, the difference among the coatings was small. The slightly lower cutting force

of the $Al_{60}Ti_{40}N$ coating can be attributed to its mechanical properties (Table 5.2).

During machining, this coating underwent elastic deformation, which might reduce

cutting force values, as reported in [24]. This observation can be validated by the fact that when its Al content is below 67 at. %, the coating possesses sufficient hot-hardness to resist the heavy loads and heat generated by the ultra-high-speed machining process [17,25]. Considering the data plotted in Fig. 5.4 after ANOVA analysis, it can be concluded that the cutting forces at this stage were similar in all coated systems. This combination had resulted in a slight reduction of the cutting forces in comparison with the 50/50 monolayer and their increase in relation to the 60/40 monolayer system.

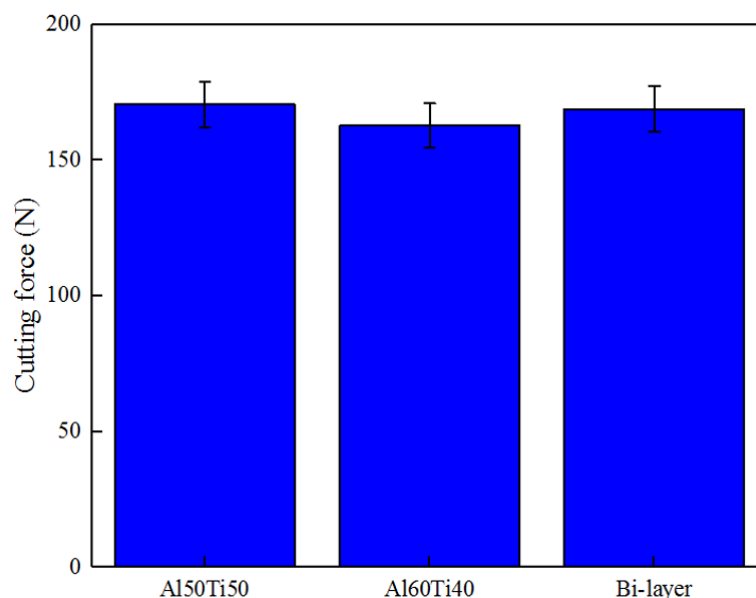Fig. 5.4. Cutting forces during the first pass.

5.3.3. Tool wear analysis

3D Progressive wear studies were performed on the cutting inserts during ultra-high-speed turning using an optical microscope, as shown in Fig. 5.5. Three cutting lengths were selected, each of which was related to the abrupt failure of the corresponding coated cutting tools as is shown in Fig. 5.3. In general, cratering was the

predominant wear mode for all of the AlTiN PVD coated tools studied during ultra-high-speed turning. The extremely high temperatures present under such machining conditions, promoted crater wear occurring on the rake face. This finding has indicated that the coating layer was able to protect the cutting edge for a substantially long time during the machining process. In all cases, the intensity of crater wear was found to be more severe than that of flank wear throughout all wear stages prior to tool failure. The cause of this crater formation was the actual interaction between the rake surface of the tool and the chips under heavy thermo-mechanical loads [25]. With growth of crater wear, the substrate became exposed, which eventually resulted in the removal of the cobalt binder due to thermal softening [26]. As time progressed, this resulted in deeper and wider crater wear. The novel bi-layer coated tool featured smaller and rounder craters compared with the other coatings until a cutting length of 2500 m was reached. This can be attributed to its combination of mechanical properties, namely the toughness of Al/Ti 60/40 in conjunction with the hardness of 50/50.
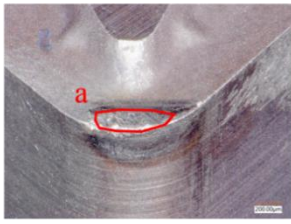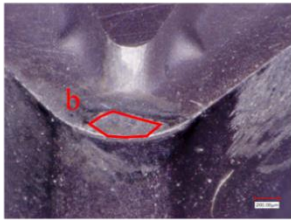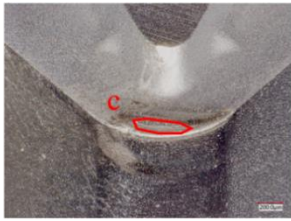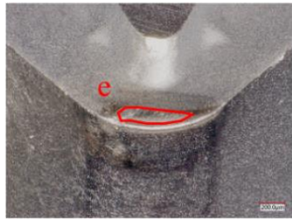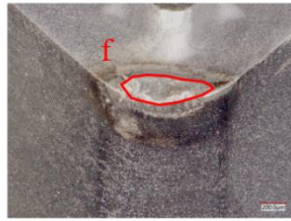
Cutting length	1500 m		Crater area
Al$_{50}$Ti$_{50}$N	(a)		a: 72431.3±3621.5 μm^2 b: 68900.1±3445.0 μm^2 c: 23422.0±1171.1 μm^2
Cutting length	**1500 m**	**2500 m**	
Al$_{60}$Ti$_{40}$N	(b)	(d)	d: 93871.0±4693.5 μm^2 e: 54354.7±2717.7 μm^2 f: 98209.9±4910.4 μm^2
Cutting length	**1500 m**	**2500 m**	**3500 m**
Bi-layer	(c)	(e)	(f)

Fig. 5.5. 3D progress wear pattern of inserts at different cutting lengths.

In order to understand the wear mechanism behind tool failure, worn cutting tools after the cutting tests were evaluated by SEM. Fig. 5.6 shows the wear patterns on the failed inserts at the end of tool life. Under such ultra-high-speed machining of austenitic stainless steel, the intense temperature and heavy load applied on the tool/chip/workpiece interfaces were the main reasons for tool failure. In general, the main wear mechanism of AlTiN PVD coated tools during ultra-high-speed machining was a combination of attrition/abrasion and adhesion. Such wear conditions resulted in intense chipping and BUE which covered the craters that had formed on the tool rake face. During cutting, the flank had become damaged and was severely affected by chipping and coating delamination, which resulted in metal-to-metal adhesion. As was

explained in [27], abrasion/attrition wear promoted workpiece material adhesion to the tool surface and generated a BUE that caused further chipping on the tool flank face. It can be seen in Fig. 5.6 that the bi-layer coating and the $Al_{50}Ti_{50}N$ coating showed a similar wear pattern on the failed insert, since the bi-layer coating contained Al/Ti 50/50 as the sublayer. However, fewer BUE marks were observed on the bi-layer coated tool, which had also featured minimal crater wear compared to the $Al_{60}Ti_{40}N$ coating, with a clear round-shape crater on the rake face. Overall, the bi-layer coating demonstrated its multi-functional capability of resisting cratering, BUE formation, and flank wear. The beneficial combination of the properties of the two component AlTiN monolayers in this novel bi-layer coating had achieved a reduction in the wear rate and as a consequence, extended the tool's life during the ultra-high-speed turning of SS304.

Fig. 5.6 also shows the EDS elemental mapping results on the worn tools. The Al signal indicated the remaining AlTiN coating on the inserts, the Fe/Cr signal confirmed the workpiece material (SS304) adhering on the tool and the W signal indicated tungsten carbide substrate exposure after the coating became worn out. This EDS result (absent Al signal in the middle with apparent W and Fe/Cr signal) provides further evidence for the wear mechanism described above wherein substrate exposure occurs on the tool rake face and becomes covered by the intense BUE formed during tool failure. In addition, the Fe/Cr signal also showed the formation of oxides on the tool flank face, which are normally contained within the BUE during high-speed machining of austenitic stainless steel.
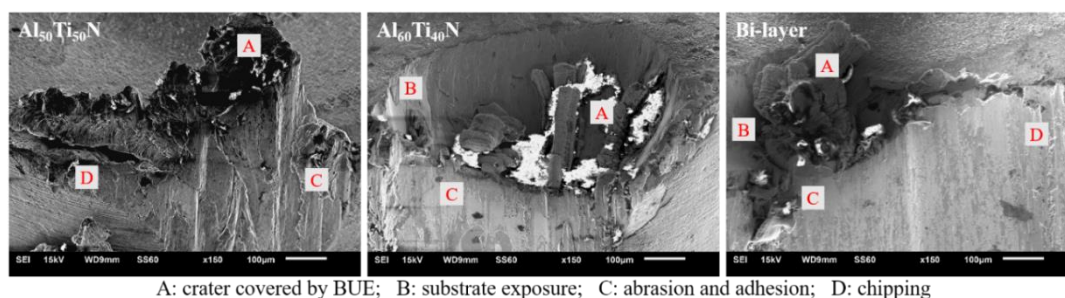
A: crater covered by BUE; B: substrate exposure; C: abrasion and adhesion; D: chipping
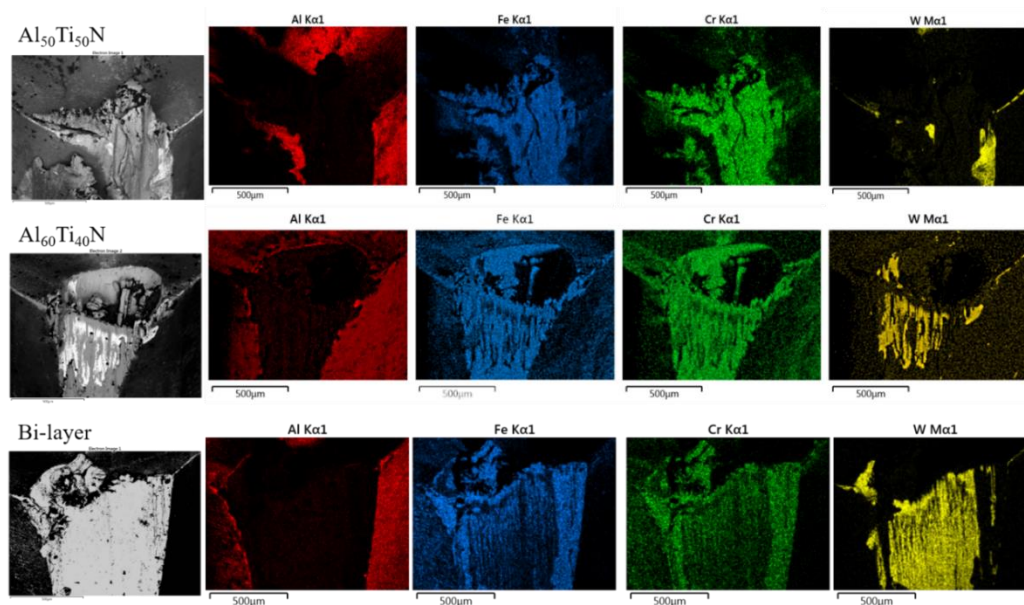
Fig. 5.6. SEM image and EDS element map of wear modes after tool failure.

Fig. 5.7 presents the volume of BUE and the volume of combined crater and flank wear after tool failure. Those measurements were performed using an Alicona microscope, following the procedures presented in the experimental procedures section. The $Al_{50}Ti_{50}N$ tool had the most severe BUE along with the most worn volume. Given the same chemical composition of the sublayer as in Al/Ti 50/50, the bi-layer coated tool showed a similar but slightly reduced volume of wear than that of the $Al_{50}Ti_{50}N$ coating. On the other hand, the volume of BUE on the bi-layer coated tool was significantly lower (similar to that of the monolayer $Al_{60}Ti_{40}N$ coated insert) which indicated minimal detachment of the coating and lateral chipping on the tool edge. This

beneficial characteristic can be attributed to the mechanical properties of this coating, as recorded in Table 5.2. Although the $Al_{60}Ti_{40}N$ coating featured the smallest wear volume following tool failure (at 2800 m cutting length), given the slower progress of wear during the cutting process (as shown in Fig. 5.5), the bi-layer coating had alleviated the wear rate and thereby achieved a much longer tool life of 3700 m. In this situation, the greater wear volume of the worn bi-layer coated tool was acceptable. Overall, the novel bi-layer coating possessed a number of beneficial mechanical properties that take advantage of both the Al/Ti 50/50 sublayer and Al/Ti 60/40 top layer, which led to better wear performance and extended tool life.

Fig. 5.7. Numerical volume of BUE and wear on the failed tool.

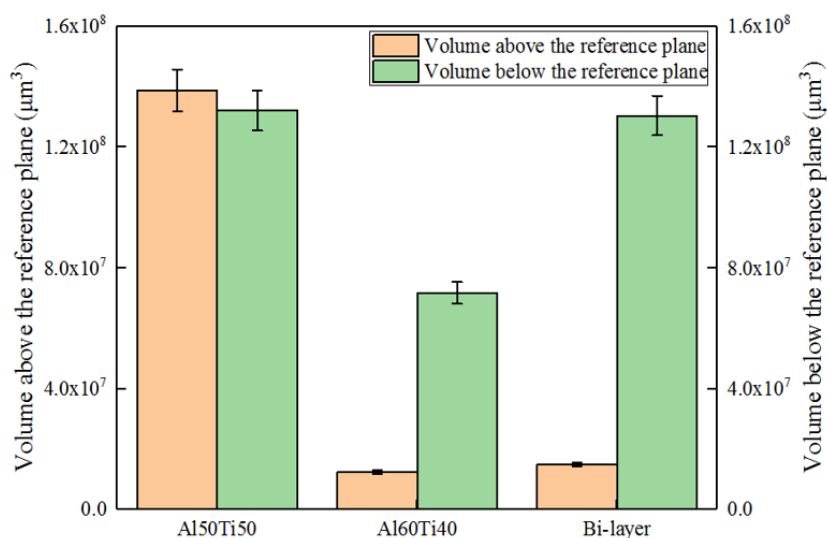## 5.3.4. Tribological characteristics evaluated through the chip formation studies

Tribological characteristics were evaluated through chip formation features during cutting as a consequence of the friction conditions at the insert/chip interface [28]. Chip

shapes, undersurface morphology and shear bands are solid indicators of the tribological conditions during cutting. Fig. 5.8 shows the chips and the data collected from the three different coatings proposed in this work. The average surface roughness of the undersurfaces of the chips produced by the bi-layer coated tool was 0.7417 μm, as was measured under an Alicona confocal microscope. This was smoother than the chips produced by the monolayer Al/Ti 60/40 (Sa = 0.9023 μm) and Al/Ti 50/50 (Sa = 1.1522 μm) coated tools. SEM images confirmed the curly shape of the chips, although the Al/Ti 50/50 chip had more of an irregular arc shape. The undersurface morphology of Al/Ti 50/50 shown in Fig. 5.8 (middle), with its evident fold and tearing marks was considered to be the worst. The metal had intensively adhered to the tool surface due to intensive friction at the interface, which caused the material to accumulate during the metal flow and eventually resulted in the emergence of material folds [27]. The chips generated by the Al/Ti 60/40 monolayer and the bi-layer coatings exhibited better undersurfaces. Although there were spots of uneven metal flow on the bi-layer chip surface and shred marks on the Al/Ti 60/40 monolayer chip, the metal was nonetheless able to more easily flow across the tool rake face due to its generally smoother average surface.

All of the shear bands of the upper surface of the chips shown in Fig. 5.8 featured a lamellar structure. The difference was in the distance between the separate tracks. The chips produced by the bi-layer coated tool had a more uniform distance compared with the other two chips. Furthermore, the shear band segment spacing of the chips produced by the bi-layer coated tool was more constant and apparently narrower as well. This superior morphology confirmed that the chips underwent plastic deformation and were produced smoothly and constantly by the bi-layer coated tool during the ultra-high-

speed turning of SS304. Considering the chips' shape and morphology, less intensive sticking and less severe tearing were shown to have occurred in the bi-layer coated tool, indicating less intensive friction at the tool/chip interface into the cutting zone.
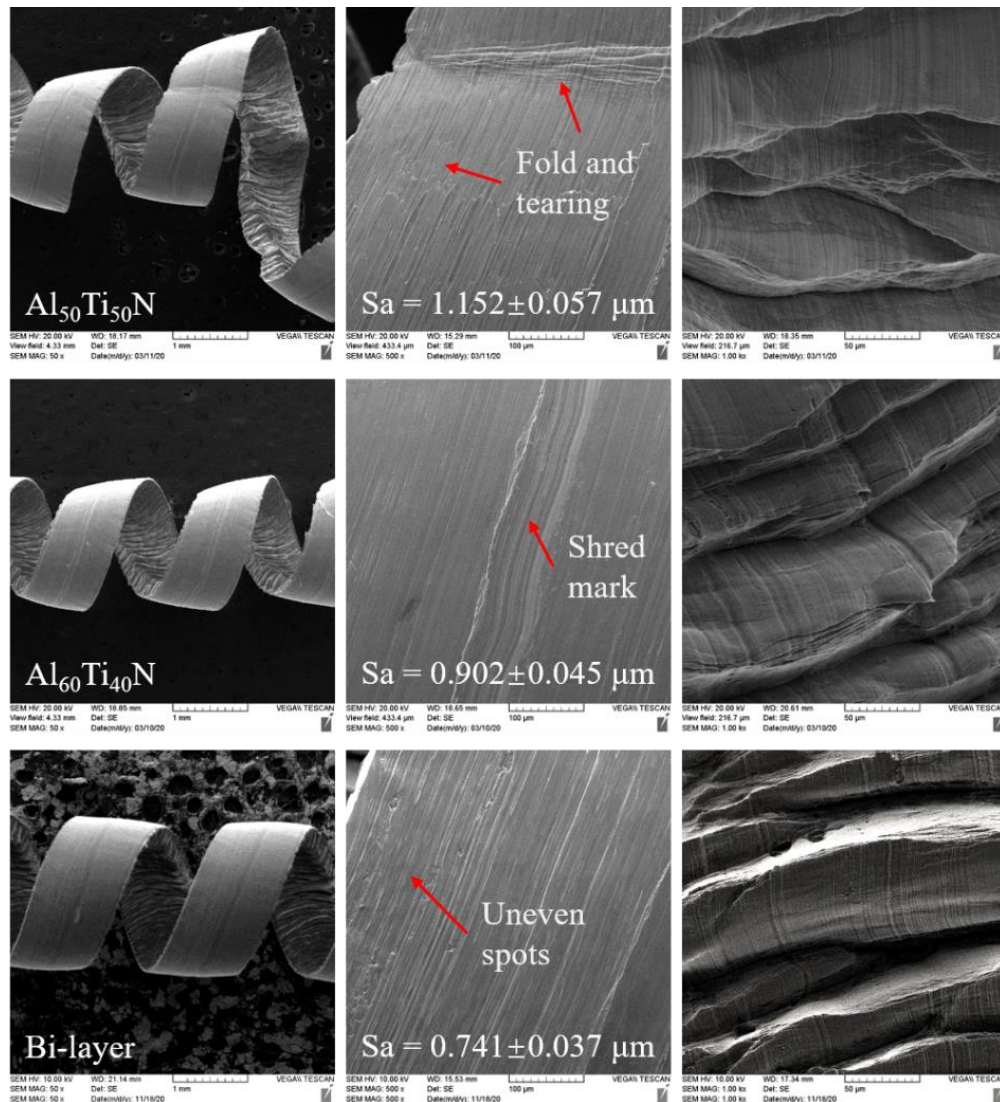

Fig. 5.8. Chip characteristics of general shape, undersurface morphology and shear band.

Chip formation numbers are presented in Table 5.3 and different comparable trends are shown in Fig. 5.9. As can be seen, the chips produced by the bi-layer coated tool had the thinnest average thickness, which resulted in the highest chip compression ratio,

with the largest shear angle and the lowest friction coefficient. These quantitative results indicated that friction between the chip and the bi-layer coated insert was improved during the machining process. A combination of the mechanical properties and microstructure of the novel bi-layer coating has reduced the friction coefficient at the cutting zone.

Another critical characteristic is the chip sliding velocity. It is clearly shown (both in Table 5.3 and Fig. 5.9) that the chip produced by the bi-layer coated tool had improved sliding velocity compared to the chips produced by the Al/Ti 60/40 and 50/50 monolayers. This indicates the rapid metal flow of the chips produced by the bi-layer coated tool. Given the accelerated metal flow, the bi-layer chips induced intense plastic deformation [18], which was also confirmed by the chip shear band characteristics presented in Fig. 5.8.

Table 5.3. Statistical characteristic of chips formed by different AlTiN coated inserts.

Coating	Bi-layer	Al/Ti 50/50	Al/Ti 60/40
Chip thickness (mm)	0.254±0.012	0.286±0.014	0.266±0.013
Tool-chip Contact Length (mm)	0.102±0.005	0.122±0.006	0.103±0.005
Chip Compression Ratio - CCR	0.59±0.030	0.52±0.026	0.56±0.028
Φ - Shear Angle (°)	31.71±1.58	28.57±1.43	30.47±1.52
β - Friction Angle (°)	18.29±0.91	21.43±1.07	19.53±0.98
ϒ - Shear Strain	1.44±0.072	1.68±0.084	1.53±0.077
Chip Sliding Velocity (m/min)	247.09±12.35	219.15±10.96	235.88±11.79
Friction Coefficient (μ)	0.61±0.03	0.77±0.04	0.67±0.03

Furthermore, as shown in Fig. 5.9, the tool-chip contact length of the bi-layer coating was slightly less than that of the Al/Ti 60/40 monolayer coating, at around 0.1 mm. Since they have the same chemical composition of the top layer, these two coatings

exhibited similar performance at the initial stage of wear. This result was related to the chip shapes and undersurface morphology as shown in Fig. 5.8. These two chips featured regular curled shapes with a high degree of curvature, which had demonstrated that the chip became quickly deformed and cut out with reduced contact length on the tool rake face. In addition, the lowest tool-chip contact length was also determined by the friction environment occurring at the cutting zone, which in turn, was related to the lowest friction coefficient and the highest chip sliding velocity. Since the bi-layer coating featured superior chip formation characteristics, the friction between the tool and chip/workpiece was minimal. This enabled a significant wear rate reduction during machining, thereby improving tool life.
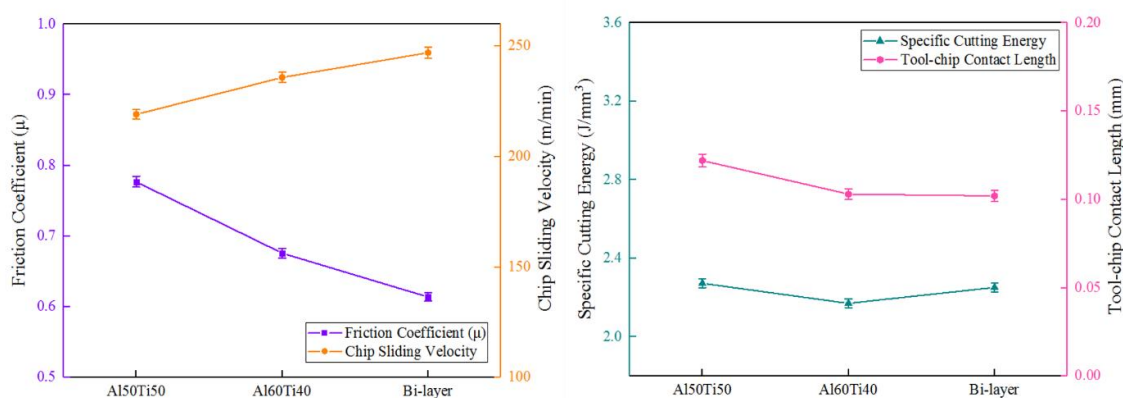
Fig. 5.9. Tribology characteristics based on chip formation data.

Cutting force was used to calculate the specific cutting energy [29]. Since the cutting forces of all the AlTiN coatings were almost the same (with a deviation less than 10 N shown in Fig. 5.4), the specific cutting energy in Fig. 5.9 was presumed to exhibit a minor variation as well. The limited reduced specific energy generated by the $Al_{60}Ti_{40}N$ coated tool can be attributed to its difference in mechanical properties. Due

to its higher toughness, this coating underwent elastic deformation during the machining process, making it better able to dissipate energy. Less energy was therefore required to cut a unit volume of workpiece material [30]. Considering all of the chip characteristics illustrated above, the bilayer coating had presented a better combination of mechanical properties, which resulted in improved wear performance.

5.3.5. Chip cross-section analysis

According to the chip tribological characteristics, the chip produced by the bi-layer coated tool had experienced accelerated metal flow, which led to intensive plastic deformation within the body of the chips. A chip cross-section study was conducted to further evaluate the degree of plastic deformation within the chips. This study had also helped explain the metal deformation mechanism occurring in the shear zone [31]. Fig. 5.10 shows the chip cross-sections along with the microstructure of each evaluated chip. Saw-tooth chips were found to have formed during the high-speed turning of stainless steels due to the extreme heat contributing to the thermal deformation of the chip [32]. The chips produced by the bi-layer coated tool were noticeably thinner and with a more rounded shape than the other two chips. The chips produced by the bi-layer coated tool in Fig. 5.10 exhibited more intensive metal flow. This was observed in conjunction with the coefficient of friction data (shown in Table 5.3). The friction between the chip and the bi-layer coated tool remained at the minimum during high-speed turning. Therefore, the curlier chips had a greater tendency to easily form and smoothly slide across the tool rake face. This had resulted in a high degree of plastic deformation in the chips generated by the bi-layer coating and contributed to the most intense metal flow at the chip/tool interface.
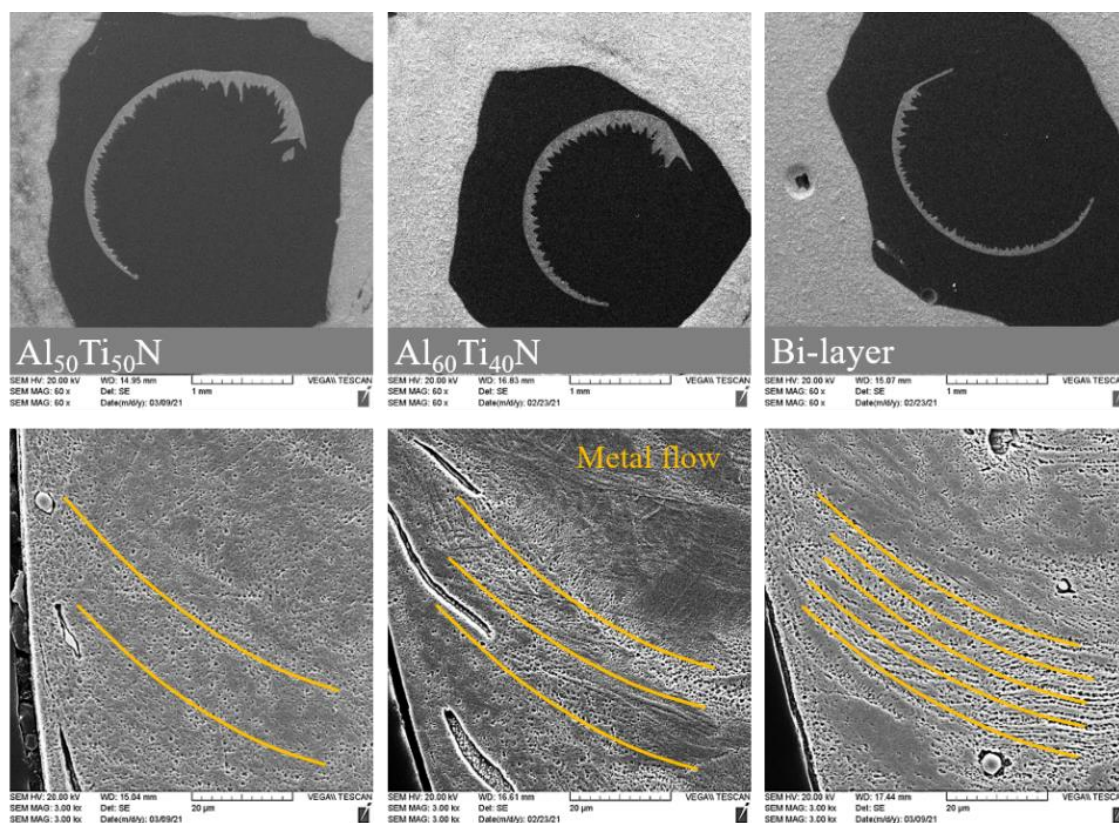
Fig. 5.10. Chip cross-section microstructure of different AlTiN coatings.

The micro-hardness distribution was measured at the chip cross-section, as shown in Fig. 5.11. This test helped evaluate the effect of strain-hardening induced into the chip. All chips exhibited a lower hardness at the chip/tool interface area (edge side). Hardness tended to increase along the outer surface (tip side) of the chips. This confirmed the incidence of the strain-hardening effect since metal along the cutting direction was heavily deformed in the primary shear zone. Although the hardness values of the chips produced by the bi-layer coated tool were lower than those of chips produced by other coated tools, the extent of hardening was the greatest, reaching 11.3 %. The chips produced by the $Al_{60}Ti_{40}N$ coated tool had the second greatest degree of hardening (with 10.3 %) and the chips produced by the $Al_{50}Ti_{50}N$ coated tool had the least range of hardening, only 8.6 %. The significant hardness variation in chips

produced by the bi-layer coated tool can be explained by the accelerated metal flow, which caused induced strain plastic deformation. Lattice stretching of the workpiece promoted by shear stress under the heavy load and thermal effect had led to different chip formation which is evident in the shear band morphology (Fig. 5.8). This theory was also confirmed in [17,18]. During the ultra-high-speed turning of SS304, the novel bi-layer coating improved the friction condition at the tool-chip interface, which was reflected in the chip formation characteristics (such as lower friction angle and higher chip compression ratio in Table 5.3).

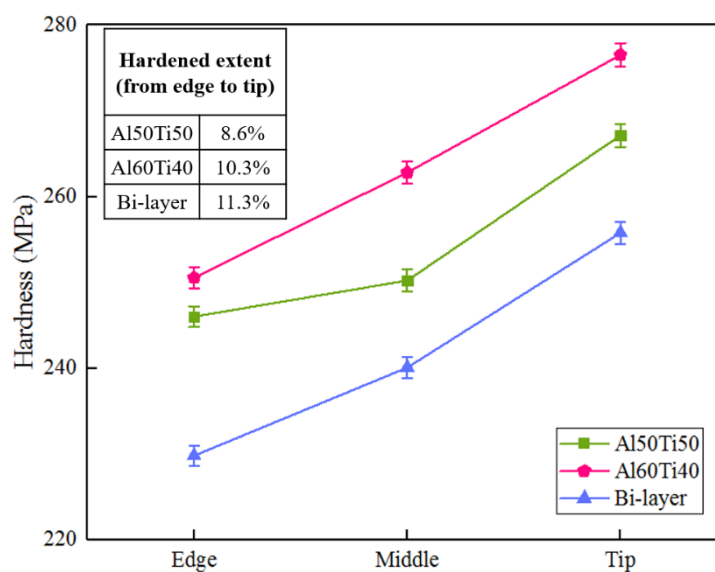Fig. 5.11. Chip cross-section hardness of different AlTiN coatings.

All of the studied chip characteristics had indicated the presence of an enhanced friction environment at the cutting zone during machining by the bi-layer coated tool. The combination of chemical composition and mechanical properties of this coating was demonstrated to be beneficial for the ultra-high-speed turning of austenitic stainless steel.

5.4. Conclusions

In this paper, a novel Al/Ti 60/40+50/50 bi-layer AlTiN PVD coating was designed and compared with an Al/Ti 60/40 and 50/50 monolayer coating under ultra-high-speed (420 m/min) finish turning of stainless steel 304. The novel bi-layer coated tool's life was found to have increased by 33 %, which can be attributed to the combination of high hardness of the underlying $Al_{50}Ti_{50}N$ layer and improved frictional characteristics of the top $Al_{60}Ti_{40}N$ layer.

Analysis of the inserts' worn area had demonstrated crater wear as the predominant wear mode due to the excessive temperature generated at high cutting speeds. Due to a combination of good adhesion and high abrasion resistance, the novel bi-layer coating had proven capable of reducing the wear rate and stabilizing the growth of crater wear, which resulted in the greatest tool life extension.

Chip formation characteristics and chip cross-section analysis had confirmed that the chips produced by the bi-layer coated tool exhibited the most intensive plastic deformation during the turning process. This can be attributed to the improved friction condition at the bi-layer coated tool/chip interface within the cutting zone, which had expedited chip flow and reduced contact with the tool rake face.

Given its favorable mechanical and tribological properties, the novel Al/Ti 60/40+50/50 bi-layer coating was found to be capable of providing multifunctionality and significantly improving tool wear performance and the ensuing tool life.

5.5. References

[1]   Q. He, Z. Jin, G. Jiang, Y. Shi, The investigation on electrochemical denatured layer of 304 stainless steel, Mater. Manuf. Process. 33 (2018) 1661–1666. https://doi.org/10.1080/10426914.2018.1453152.

[2]   C. Hong, J. Shi, L. Sheng, W. Cao, W. Hui, H. Dong, Influence of hot working on microstructure and mechanical behavior of high nitrogen stainless steel, J. Mater. Sci. 46 (2011) 5097–5103. https://doi.org/10.1007/s10853-011-5439-2.

[3]   A. Di Schino, J.M. Kenny, Grain size dependence of the fatigue behaviour of a ultrafine-grained AISI 304 stainless steel, 57 (2003) 3182–3185. https://doi.org/10.1016/S0167-577X(03)00021-1.

[4]   P.S. Bapat, P.D. Dhikale, S.M. Shinde, A.P. Kulkarni, S.S. Chinchanikar, A Numerical Model to Obtain Temperature Distribution During Hard Turning of AISI 52100 Steel, Mater. Today Proc. 2 (2015) 1907–1914. https://doi.org/https://doi.org/10.1016/j.matpr.2015.07.150.

[5]   J.M.F. d. Paiva, R.D. Torres, F.L. Amorim, D. Covelli, M. Tauhiduzzaman, S. Veldhuis, G. Dosbaeva, G. Fox-Rabinovich, Frictional and wear performance of hard coatings during machining of superduplex stainless steel, Int. J. Adv. Manuf. Technol. 92 (2017) 423–432. https://doi.org/10.1007/s00170-017-0141-4.

[6]   I. Korkut, M. Kasap, I. Ciftci, U. Seker, Determination of optimum cutting parameters during machining of AISI 304 austenitic stainless steel, Mater. Des. 25 (2004) 303–305. https://doi.org/https://doi.org/10.1016/j.matdes.2003.10.011.

[7]   A.I. Fernández-Abia, J. Barreiro, J. Fernández-Larrinoa, L.N.L. de Lacalle, A. Fernández-Valdivielso, O.M. Pereira, Behaviour of PVD Coatings in the Turning of Austenitic Stainless Steels, Procedia Eng. 63 (2013) 133–141.

https://doi.org/https://doi.org/10.1016/j.proeng.2013.08.241.

[8] Q.F.T. Wang, Y.L.Z. Wu, T. Zhang, T. Li, Microstructure and Corrosion Resistance of the AlTiN Coating Deposited by Arc Ion Plating, Acta Metall. Sin. (English Lett. 29 (2016) 1119–1126. https://doi.org/10.1007/s40195-016-0497-8.

[9] X. Wang, P.Y. Kwon, D. Schrock, D. (Dae-W. Kim, Friction coefficient and sliding wear of AlTiN coating under various lubrication conditions, Wear. 304 (2013) 67–76. https://doi.org/https://doi.org/10.1016/j.wear.2013.03.050.

[10] P. Sahoo, K. Patra, V.K. Singh, M.K. Gupta, Q. Song, M. Mia, D.Y. Pimenov, Influences of TiAlN coating and limiting angles of flutes on prediction of cutting forces and dynamic stability in micro milling of die steel (P-20), J. Mater. Process. Technol. 278 (2020) 116500. https://doi.org/https://doi.org/10.1016/j.jmatprotec.2019.116500.

[11] J.L. Endrino, G.S. Fox-rabinovich, C. Gey, Hard AlTiN , AlCrN PVD coatings for machining of austenitic stainless steel, Surf. Coatings Technol. 200 (2006) 6840–6845. https://doi.org/10.1016/j.surfcoat.2005.10.030.

[12] W. Kalss, A. Reiter, V. Derflinger, C. Gey, J.L. Endrino, Modern coatings in high performance cutting applications, Int. J. Refract. Met. Hard Mater. 24 (2006) 399–404. https://doi.org/https://doi.org/10.1016/j.ijrmhm.2005.11.005.

[13] G.S. Fox-Rabinovich, A.I. Kovalev, M.H. Aguirre, B.D. Beake, K. Yamamoto, S.C. Veldhuis, J.L. Endrino, D.L. Wainstein, A.Y. Rashkovskiy, Design and performance of AlTiN and TiAlCrN PVD coatings for machining of hard to cut materials, Surf. Coatings Technol. 204 (2009) 489–496. https://doi.org/10.1016/j.surfcoat.2009.08.021.

[14]   L. Chen, J. Paulitsch, Y. Du, P.H. Mayrhofer, Thermal stability and oxidation
        resistance of Ti–Al–N coatings, Surf. Coatings Technol. 206 (2012) 2954–2960.
        https://doi.org/https://doi.org/10.1016/j.surfcoat.2011.12.028.

[15]   C. He, J. Zhang, G. Song, G. Ma, Z. Du, J. Wang, D. Zhao, Microstructure and
        mechanical properties of reactive sputtered nanocrystalline (Ti,Al)N films, Thin
        Solid   Films.   584   (2015)   192–197.
        https://doi.org/https://doi.org/10.1016/j.tsf.2014.12.027.

[16]   M. Witthaut, R. Cremer, A. von Richthofen, D. Neuschütz, Improvement of the
        oxidation behavior of Ti1-xAlxN hard coatings by optimization of the Ti/Al ratio,
        Fresenius.   J.   Anal.   Chem.   361   (1998)   639–641.
        https://doi.org/10.1007/s002160050976.

[17]   Q. He, J.M. Paiva, J. Kohlscheen, B.D. Beake, S.C. Veldhuis, Study of wear
        performance and tribological characterization of AlTiN PVD coatings with
        different Al/Ti ratios during ultra-high speed turning of stainless steel 304, Int. J.
        Refract.   Met.   Hard   Mater.   (2021)   105488.
        https://doi.org/https://doi.org/10.1016/j.ijrmhm.2021.105488.

[18]   Q. He, J.M. Paiva, J. Kohlscheen, B.D. Beake, S.C. Veldhuis, An integrative
        approach to coating / carbide substrate design of CVD and PVD coated cutting
        tools during the machining of austenitic stainless steel, 46 (2020) 5149–5158.
        https://doi.org/10.1016/j.ceramint.2019.10.259.

[19]   J. Xiong, Z. Guo, M. Yang, W. Wan, G. Dong, Tool life and wear of WC–TiC–
        Co ultrafine cemented carbide during dry cutting of AISI H13 steel, Ceram. Int.
        39   (2013)   337–346.
        https://doi.org/https://doi.org/10.1016/j.ceramint.2012.06.031.

[20] ISO 4499-2:2008, Hardmetals — Metallographic determination of microstructure — Part 2: Measurement of WC grain size, (n.d.).

[21] J. García, V.C. Ciprés, A. Blomqvist, B. Kaplan, Cemented carbide microstructures: a review, Int. J. Refract. Met. Hard Mater. 80 (2019) 40–68. https://doi.org/https://doi.org/10.1016/j.ijrmhm.2018.12.004.

[22] J. Kohlscheen, T. Shibata, Phase and Residual Stress Evaluation of Dual-Phase Al70Cr30N and Al80Cr20N PVD Films, Crystals. 9 (2019). https://doi.org/10.3390/cryst9070362.

[23] A. Kleinbichler, M.J. Pfeifenberger, J. Zechner, S. Wöhlert, M.J. Cordill, Scratch induced thin film buckling for quantitative adhesion measurements, Mater. Des. 155 (2018) 203–211. https://doi.org/https://doi.org/10.1016/j.matdes.2018.05.062.

[24] J. Rajaguru, N. Arunachalam, Coated tool Performance in Dry Turning of Super Duplex Stainless Steel, Procedia Manuf. 10 (2017) 601–611. https://doi.org/https://doi.org/10.1016/j.promfg.2017.07.061.

[25] J. Kohlscheen, C. Bareiss, Effect of Hexagonal Phase Content on Wear Behaviour of AlTiN Arc PVD Coatings, (2018). https://doi.org/10.3390/coatings8020072.

[26] D. Jianxin, Z. Jiantou, Z. Hui, Y. Pei, Wear mechanisms of cemented carbide tools in dry cutting of precipitation hardening semi-austenitic stainless steels, Wear. 270 (2011) 520–527. https://doi.org/https://doi.org/10.1016/j.wear.2011.01.006.

[27] A. Biksa, K. Yamamoto, G. Dosbaeva, S.C. Veldhuis, G.S. Fox-rabinovich, A. Elfizy, T. Wagg, L.S. Shuster, Tribology International Wear behavior of adaptive

nano-multilayered AlTiN / Me x N PVD coatings during machining of aerospace alloys, Tribiology Int. 43 (2010) 1491–1499. https://doi.org/10.1016/j.triboint.2010.02.008.

[28] E.M. Trent, P.K. Wright, Metal Cutting, 2000. https://doi.org/10.1016/B978-075067069-2/50012-7.

[29] M. Shaw, Metal cutting principles, 2°, Oxford Unversity Press, New York, 2005.

[30] W. Polini, S. Turchetta, Force and specific energy in stone cutting by diamond mill, Int. J. Mach. Tools Manuf. 44 (2004) 1189–1196. https://doi.org/https://doi.org/10.1016/j.ijmachtools.2004.04.001.

[31] J. Nomani, A. Pramanik, T. Hilditch, G. Littlefair, Chip formation mechanism and machinability of wrought duplex stainless steel alloys, (2015) 1127–1135. https://doi.org/10.1007/s00170-015-7113-3.

[32] A.I. Journal, R.S. Pawade, S.S. Joshi, MECHANISM OF CHIP FORMATION IN HIGH-SPEED TURNING OF INCONEL 718, 0344 (2011). https://doi.org/10.1080/10910344.2011.557974.

Chapter 6: Conclusions and Future work

6.1. General Conclusions

Austenitic stainless steels have a high work-hardening level and low thermal conductivity as a result of its chemical composition made up predominantly of chromium (Cr) and nickel (Ni). This leads to severe machining problems as associasted with high cutting forces, unstable chip formation, and rapid tool failure. In addition, the friction force at the tool-chip interface is elevated due to work hardening, which leads to a high localized temperature and causes diffusion and oxidation at the tool-workpiece interface. To solve these challenges, the combination of coating and substrate system was studied to sustain the heavy load and high temperatures experienced during the high-speed machining of SS304. Furthermore, a novel self-adaptive bilayer AlTiN PVD coating was developed to address the combined wear mechanism of oxidation, diffusion, and abrasion/attrition, and to improve tool life.

In order to develop a novel self-adaptive AlTiN PVD coating, this research was divided into four different studies, each striving to understand a different aspect of the coating/substrate system that is important for high-speed semi-finish/finish turning of SS304. First, the mechanical properties, microstructure, and chemical composition of the coating/substrate system were studied. Wear mechanisms and tribological characteristics during the high-speed turning of SS304 were systematically focused and investigated. The effects of different cooling conditions and the coating's chemical composition were analyzed in detail for high-speed machining applications. Finally, a novel bilayer AlTiN PVD coating was designed and developed based on the previous findings and analyses.

In each study, machining experiments and advanced characterization were conducted as follows: a) XRD and residual stress measurements on the coating surface; b) SEM/EDS/EBSD observations on the coating/substrate system, tool wear mechanisms, chip formation morphology and surface integrity of the machined workpiece; c) nano-indentation and scratch tests in order to evaluate the mechanical properties of the chip cross-section and coating/substrate system; d) optical 3D microscopy and white light interferometry microscopy to measure surface roughness of the coating, chips, and machined workpiece as well as the tool wear volume; and e) cutting force collection during the initial turning stage. Based on these detailed experimental and analytical studies, the major conclusions of this research can be summarized below:

1. The CVD 1 coating/substrate system (TiN-TiCN-Al_2O_3 coating + WC- 10 % Co- 2.6 % Ti substrate) performed desirably due to a combination of factors (e.g., better plasticity and better load carrying capacity) contributing to longer tool life during the high-speed semi-finish turning of SS304. The enhanced mechanical properties of this coating/substrate system affected tribological characteristics during cutting such as CCR, metal flow and shear band formation, wear performance, and overall tool life.

2. Analysis of wear performance showed that the tool that used an AlTiN PVD coating/substrate system for high-speed semi-finish/finish turning of SS304 failed due to intensive crater wear instead of the regularly observed flank wear. This was a result of the intense temperatures generated on the tool rake face under high cutting speeds, which caused diffusion and consequently intensive chemical wear.

3. The expected high oxidation resistance of the coating layer along with an Al/Ti atomic ratio over 67/33 was not a decisive factor under the considered conditions. Instead, the optimal combination of superior substrate adhesion and high hardness rendered the monolayer Al/Ti 60/40 coated insert capable of stabilizing the worn area around the crater. Therefore, the crater's depth could grow evenly with moderate flank wear, resulting in the longest tool life out of the five different Al/Ti ratios.

4. Under different cooling conditions, tool life results showed that all the inserts performed better in the presence of coolant for the high-speed machining of SS304, with cutting length extended by 2-3 times. Among them, the monolayer Al/Ti 60/40 coated insert possessed the longest tool life of 7,000 m under wet conditions, and 2,500 m under dry conditions.

5. The characteristics of the chip were analyzed to reveal that the friction at the cutting zone was generally lower when a coolant was present, but the coating system used were found to be effective at reducing the cutting forces under dry turning conditions thanks to the formation of alumina at the first stage of the cutting process. In addition, the monolayer Al/Ti 60/40 coated insert produced improved chip formation characteristics such as high CCR, high chip sliding velocity, and low TCCL. This indicates that the enhanced mechanical properties of the monolayer Al/Ti 60/40 coated insert yielded a lower intensity of friction between the tool/chip interface.

6. A novel Al/Ti 60/40+50/50 bilayer AlTiN PVD coating was designed. This novel self-adaptive bilayer coating was found to increase tool life by 33 % compared to the best monolayer Al/Ti 60/40 coated insert. This improved

performance was attributed to the combination of the high hardness of the underlying Al/Ti 50/50 layer and the improved frictional characteristics of the top Al/Ti 60/40 layer.

In summary, the selection and design of the self-adaptive AlTiN PVD coating for high/ultra-high speed semi-finish/finish turning of austenitic stainless steels was based on the dominant tool wear mechanisms and tribological characteristics occurring at the tool/chip/workpiece interface. The major focus of this research was to identify the coating's combination of mechanical properties and chemical composition, which is associated with tribological characteristics at the deformation zone. This resulted in improved wear performance and extended tool life. This improved performance was attributed to the ability of the coating to address the underlying dominant tool wear mechanisms experienced during the high-speed turning of SS304.

6.2. Research Contributions

The main contributions of this research can be summarized as follows:

1. An advanced study of different PVD and CVD coating/substrate systems was performed. This provided the results needed to form a comprehensive understanding of the correlation between different grades of substrates and the coatings which were deposited over them. This study provided needed information on the mechanical properties and tool wear performance during the high-speed machining of stainless steels.

2. The dominant tool wear mechanism of AlTiN PVD coatings with different Al/Ti ratios during high/ultra-high speed turning of austenitic stainless steel under various cooling conditions was identified and understood. It was established that a combination of oxidation/diffusion wear mechanisms

resulted in cratering whereas abrasion/attrition led to catastrophic failure on the flank face. This combination of wear mechanisms dictates the overall wear behaviour and tool life of tools coated with an AlTiN coating. Different Al/Ti ratios were considered to better understand the role these elements played in providing protection and lubracation.

3. Tribological characteristics present at the tool/chip interface were observed and analyzed for AlTiN PVD coatings with different Al/Ti ratios. The chip formation mechanism and chip cross-section studies were evaluated in detail. The findings were also correlated with tool wear performance and the coating's mechanical properties in order to understand the coating/substrate behaviour during high/ultra-high speed turning of austenitic stainless steel better.

4. A novel self-adaptive bilayer AlTiN PVD coating was designed and developed. This coating was applied in the ultra-high speed finish turning of austenitic stainless steel. An understanding of what is driving the performance improvement associated with the new coating as compared to other coatings was studied. A combination of mechanical properties, chemical composition, microstructure, and tribological characteristics of this bilayer AlTiN PVD coating was determined to be capable of providing multifunctionality and significantly improving tool wear performance and ultimately extending tool life.

In this research, a novel self-adaptive bilayer AlTiN PVD coating was designed and developed. The effect of the coating/substrate system properties and tribological characteristics was investigated in detail. Improved wear performance and extended tool life were achieved by the novel bilayer coating for the high/ultra-high speed turning

of austenitic stainless steel. The knowledge gained and the research approach adopted can be implemented to design PVD coatings for various workpiece materials, especially difficult-to-cut materials, to achieve similar results.

6.3. Recommendations for Future Research

In the current study, it was demonstrated that tool life can be significantly improved for turning operations by designing PVD coatings with a combination of mechanical properties, chemical composition, and tribological characteristics that specifically address the complex wear mechanisms involved. Other workpiece materials and other applications, such as drilling and milling, should be studied to better understand the full potential of this coating.

Using the bilayer AlTiN PVD coating developed as a base, other monolayer or multilayer coatings with different alloying elements that can generate favourable tribo-films should be experimentally studied to further improve tool life. According to the literature, WC/C, TiB_2, and/or CrB_2 have also been shown to provide lubrication and oxidation resistance. Therefore, these layers should be deposited on the outer surface over top of the AlTiN PVD coating in an effort to further improve tool performance.

Furthermore, the PVD technique that was used for this research was cathodic arc deposition. Different PVD methods such as high-power impulse magnetron sputtering (HiPIMS) should be tested to assess if their deposition properties lead to an AlTiN-based coating with the same chemical composition but improved microstructure and surface properties which can sustain high cutting speeds while improving tool life.